AN ANALYSIS OF THE TRANSIENT RESPONSE OF

THERMAL PROTECTION SYSTEMS

Submitted in Partial Fulfillment of the Requirements for the
Degree of Master of Science in Engineering

by

Frank Campanile

The School of Engineering

UNIVERSITY OF DAYTON

Dayton, Ohio

December, 1968

Approved:

Chairman, Advisory Committee

Director, Graduate Programs

Dean, School of Engineering

ACKNOWLEDGEMENTS

The author wishes to acknowledge his indebtedness to his advisor, Dr. L. I. Boehman, whose advice and encouragement were largely responsible for this study being undertaken and accomplished. I also wish to express my appreciation to the United States Air Force for its financial support during my graduate studies.

I wish to express my gratitude to the members of the Plastics and Composites Branch of the Air Force Materials Laboratory for their support in furnishing materials specimen and data. Particularly, I would like to thank Mr. D. L. Schmidt and Dr. M. Manoff of the Ablative Plastics Group; without their assistance this study could not have been accomplished. The cooperation and assistance of the following individuals of the Aeronautical Systems Division are gratefully acknowledged: Mr. L. E. Miller and Dr. W. L. Hankey, who provided valuable counsel in the preparation of certain sections of this investigation; Mr. H. E. Petersen for his advice in programming the MIMIC computer program; Mr. G. K. Cunningham for his graphics support; and Mrs. Frances Jarnagin for her fine typing assistance.

The assistance and advice of the following members of the University of Dayton Research Institute are gratefully acknowledged: Messrs. J. C. Wurst and D. A. Gerdeman, as well as the counsel of Dr. P. Bauer.

Finally, I would especially like to thank my wife, Kay, for her typing assistance and also for her encouragement, patience, and understanding throughout my entire graduate studies.

ABSTRACT

This study outlines a method of reducing a partial differential equation, such as the heat-conduction equation, to a system of ordinary differential equations. The system of equations is then solved utilizing the MIMIC computer program whose specific purpose is to provide digital solution, on an IBM 7090 (7094) computer, for systems of ordinary differential equations.

The ultimate goal of this analysis is to apply the aforementioned technique to study the thermal response of ablators. The inherent nonlinearity of the heat conduction equation, due to the moving boundary, virtually excludes analytical solutions to the problem and forces the use of numerical techniques.

Differential equations governing the transient response of thermal protection systems to a hyperthermal re-entry environment are presented. A simplified analysis of a charring ablator, illustrating the various modes of heat dissipation, is given in detail. The analysis is shown to be adequate for studying the thermal response of not only charring ablators, but also heat-sink thermal protection systems, melting, sublimers, and impregnated ceramic ablators, by comparing predicted results with known analytical solutions, other ablation models, and test results. Teflon, a classic sublimer, and Carbon Phenolic, a modern charring ablator, were tested in a 100 KW arc heater facility at the University of Dayton in order to obtain some experimental results.

Finally, the model is exercised by designing an ablator thermal protection system for several classes of re-entry vehicles.

TABLE OF CONTENTS

TABLE OF CONTENTS CONTINUED

NOMENCLATURE

A	area
B	collision frequency
BP	ballistic parameter = W/C_dA
C	integration constants
c	specific heat at constant pressure
C_f	skin friction coefficient
C_{O_2}	mass fraction of oxygen in the free stream
D	aerodynamic drag
E	activation energy
F	heat of fusion of ice
f	porosity
h,H	enthalpy
H_p	heat of pyrolysis
h_c	heat of combustion
$\bar{h}_c$	convective heat transfer
h_d	heat of depolymerization
h_f	heat of fusion
k	thermal conductivity
k_p	permeability
L	aerodynamic lift
L_o	initial ablator thickness
M	molecular weight
$\dot{m}$	mass loss rate
N,n	number of slices ablator is cut for finite difference formulation
$\dot{m}_p$	degradation rate of virgin material

NOMENCLATURE CONTINUED

N_{Le}	Lewis Number
N_{Re}	Reynolds Number
P	pressure
P_{O_2}	partial pressure of molecular oxygen
Q	total heat
Q^*	thermochemical heat of ablation
q	dynamic pressure
$\dot{q}$	heat flux
R	gas constant
R_n	nose cap radius
s	distance that surface has receded from initial boundary
$\dot{s}$	recession rate
T	temperature
T_w	substrate temperature, or wall temperature
t	time
V	volume, velocity
V_c	circular velocity
V_w	steady state ablation velocity
W	weight
w	thickness of substrate material
x	distance
X_{O_2}	mole fraction of oxygen

NOMENCLATURE CONTINUED

Greek Symbols

α	thermal diffusivity, absorptivity
$\bar{\alpha}$	angle of attack
β	transpiration factor
γ	flight path angle
Γ	gasification ratio
δ	ablated thickness
Δ	incremental thickness
ϵ	emissivity
η	transpiration factor coefficient
λ	weight of char removed per unit weight of oxygen
θ	angular distance
μ	viscosity
Λ	fin or leading edge sweep angle
ξ	dimensionless or transformed coordinate
ρ	density
σ	Stefan-Boltzmann Radiation constant, stress
τ	shear stress
ψ	transpiration blocking function
∇	Laplacian Operator

Subscripts

s	surface, stagnation
a	ablation zone
c	char, cone
v	virgin plastic

Subscripts continued

aero	aerodynamic
rad	radiation
re-rad	reradiation
g	escaping gases
comb	combustion
∞	free stream
w	wall, substrate
e	edge of boundary layer
i	initial
m	melting
ss	steady state
int	interior
col	coolant
FP	flat plate
L	laminar
T	turbulent
SL	sea level
LE	leading edge
F	fin
p	virgin plastic
d	diffusion controlled
r	reaction controlled
tra	transition
pyr	pyrolysis
o	reference values

Superscripts

' transformed coordinate

. derivative with respect to time

LIST OF TABLES

LIST OF ILLUSTRATIONS

LIST OF ILLUSTRATIONS CONTINUED

I. INTRODUCTION

Bodies traveling in a fluid experience dynamic heating, the magnitude of which depends upon the body configuration and the environmental parameters. At a given altitude and configuration the amount of heating experienced is dependent directly on speed. Subsonic aircraft do not encounter heating problems but supersonic aircraft experience some heating for Mach numbers greater than two. The normal mode of thermal protection for this class of vehicle is normally the heat sink. Even the first re-entry missiles such as the Thor, Atlas, and Titan were protected by blunt heat sink structures fabricated of copper or beryllium. Actually, heat sinks do not solve the re-entry problem; they mostly avoid it. A heat sink works by the absorption and storage of heat. An effective heat sink material must have high specific heat and high thermal conductivity, so that the heat can be carried away from the surface before surface temperatures build up to the melting point. No matter how good a material performs as a heat sink, it is limited as to the amount of heat it can absorb as shown in Table 1. The reason heat sinks were used as the first thermal protection systems was not because they were efficient, but for the fact that they were available, easy to manufacture, reliable and amenable to analysis.

With the advent of modern ICBM's and their high flight speeds, aerodynamic heating increases to a point where some added form of thermal protection is necessary to prevent thermally induced thermostructural failure. With higher heat fluxes, the heat sink concept

TABLE 1. HEAT ABSORBING CAPABILITIES OF MATERIALS

Material	Heat Required to Raise to Melting Temp BTU/LB (0^o-T_m)	Heat of Fusion		Heat of Vaporization		Total Heat Absorbed (Including Decomposition) BTU/LB (80 - 8530^{o}F)
		BTU/LB @ 1 ATMO	Temp ^{o}F	BTU/LB @ 1 ATMO	Temp ^{o}F	
Copper	150	88	1980	3180	4170	3400
Beryllium	1600	700	2462	6500	2732	12000
Aluminum	280	170	1220	3590	3270	5800
Graphite	4100	?	6330	21450	7580	30000
Tungsten	770	100	6100	1530	10500	2400
Molybdenum	420	200	4757	3000	6692	3800
Water	15	144	32	973	212	28440
Teflon	185	37	620	680	1125	8000
Magnesium Oxide	--	1920	5070	--	5715	10090
Silicone Carbide	--	--	--	--	4892	7050
Beryllium Oxide	--	3400	4620	13400	7700	12000

Sources: 1. H. A. King, "Proceeding of an International Symposium on High Temperature Technology," Stanford Research Institute, McGraw Hill, 1959.
2. I. Gruntfest, "The Use of Plastics at High Temperatures," SAE National Aeronautical Meeting at L. A., Sept. 29, 1958.

was no longer adequate and more complex thermal protection techniques of transpiration, film cooling, or ablation were required. Ablation has proven the simplest and most reliable to utilize. Numerous studies (Ref. 1, 2, 3) and reviews have been made of this mechanism and of the potential of ablative materials.

The principle behind ablation is simply that a material will absorb heat as it changes from one physical state into another. Thus, ablation can be defined as the thermal degradation of a material by the absorption of energy resulting from the high velocities and aerodynamic heating encountered by space vehicles upon re-entering the earth's atmosphere. This near-orderly removal of material by melting, subliming, or pyrolysis, has already proven to be an effective and efficient heat protection system for some re-entry vehicles and rocket nozzles.

Unlike heat sink material, ablation material should have a low thermal conductivity, producing high temperature gradients, so that the surface builds up to the material degradation point while the material underneath stays comparatively cool and retains its structural integrity.

Modern heat shield designers are faced with the problem of thermal protection against a wide realm of re-entry vehicles as illustrated in Figure 1. The different re-entry trajectories give diverse heat flux versus time histories. These heat fluxes range in peak heating of

1. Schmidt, D. L., "Behavior of Plastics in Re-entry Environments," Modern Plastics, Nov. 1960.
2. Adams, Mac C., "Recent Advances in Ablation," ARS Journal, Sep. 1959.
3. Scala, S. M., Gilbert, L. M., "Thermal Degradation of a Char-Forming Plastic During Hypersonic Flight," ARS Journal, June 1962.

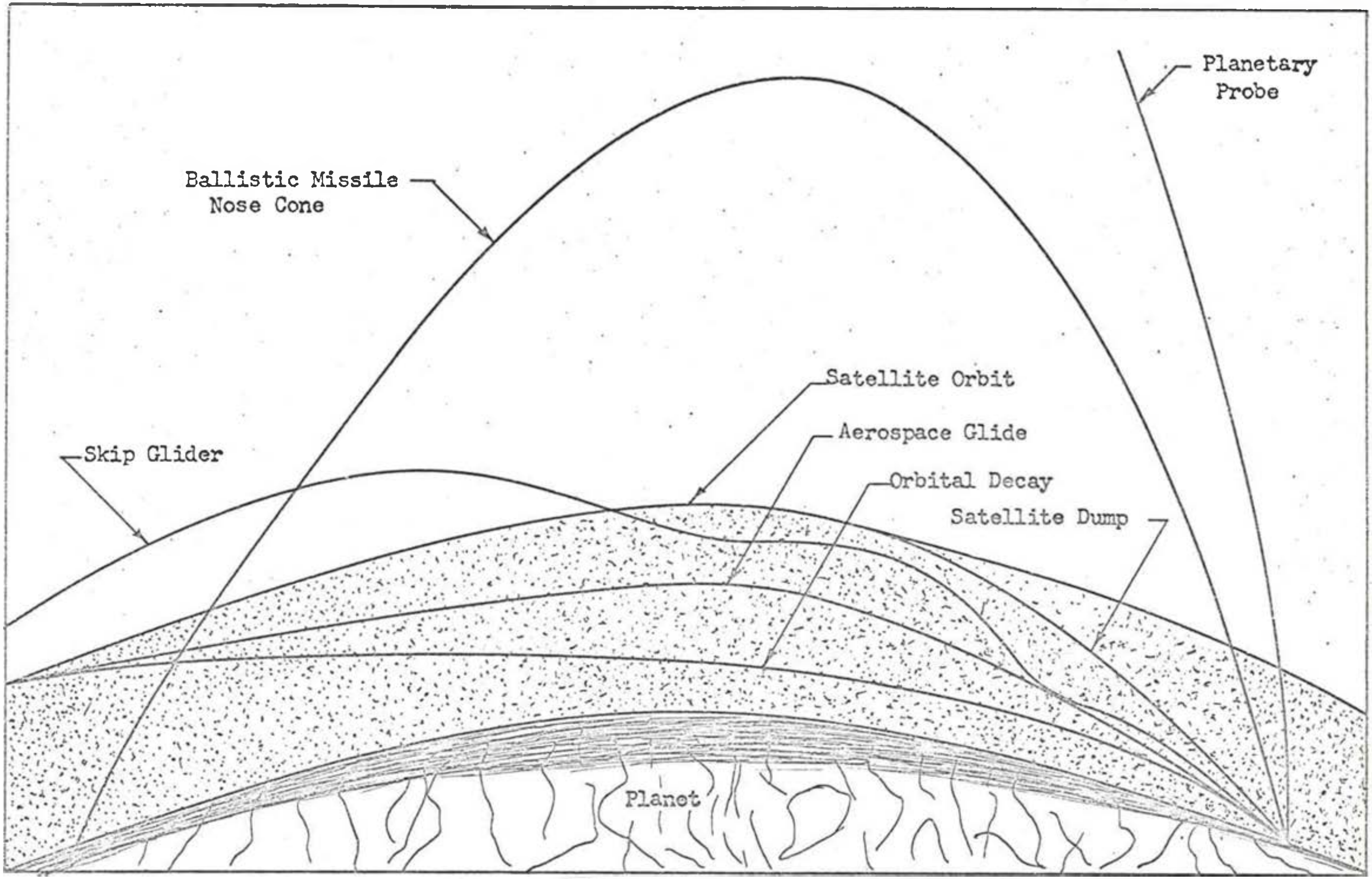

Figure 1. Typical Re-entry Trajectories

2000 BTU/ft^2 sec which last for several seconds, for an ICBM trajectory, to lifting bodies heat fluxes which may be of the order of 20 BTU/ft^2 sec but which may last for over one hour. To combat this problem heat shield designers developed a new array of materials which range from improved ceramics to ablators. Of great interest as ablators is the particular group of composite polymer systems commonly referred to as reinforced plastics. Basically, these materials are composed of organic resins combined with organic or inorganic fibers of materials such as glass, carbon, asbestos, ceramics, or nylon. These fibers serve as reinforcement similar to that of steel in reinforced concrete. These materials have found wide use in rocket nozzles, manned re-entry vehicles, and ICBM heat shields due to their light weight, reliability, good thermal shock characteristics, and ease of fabrication, and are comparatively inexpensive compared to ceramics.

Table 1 shows the heat absorption characteristics of heat sink, ceramics, and ablator materials. This table shows that water up to decomposition contains a large amount of potential enthalpy and potentially it is one of the best materials. However, keeping it around to reap all its benefits is a problem. Materials which initially degrade into a liquid phase or char present this particular problem. The shear and pressure forces as well as mechanical degradation, especially in a turbulent aerodynamic environment; sweep the liquid phase away and thus decrease the efficiency of the heat shield. It is thus important to utilize the heat of vaporization and decomposition of the materials. Magnesium oxide, for example, is believed to sublime with some decomposition occurring simultaneously. It is also suspected that an increase in pressure of a few atmospheres suppresses decomposition and permits melting. Thus, its potential heat capacity may not be realized when the liquid flows away under surface shear force (Ref. 4).

Since the heat of vaporization or degradation is much higher than the heat of fusion, as seen in Table 1, the analysis proposed in this study will concentrate on materials which sublime or degrade by charring rather than on materials which melt.

Aside from impregnated ceramics two types of ablators have come into prominence - sublimers and char formers. In this analysis the sublimers are treated as ablating at a fixed temperature. For subliming ablators the surface temperature is taken as the ablation temperature during the ablation process. The char forming ablators are also treated as ablating at a fixed temperature, even though this is only approximately true in both instances. However, the surface temperature of the char layer, which is obtained from a heat balance at the surface, can sustain high temperatures and thus reject much of the heat by reradiation.

Even though many organic and reinforced plastics have been already used to protect vehicles from short term high heat flux aerodynamic heating, the behavior of these materials under ablating conditions is quite complex and thus not completely understood. The various additives that are used can change the mechanism of decomposition of the phenolics or epoxy resins inherent in these materials. The thermal response of the material can vary from a Teflon-type degradation

---

4. Scala, E., "Composite Materials for Thermal Protection," Presented at Southwestern Metal Congress (American Society for Metals), Dallas, Texas, May 9, 1960.

leaving no residue, to a charring phenolic leaving practically a graphite coating.

The first ablation heat shield designers utilized the effective heat of ablation, an experimentally determined property defined in Appendix I, to design thermal shields. Since then, many theoretical analysis of varying degrees of sophistication (Ref. 5, 6) have been proposed and utilized in order to assess the transient thermal response of ablators. It has been pointed out in the foregoing discussion that ablation usually involves the removal of material. Thus, the application of heat to a moving boundary produces nonlinear differential equations. The resulting equations cannot be solved analytically without making gross simplifying assumptions. Even the design of heat sink thermal devices and radiating ceramics defies the use of analytical solution if the heat input is a function of time and/or the material properties are functions of one or more thermodynamic properties.

Thus, due to the nonlinearity of the equations involved in designing thermal protection systems, several procedures which utilize numerical techniques to solve the resulting equations have been proposed. In order to solve a heat transfer problem which is described by nonlinear differential equations one must resort to an analog computer simulation (Ref. 7) or solve the problem on a digital computer

---

5. Swann, R. T., "Approximate Analysis of the Performance of Char-Forming Ablators," NASA TR R-195, June 1964.
6. Swann, R. T., Pittman, C. M., Smith, J. C., "One-Dimensional Numerical Analysis of the Transient Response of Thermal Protection Systems," NASA TN D-2976, Sept. 1965.
7. Hurwicz, H., Fifer, S., Kelly, M., "Multidimensional Ablation and Heat Flow During Re-entry," Journal of Spacecraft and Rockets, Jan. 1964.

by numerical methods (Ref. 6). Solving the problem on an electric analog computer involves the use of skilled people and much equipment while the common complaint of solving this problem by strict numerical methods on the digital computer is the excessive amount of computer time. The proposed use of the MIMIC computer program seems to eliminate some of these problems in that it is simple to use and achieves the desired solutions quickly.

For heat sink type materials, such as copper or beryllium, properties such as conductivity, density, and specific heat are well established. For ablative materials, however, with their chemistry of decomposition and transient property changes, the thermal properties are difficult to obtain. The ablative materials are less well developed or characterized and are frequently of so inconsistent quality that the thermal properties vary from sample to sample. Often a range of values for the different properties is reported. These values can vary by as much as plus or minus ten per cent. Also, it has been stated previously that the behavior of these materials under ablating conditions is complex and not fully understood. Another problem in achieving accuracy is the errors inherent in determining heating input rates. Under the best of conditions, convective heat flux input can be predicted with an error of plus or minus twenty per cent for high speed flight, and the accuracy of estimated heat fluxes from radiating hot gases is considerably poorer. The desired objective of thermal analysis is to predict structural response with an accuracy of plus or minus twenty per cent (Ref. 4).

---

6. Ibid.
4. Ibid.

In view of the foregoing, an analysis which attempts to be too refined does not seem to be justifiable. This is especially true since, due to the degree of uncertainty involved, the designer is forced to use some measure of conservatism after he obtains the design parameters. However, the model should be sensitive to all thermodynamic properties and account for all the various heat input and heat dissipation mechanisms.

II. THEORETICAL ANALYSIS

When a material undergoes ablation, heat to the surface is generated by convective aerodynamic heating as well as by shock wave radiation and combustion. Combustion can be of two types, gas-phase combustion and surface combustion. This heat input is dissipated when the ablative material acts initially as a heat sink, since the heat entering the surface is conducted into the ablator material and stored. Since ablators normally have low thermal diffusivities due to very low conductivities, the surface temperature rises rapidly until the ablation temperature, T_a, is reached and thermal degradation of the material begins. During the thermal degradation, the ablator pyrolyzes, sublimes or forms a char, giving off gases. Thus, part of the original heat input is dissipated by the phase change and by the gases being injected into the boundary layer producing a heat absorption, or heat blockage effect, by the process of transpiration cooling. The surface, especially on char formers, reaches high temperatures and thus rejects some of the heat by reradiation.

The objective of this analysis is to formulate an ablation model which will predict surface recession and backface temperature, as well as the temperature distribution within the material, for a heat shield under various re-entry conditions or from diverse external heat fluxes. The important heat transfer mechanisms for which an understanding is required before predicting recession rate and temperature distribution are shown schematically in Figure 2. The heat transfer mechanisms will be discussed in the subsequent section.

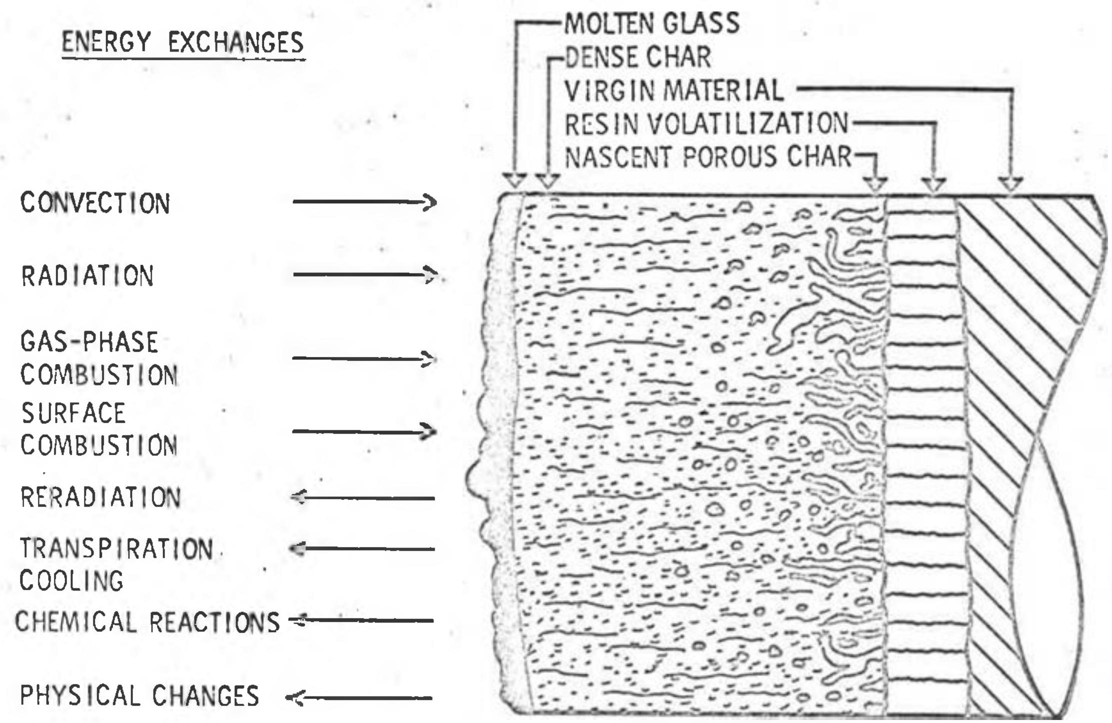

Figure 2. Heat Transfer Mechanisms for a Typical Char Forming Reinforced Plastic.

Ablative materials have low strength at elevated temperatures. Thus, they are normally bonded or mechanically attached to a metal substructure which acts as a bearer of the aerodynamic loads. The bonding or metal structure must be maintained at a reasonable temperature to prevent catastrophic failure. Thus, low thermal conductivity of the ablators is imperative. Modern epoxy bonding agents lose their adhesive qualities in the neighborhood of 600°F. Conventional structures, like aluminum, begin to lose their strength at around 400°F, while refractory structures can be heated to higher temperatures.

Figures 3a and 3b show a schematic of the thermal protection system to be analyzed prior to and after ablation has started.

In the following analysis one square foot of material is assumed; the flow is one dimensional and all heat flow is normal to the surface.

2.1 Thermal Analysis before Ablation

The heat input, $\dot{q}_{in}$, to an ablating heat shield prior to ablation is given by:

$$\dot{q}_{in} = \dot{q}_{aero} + \alpha\, \dot{q}_{rad} - \dot{q}_{re\text{-}rad} \tag{1}$$

where:

$\dot{q}_{aero}$ = convective aerodynamic heating to surface

$\alpha\, \dot{q}_{rad}$ = radiation from the shock wave preceeding the body

$\dot{q}_{re\text{-}rad}$ = amount of heat that is reradiated from the virgin material ($\Lambda\, \epsilon_v\, \sigma\, T_s^{\,4}$)

In order to illustrate the method of reducing partial differential equations to a set of ordinary differential equations we can consider the case before ablation or mass loss begins. For this case we have a nonablating homogeneous solid and the one-dimensional Fourier

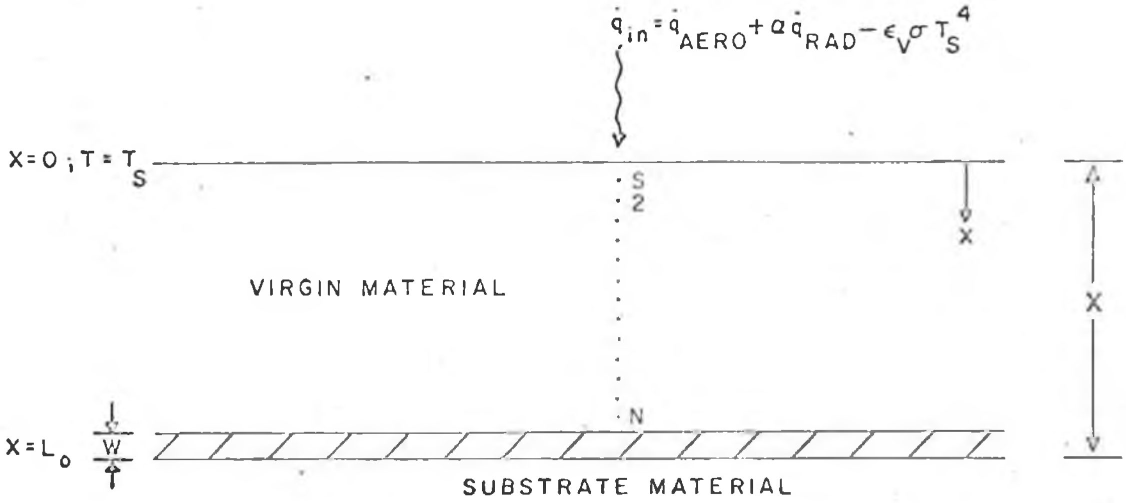

Figure 3a. Ablator Prior to Ablation

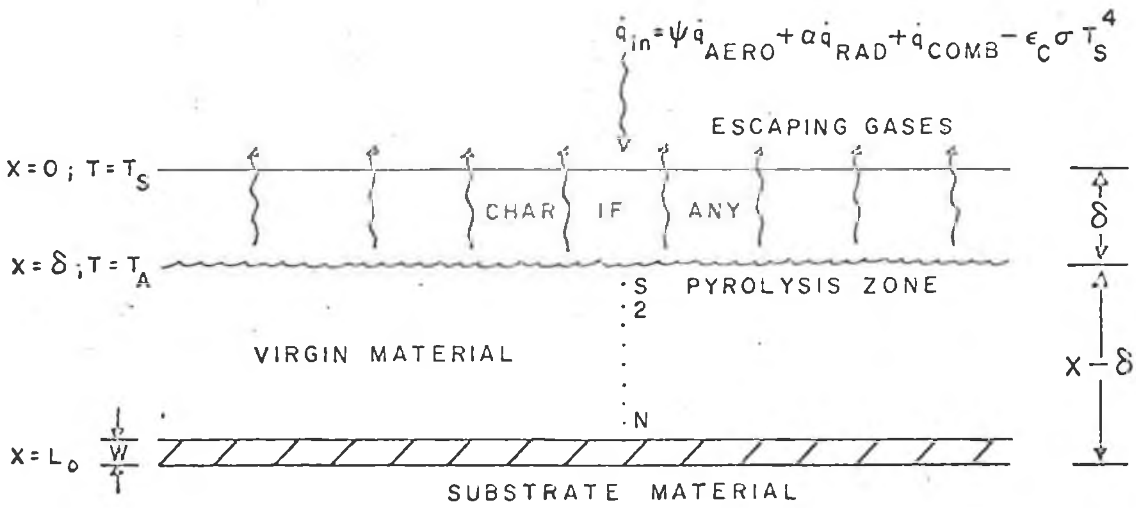

Figure 3b. Ablator During Ablation

heat conduction equation applies:

$$\rho_v C_v \frac{\partial T}{\partial t} = k_v \frac{\partial^2 T}{\partial x^2} \tag{2}$$

subject to the following boundary and initial conditions:

at $x = 0$; $\dot{q}_{aero} = k_v \left(\frac{\partial T}{\partial x} \right)_{x=0} + \epsilon_v \sigma T_s^4$

at $x = L_o$; $\rho_v C_v \frac{\partial T}{\partial t} = k_v \frac{\partial^2 T}{\partial x^2}$

at $t = 0$; $T = T_1$

Equation 2 can be approximated by a system of difference-ordinary differential equations. The difference-differential equations can be derived by a purely formalistic approach as demonstrated in Appendix II or by the method which follows, which in essence performs a heat balance on each node.

Let the region $0 \leq x \leq L_o$ be divided into N sections, each of width Δx, where $N \Delta x = L_o$. Let x_1 be the coordinate of the center of first cell and $T(x_1, t) = T_1$ be a representation of the average temperature over the width Δx of the first cell. This technique can be extended to the Nth cell.

A thermal balance for each cell will satisfy the following conditions:

Heat in = heat stored + heat out (3)

The heat balance for the first cell then takes the following form:

$$\dot{q}_{in} = \rho_s C_s V_s \frac{dT_s}{dt} + k_2 \frac{A(T_s - T_2)}{\Delta x} \tag{4}$$

Since the volume element $V_s = A_s \Delta x$ and the area is assumed equal to unity, the system of equation reduces to:

for first node: $\dot{q}_{in} = \rho_s C_s \Delta x \frac{dT_s}{dt} + \frac{k_2 (T_s - T_2)}{\Delta x}$

and for the subsequent nodes:

$$
\begin{aligned}
\frac{k_2(T_s - T_2)}{\Delta x} &= \rho_2\, C_2 \frac{dT_2}{dt} + \frac{k_3(T_2 - T_3)}{\Delta x} \\
\frac{k_3(T_2 - T_3)}{\Delta x} &= \rho_3\, C_3 \frac{dT_3}{dt} + \frac{k_4(T_3 - T_4)}{\Delta x} \\
&\vdots \\
\frac{k_{N-1}(T_{N-1} - T_N)}{\Delta x} &= \rho_N\, C_N \frac{dT_N}{dt} + \frac{k_N(T_N - T_W)}{\Delta x} \\
\frac{k_N(T_N - T_W)}{\Delta x} &= \rho_N\, C_N\, w \frac{dT_w}{dt}
\end{aligned}
\tag{5}
$$

Note that from the system of equations presented in Equation 5 the surface temperature T_s is not really the true surface temperature, but a temperature of the slab some finite distance below the surface. However, the spacing between nodes Δx does not need to be constant and a much smaller increment can be assumed for the first node. In this fashion, the true surface temperature can be approximated. By making the temperature of the center of the cell represent the temperature of the entire cell we invoke the concept of "thermally thin." This implies no temperature gradients within a given cell. Because of this, each node should be made small enough to retain the accuracy required to satisfy this assumption.

In the formulation of the last equation, in the system of equations presented in Equation 5, we have neglected the effect of the bonding agent or attachment mechanism between the ablator and the substrate material. This heat resistance can be taken into account, but has been neglected in this analysis. Essentially, we are saying that the bonding agent or the attachment offers no resistance to the flow of heat (i.e., infinite conductivity).

Various boundary conditions can be applied to the last node. The boundary condition applied here is that the substrate material acts as a heat sink. In the formulation of equations in Appendix II, the last node was assumed to be thermally insulated. This means that no flow of heat flows across the last node (i.e., temperature gradient, $\frac{\partial T}{\partial x} = 0$). Several other boundary conditions will be covered in a subsequent section.

If we define the thermal diffusivity, α, as $\alpha = \frac{k}{\rho c}$, then the system of equation presented by Equation 5 can be written as:

$$
\begin{aligned}
\dot{T}_s &= \frac{dT_s}{dt} = \frac{\alpha_s}{k_s \Delta x} \dot{q}_{in} + \frac{\alpha_2}{(\Delta x)^2} (T_s - T_2) \\
\dot{T}_2 &= \frac{dT_2}{dt} = \frac{\alpha_2}{(\Delta x)^2} (T_s - T_2) - \frac{\alpha_3}{(\Delta x)^2} (T_2 - T_3) \\
\dot{T}_3 &= \frac{dT_3}{dt} = \frac{\alpha_3}{(\Delta x)^2} (T_2 - T_3) - \frac{\alpha_4}{(\Delta x)^2} (T_3 - T_4) \\
&\vdots \\
\dot{T}_N &= \frac{dT_N}{dt} = \frac{\alpha_N}{(\Delta x)^2} (T_{N-1} - T_N) - \frac{\alpha_N}{(\Delta x)^2} (T_N - T_W) \\
\dot{T}_W &= \frac{dT_W}{dt} = \frac{k_W}{\rho_W C_W w \Delta x} (T_N - T_W)
\end{aligned}
\tag{6}
$$

Given an initial temperature distribution, T_i, this set of equations is solvable for T_s through T_W. This set of equations can be programmed and solved by finite difference by the MIMIC (Ref. 8) computer program which integrates Equation 6 with the given temperature distribution, T_i, as an initial value. The MIMIC computer program is discussed in Appendix III. Thus, the temperatures are obtained from the system of equation shown in Equation 7:

$$
\begin{aligned}
T_s &= T_i + \int_o^t \dot{T}_s \, dt \\
T_2 &= T_i + \int_o^t \dot{T}_2 \, dt \\
T_3 &= T_i + \int_o^t \dot{T}_3 \, dt \\
&\vdots \\
T_N &= T_i + \int_o^t \dot{T}_N \, dt \\
T_W &= T_i + \int_o^t \dot{T}_W \, dt
\end{aligned}
\qquad (7)
$$

The MIMIC computer program employs a fourth order variable step Runge-Kutta method to perform the required integration.

Since this is a numerical method of solving Equation 2, the heat input, $\dot{q}_{in}$, can be a function of time, and the thermophysical properties (i.e., k, ρ, or C_p) can be either a constant or a function of two thermodynamic variables - for example, temperature and pressure.

---

8. Sansom, F. J., Petersen, H. E., "MIMIC Programming Manual," SEG-TR-67-31, Wright-Patterson AFB, Ohio, Aeronautical Systems Division, July 1967.

We have shown a method whereby the one-dimension Fourier heat conduction equation is reduced to a system of ordinary differential equations and subsequently solved by the MIMIC computer program. The problem of multidimensional heat conduction consists of finding a solution to the general heat conduction equation:

$$\rho c \frac{\partial T}{\partial t} = \nabla^2 kT \tag{8}$$

Appendix II will illustrate that the aforementioned method, of solving a partial differential equation with non-linear boundary conditions, can be readily extended to two and three-dimension heat flow problems. The preceding problem has been solved in a cartesian coordinate system. The method can, however, be extended to encompass cylindrical and spherical coordinate systems.

2.2 Thermal Analysis During Ablation

In the initial phase of heating, the energy is transferred to the ablating body. The body behaves as a heat sink, and the surface temperature increases. This behavior is described by Equation 7. When the surface reaches the ablating temperature, T_a, the surface material begins to absorb heat by decomposition evolving gases and for a charring ablator a porous coke like residue is also formed. It is this phase of the ablator's behavior which is the current subject of our discussion. The interface between the porous char and the essentially virgin material moves into the surface at a rate which depends on the severity of the aerodynamic conditions, particularly heating.

The gases which are generated at the moving interface during this process diffuse through the porous char layer and into the boundary layer, and thus block some of the convective heat by the transpiration cooling effect. Transpiration cooling acts as a negative feedback in the ablative process. It will be shown that as the heat input increases the heat blocked by transpiration increases and thus reduces the amount of heat conducted into the material. Thus, transpiration effect is reduced as the rate of mass loss decreases. When the transpiration effect is reduced, the char surface temperature rises and heat is rejected by reradiation. Reradiation is high in charring ablators because of the high surface temperature that they can support and because of the high emissivity.

The char layer thickness also acts as an insulator. As the char layer thickens, the rate at which heat reaches the interface is reduced and the recession rate is reduced. Many authors (Ref. 9) believe that a steady state char thickness develops on an ablative material. By this it is meant that a fairly constant char layer is maintained (i.e., the rate of recession of the char is equal to the rate of recession of the virgin material interface). The analysis contained in the following pages of this section will hold for whenever the interface temperature equals or exceeds the ablation temperature.

In order to assess all the assumptions made in this analysis we will start with the general energy equation for one component in terms of temperature (Ref. 10).

---

9. Gruntfest, I., "The Outlook for Ablating Heat Protection Systems," AFOSR Conference on Aerodynamically Heated Structures, July 25-26, 1961, Arthur D. Little, Inc., Cambridge, Mass.
10. Bird, R. B., Stewart, W. E., Lightfoot, E. N., Transport Phenomena, John Wiley & Sons, Inc., New York, 1960.

$$\rho c \frac{DT}{Dt} = - \nabla \cdot \dot{q} + \left(\frac{\partial \ln 1/\rho}{\partial \ln T} \right)_p \frac{DP}{Dt} - \tau : \nabla V - (\overline{R}) + S_e \tag{9}$$

where $\frac{DT}{Dt}$ is the substantial derivative

$$\frac{DT}{Dt} \equiv \frac{\partial T}{\partial t} + V_x \frac{\partial T}{\partial x} + V_y \frac{\partial T}{\partial x} + V_z \frac{\partial T}{\partial y} \tag{10}$$

The following assumptions are made:

1. Assume one-dimensional flow (x-direction only).
2. Neglect viscous dissipation effects ($\tau : \nabla V = 0$).
3. Assume constant pressure ($\frac{DP}{Dt} = 0$).
4. Neglect sources ($S_e = 0$).
5. Neglect internal radiation ($\overline{R} = 0$).
6. Neglect density variation in pyrolysis zone.
7. Assume a constant ablation temperature, T_a; this temperature occurs in a plane at the char-virgin material interface.
8. The products of decomposition are a char layer and a gas.
9. The rate of formation of the gas, $\dot{m}_g$, is a constant fraction of the rate of decomposition of the virgin material, $\dot{m}_p$, such that $\Gamma = \dot{m}_g/\dot{m}_p$.
10. The temperature of the escaping gas is in equilibrium with the temperature of the char.

Purely one dimensional heat transfer problems probably do not exist. This assumption is frequently made, however, for the sake of simplicity. If the gradients in one direction are much greater than those in the other directions, the system can be adequately approximated by the one-dimensional case and design information may be obtained. The work done on the gas by the pressure forces and the viscous dissipation effects, assumptions 2 and 3, are normally neglected in analyses of this type, unless boundary layer interactions are being studied. No heat sources are assumed present and the material will be treated as being opaque to radiation.

The pyrolysis of ablative plastics is very complex. The products of decomposition are a porous char, and various gases. Liquid also forms when inorganic reinforcement agents are added. The thermal degradation of the original material is given by the Arrhenius relation (Ref. 11):

$$\dot{m}_p\ (x,t) = \frac{\partial \rho}{\partial t} = - B\ e^{-E/RT}\ \rho_p\ \left(\frac{\rho - \rho_c}{\rho_p}\right) \qquad (11)$$

where ρ is the instantaneous bulk density of the material. The collision frequency factor, B, activation energy, E, and the order of the reaction, n, are determined from thermogravimetric analysis (TGA) and are often of inconsistent quality. TGA of ablative materials, shown in Figure 4, are frequently used to determine the nature of a material's decomposition process. The material is heated in an inert atmosphere with a known heating rate, and thus provide a dynamic weight loss versus temperature curve. From curves similar to those shown in Figure 4, the following can be obtained: the temperature at which initial decomposition takes place, the temperature range over which the major decomposition of the resin occurs, the weight loss corresponding to each decomposition step, the weight of char remaining after decomposition, and from the relative displacement on the temperature axis

---

11. Mathieu, R. D., "Mechanical Spallation of Charring Ablators in Hyperthermal Environments," AIAA Journal, Sept. 1964.

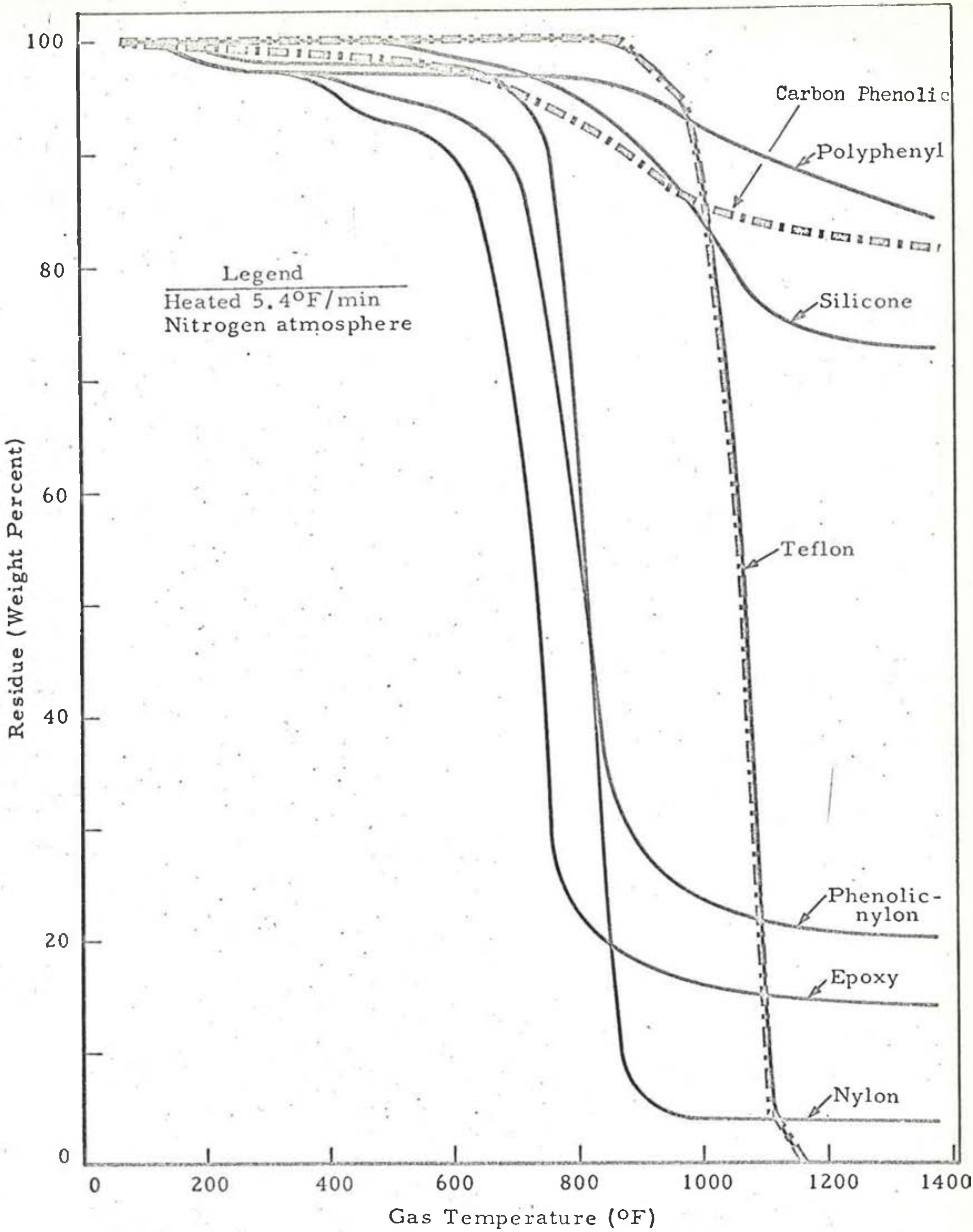

Figure 4. Thermogravimetric Analysis (TGA) of Several Ablative Plastics.

of the weight-loss curve the Arrhenius constants for the decomposition reactions are obtained. Curves similar to Figure 4 are of such a nature that many curve-fits of varying reaction order, n, can be used. Because of this, it is doubtful that using TGA data and Equation 11 would increase the accuracy of an ablative analysis. However, this technique is in wide use (Ref. 12) even though the Arrhenius constants reported in the current literature have a great deal of scatter.

Pyrolysis experiments reported in (Ref. 13) indicate that the thermal degradation of polymers occurs over a narrow temperature range. This is also borne out by Figure 4. This leads to a justification of assumptions 6 and 7. The density changes reported by (Ref. 14) are of the order of fifteen per cent in the reaction or pyrolysis zone.

Assumptions 8 and 9 are plausible, but the gasification ratio, Γ, may be a difficult parameter to obtain for some charring materials. For subliming materials, such as Teflon, the value of the gasification ratio is unity.

As the gases pass through the char layer, a convective heat transfer exists between the gas and the char layer. Analyses have been postulated where a constant gas temperature has been assumed. Another assumption (Ref. 15) postulates that the temperature of the char and

---

12. Kauzlarich, J. J., "Ablation of Reinforced Plastic for Heat Protection," Journal of Applied Mechanics, Mar. 1965.
13. Madorsky, S. L., Straus, I., "Thermal Degradation of Polymers at High Temperatures," NBS Journal of Research, Vol. 63A, 1959.
14. Beecher, N., Rosensweig, "Ablation Mechanisms in Plastics with Inorganic Reinforcement," ARS Journal, April 1961.
15. Barriault, R. J., Yos, J., "Analysis of the Ablation of Plastic Heat Shields that Form a Charred Surface Layer," ARS Journal, Sept. 1960.

the gas is the same and is a constant. A detailed analysis would probably show that neither assumption is true. The case where the char and gas temperature are in thermal equilibrium has been assumed in this analysis, since it was felt that this case may be closer to the real physical process since some of the gases are evolved from the char itself.

Under the foregoing assumptions and upon substitution of the Fourier heat conduction equation into Equation 9 the following equation results:

$$\rho c \frac{\partial T}{\partial t} = k \frac{\partial^2 T}{\partial x^2} + \rho V_x C \frac{\partial T}{\partial x} \tag{12}$$

Thus, when the surface temperature, T_s, reaches the ablation temperature, T_a, ablation starts and a char is formed. Figure 3-b shows this case schematically. It is again assumed that all heat flow is normal to the surface, and that the transpiring gases through the char are at the same temperature as the char.

The energy balance in the char layer becomes, at $0 \leq x \leq \delta$:

$$\rho c\, C_c \frac{\partial T}{\partial t} = k_c \frac{\partial^2 T}{\partial x^2} + \dot{m}_g C_g \frac{\partial T}{\partial x} \tag{13}$$

(Heat Stored) = (Heat Conducted) + (Heat absorbed by transpiring gases)

while in the virgin uncharred material the heat conduction equation, Equation 2, applies. Thus:

$$\text{at } \delta \leq x \leq L_o; \quad \rho_v C_v \frac{\partial T}{\partial t} = k_v \frac{\partial^2 T}{\partial x^2} \tag{14}$$

The following boundary conditions apply:

$$\text{at } x = 0; \quad \dot{q}_{in} = - k_c \left(\frac{\partial T}{\partial x}\right)_{x=0} \tag{a}$$

$$\text{at } x = \delta; \quad -k_c \left(\frac{\partial T}{\partial x} \right)_{x=\delta} = \dot{m}_p H_p - k_v \left(\frac{\partial T}{\partial x} \right)_{x=\delta} \qquad \text{(b)}$$

$$T = T_a \quad \text{(a constant)} \qquad \text{(c)}$$

$$\text{at } x = L_o; \quad -k_v \left(\frac{\partial T}{\partial x} \right)_{x=L_o} = -k_w \left(\frac{\partial T}{\partial x} \right)_{x=L_o} \qquad \text{(d)}$$

The initial temperature distribution is obtained from the solution of Equation 7. The thickness of material to which Equations 13 and 14 apply varies with time in a manner which is determined by the boundary conditions.

The two boundary conditions at the char-virgin material interface state that the heat conducted to the pyrolysis interface must be either absorbed by pyrolysis reactions or conducted into the virgin material and that the temperature of the char and virgin material at the pyrolysis interface must be equal.

When the material begins to ablate the heat input is given by:

$$\dot{q}_{in} = \psi \dot{q}_{aero} + \alpha \dot{q}_{rad} + \dot{q}_{comb} - \epsilon_c \sigma T_s^4 \qquad (15)$$

where ψ is a number less than one and is the ratio of convective heat flux with mass injection to convective heat flux without mass injection. This parameter ψ introduces the transpiration effect due to the escaping gases. It blocks convective heat, but not radiant heat. This blockage effect will be discussed in the next section.

Thus far, we have one boundary condition at the heated surface - the energy balance. Another boundary condition is required at the heated surface. Either the rate of removal of material at the surface or the temperature of the surface must be known.

The discussion that follows will describe a method, by a quasi-steady state analysis, whereby an expression will be found for the mass loss rate. If the mass loss rate is known, the recession rate can be determined. However, if the recession rate is known apriori, by means of test, oxidation, or some other mechanism, then this can be used as an input to the model in lieu of the derived expression for mass loss rate. Equations 13 and 14 and their associated boundary conditions will be reduced to a set of ordinary differential equations and solved by the MIMIC computer program provided that an expression for the mass loss rate of the gas, $\dot{m}_g$, is found.

In order to obtain the mass loss rate, $\dot{m}_g$, we will assume that quasi-steady state conditions exist. The heating rate, $\dot{q}_{in}$, will still be a function of time, but $\frac{\partial T}{\partial t}$ will be set to zero in Equation 13. Since the heat conducted into the virgin plastic is known from the solution of Equation 7, it can be eliminated from Boundary Condition b by defining the net heat input as:

$$\dot{q}'_{in} = \psi \dot{q}_{aero} + \alpha \dot{q}_{rad} + \dot{q}_{comb} - \dot{q}_{cond} - \epsilon_c \sigma T_s^4 \tag{16}$$

With the time dependence removed, Equation 13 becomes:

$$k_c \frac{d^2T}{dx^2} + \dot{m}_g C_g \frac{dT}{dx} = 0 \tag{17}$$

Upon integrating twice the following results:

$$\frac{dT}{dx} = C_4 \frac{\dot{m}_g C_g}{k_c} e^{-(\dot{m}_g C_g x/k_c)} \tag{18}$$

and

$$T = C_3 - C_4 e^{-(\dot{m}_g C_g x/k_c)} \tag{19}$$

where:

$$C_3 = \frac{e^{-(\dot{m}_g C_g C_2/k_c)}}{\dot{m}_g C_g} - \frac{1}{\dot{m}_g C_g} e^{-\ln C_1} \tag{20}$$

$$C_4 = - \frac{1}{\dot{m}_g \; C_g} \tag{21}$$

C_1 and C_2 are the original integration constants. Utilizing Boundary Conditions a and c on Equations 7 and 8 we obtain:

$$C_3 = T_a + C_4 \; e^{-(\dot{m}_g \; C_g \; \delta_c/k_c)}$$

and

$$C_4 = \frac{-\dot{q}'_{in}}{\dot{m}_g \; C_g}$$

Upon the substitution of these two constants into Equation 19 we obtain the temperature distribution:

$$T = T_a + \frac{\dot{q}'_{in}}{\dot{m}_g \; C_g} \left(e^{-[x]} - e^{-[\delta_c]}\right) \tag{24}$$

where:

$$e^{-[x]} = e^{-\dot{m}_g \; C_g \; x/k_c}$$

and

$$e^{-[\delta_c]} = e^{-\dot{m}_g \; C_g \; \delta_c/k_c}$$

From Equation 24 a quasi-steady state expression for the surface temperature, T_s, can be obtained. Thus,

at $x = 0$; $T = T_s$

therefore:

$$T_s = T_a + \frac{\dot{q}'_{in}}{\dot{m}_g \; C_g} \left(1 - e^{-[\delta_c]}\right) \tag{25}$$

In the model formulation the surface temperature will not be obtained from this expression. It will be obtained instead from an energy balance at the surface. However, this expression does show that the surface temperature is a function of the mass loss rate of the gas, $\dot{m}_g$.

If we substitute C_4 into Equation 18, the following relation results:

$$- k_c \frac{dT}{dx} = \dot{q}'_{in} e^{-[x]} \tag{26}$$

Then, using Boundary Condition b and remembering that we have accounted for the heat conducted into the virgin material by placing it into the $\dot{q}'_{in}$ term, we obtain:

$$- k_c \frac{dT}{dx} = \dot{m}_p H_p \tag{27}$$

At $x = \delta$ Equations 26 and 27 are equal and utilizing the gasification ratio, $\Gamma = \dot{m}_g/\dot{m}_p$, we can obtain the quasi-steady state mass loss rate of the gas. This results in:

$$\dot{m}_g = \frac{\Gamma}{H_p} \dot{q}'_{in} e^{-[\delta_c]} \tag{28}$$

This expression can be used to rewrite the surface temperature given by Equation 25. The substitution yields:

$$T_s = T_a + \frac{1}{C_g} [\frac{H_p}{\Gamma} (e^{[-\delta_c]} - 1)] \tag{29}$$

We will make use of Equation 28 in the formulation of our model. Note that Equation 28 is an implicit function. The equation can be linearized, and solved explicitly for $\dot{m}_g$, by taking the first two terms of the Maclaurin's Expansion Theorem. This yields:

$$\dot{m}_g = \frac{\Gamma}{H_p} \dot{q}'_{in} (1 - \dot{m}_g C_g \delta_c/k_c) \tag{30}$$

Equation 30 will only be valid for small mass loss rate. However, this simplifying assumption, of Equation 28, is not necessary since the MIMIC computer program is equipped to iteratively solve implicit functions.

From Equation 28 and the definition of the gasification ratio we can predict the following: The virgin material mass loss rate, $\dot{m}_p$, the virgin material recession rate, $\dot{\delta}$, and the char production rate, $\dot{\delta}_c$.

The virgin material recession rate is:

$$\dot{\delta} = \frac{\dot{m}_g}{\Gamma \rho_v} \tag{31a}$$

while the amount ablated is:

$$\delta = \frac{1}{\Gamma \rho_v} \int_0^t \dot{m}_g \, dt \tag{31b}$$

Since it has been assumed that the only products of pyrolysis are a gas and a char, the following is true:

$$\dot{m}_p = \dot{m}_g + \dot{m}_c \tag{32}$$

Using the definition of gasification ratio the mass rate of char formation results:

$$\dot{m}_c = \dot{m}_g \left(\frac{1 - \Gamma}{\Gamma} \right) \tag{33}$$

Then, since:

$$\rho_c \, dx = \dot{m}_c \, dt \tag{34}$$

integrating Equation 34 yields the amount of char formed:

$$\delta_c = \frac{1}{\rho_c} \int_0^t \dot{m}_c \, dt \tag{35}$$

Combining Equations 33 and 35 results in:

$$\delta_c = \frac{1}{\rho_c} \left(\frac{1 - \Gamma}{\Gamma} \right) \int_0^t \dot{m}_g \, dt \tag{36}$$

Equation 36 will predict a char layer buildup unless some char removing mechanisms are incorporated into the model. The simplest expedient is to limit the char layer thickness to some finite value. Many authors (Ref. 12) state that the char layer thickness is quite small when subjected to hyperthermal environment, and suggest that the advantages of a stable char layer be not utilized in designing thermal protection system for the sake of conservatism. The relative importance of the mechanisms involved in char removal from specific materials is not well established (Ref. 16), and is the subject of much research and discussion. Char removal may be caused by many factors. These include oxidation of char surface, erosion by surface shear stresses, spallation due to internal pressure buildup, thermal stresses and even sublimation of the char at high temperatures. Char removal mechanism will be discussed in a subsequent section.

The final item that must be obtained for our model is the temperature distribution within the char. If Equation 19 is subjected to the following char layer boundary condition:

at $x = 0$; $T = T_s$

at $x = \delta$; $T = T_a$

the following result:

$$C_3 = T_s + C_4 \tag{37}$$

and

$$C_4 = \frac{C_3 - T_a}{e^{-[\delta_c]}} \tag{38}$$

---

12. Ibid.
16. Schnider, P. J., Dolton, T. A., Reed, G. W., "Char Layer Structural Response in High Performance Ballistic Re-entry," AIAA Paper No. 66-424, AIAA Fourth Aerospace Science Meeting, Los Angeles, Cal., June 27-29, 1966.

Substituting Equations 37 and 38 yield after some algebraic manipulation that the temperature distribution in the char layer is given by:

$$T_x = \frac{T_a - T_s\, e^{-[\delta_c]} + (T_s - T_a)\, e^{-[x]}}{1 - e^{-[\delta_c]}} \tag{39}$$

The system of equation given by Equations 13 and 14 and their associated boundary conditions can be reduced to a system of ordinary differential equations by the methods outlined in the early portion of this section and in Appendix II. However, due to the fact that the boundary moves at a velocity $\dot{\delta}$ it is found expedient to use a transformation suggested by (Ref. 15). This technique will be illustrated by using Equation 14 which has the form:

$$\frac{\partial T}{\partial t} = \alpha \frac{\partial^2 T}{\partial x^2}$$

The transformation into a moving frame coordinate, x', is:

$$x' = x - \delta \tag{40}$$

where:

$$\delta = \int_0^t \dot{\delta}\, dt \tag{41}$$

Here δ and $\dot{\delta}$ are functions of time. The temperatures are of course the same in the two coordinate systems. However, the time derivatives of temperature are different. The relation is found by taking the partial derivative of Equation 41 with respect to time. This results in:

$$\frac{\partial T(x)}{\partial t} = \frac{\partial T'(x')}{\partial t} - \dot{\delta}\, \frac{\partial T(x)}{\partial x} \tag{42}$$

---

15. Ibid.

Using Equation 42 the differential equation for the temperature distribution, Equation 14, in a moving frame of reference becomes:

$$\frac{\partial T'}{\partial t} = \alpha \frac{\partial^2 T'}{\partial x'^2} + \dot{\delta} \frac{\partial T'}{\partial x'} \tag{43}$$

Using the method outlined in Appendix II the system of differential equation which replaces Equation 43 becomes:

$$\begin{aligned}
\frac{dT_1}{dt} &= \frac{\alpha}{(\bar{\Delta x})^2}(T_2 - T_1) - \frac{\alpha}{(\bar{\Delta x})^2}(T_1 - T_o) + \frac{\dot{\delta}}{\bar{\Delta x}}(T_1 - T_o) \\
\frac{dT_2}{dt} &= \frac{\alpha}{(\bar{\Delta x})^2}(T_3 - T_2) - \frac{\alpha}{(\bar{\Delta x})^2}(T_2 - T_1) + \frac{\dot{\delta}}{\bar{\Delta x}}(T_2 - T_1) \\
&\vdots \\
\frac{dT_n}{dt} &= \frac{\alpha}{(\bar{\Delta x})^2}(T_{n+1} - T_n) - \frac{\alpha}{(\bar{\Delta x})^2}(T_n - T_{n-1}) + \frac{\dot{\delta}}{\bar{\Delta x}}(T_n - T_{n-1})
\end{aligned} \tag{44}$$

where

$$\bar{\Delta x} = \frac{L_o - \delta}{N}$$

In Equation 44 the primes have been omitted for simplicity, but it is understood that we are using the transformed coordinates. The boundary conditions associated with Equation 14 are also transformed by means of Equations 40 and 41. The transformed boundary conditions are then used to eliminate the last two terms in the first and final equations of Equation 14.

Note that both sets of equations (i.e., Equations 7 and 44) need not be programmed in the model. One needs to use only the equations for the period after ablation starts. This is evident from Equation 44. We see that Equation 44 reduces to Equation 7 for the no ablation case.

This is true since for the no ablation case both $\dot{\delta}$ and δ will be zero. The boundary conditions are likewise satisfied.

This analysis has, for the sake of completeness, assumed a char to be formed at the surface. The analysis works as well for a subliming material, such as Teflon, if we assume a zero char thickness and a gasification ratio of unity.

In a following section another method of handling the ablation or moving boundary problem will be presented. The material in question will be the behavior of ice. Ice melts at a fixed temperature with the absorption of a given amount of energy - heat of fusion. At that time a new dimensionless transformation in the moving coordinate frame of reference will be introduced.

It has been proposed in this analysis to use a quasi-steady state analysis. By this we intend to solve a transient problem by introducing a mass loss rate, $\dot{m}_g$, which has been essentially obtained by steady state considerations. This assumption has some merit as will be subsequently shown. The time to reach steady state conditions, t_{ss}, has been derived by (Ref. 17) and is given by:

$$t_{ss} = \alpha \left(\frac{\rho Q^*}{\dot{q}_{in}} \right)^2 = \alpha \left(\frac{1}{V_w} \right)^2 \tag{44a}$$

Here V_w is analogous to $\dot{\delta}$ and is the steady state linear ablation rate of the material. The logic behind the derivation of Equation 44a is shown in Appendix I. This equation has been shown to be true, by experiments, for materials which have a low thermal conductivity.

---

17. Brogan, T., "The Electric Arc Wind Tunnel - A Tool for Atmospheric Re-entry Research," ARS Journal, Sept. 1959.

Many ablative materials fall into this category. Figure 5 shows a plot of Equation 44a. Since ablators are normally used to protect against high heating rates, Figure 5 shows that for incident heating rates of 1000 BTU/ft^2 sec Teflon will reach steady state ablation within a fraction of a second.

Boundary Conditions

The proposed model can be used to investigate numerous heat transfer problems. The problems range from the heat conduction problem, which does not have a moving boundary, to a charring ablator which has two moving boundaries. To provide maximum flexibility the model is able to accept a variety of boundary conditions.

The surface boundary condition may be any of the following with or without a moving boundary:

a. Various heat fluxes which are constants or a function of time.

b. Surface temperature which is a constant or a function of time.

The following surface recession mechanisms can be used:

a. Surface recession as a function of temperature, time, or a constant can be used.

b. By the provision of the double table lookups inherent in the MIMIC computer program, the surface recession rate can be a function of any two variables - for example, temperature and pressure.

c. Ablation at a given temperature which may be a function of ablation rate (i.e., sublimation rate given by Equation 28).

d. Ablation as a result of a chemical process such as oxidation.

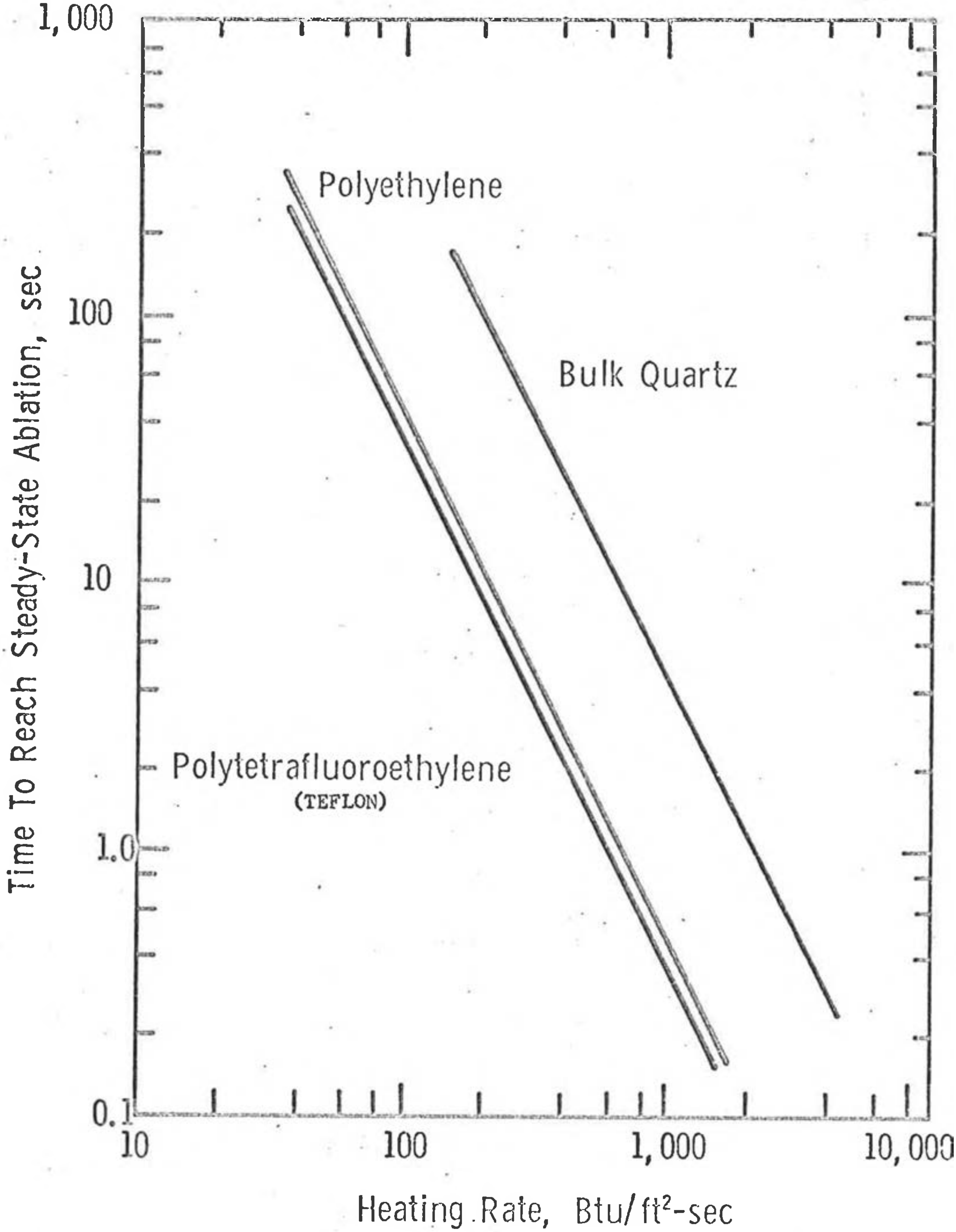

Figure 5. Time to Reach Steady State Ablation.

e. Removal of char at a rate which is determined by spalling, aerodynamic shear or thermal stresses.

Some of the equations which describe char removal mechanisms, such as spalling, oxidations and sublimation, will be covered in a subsequent chapter on char removal mechanisms. The aforementioned boundary conditions can be used as table lookups or computed dynamically. For example, the equations of motion can be programmed and the resulting trajectory can be used to derive the aerodynamic and radiant heating by means of equations. Subsequently, the surface temperature can be found by means of an energy balance. This method was used in the formulation of the first equation of the set of equations presented in Equation 6.

The heat loss to the interior environment for the last node, at the substrate structure, can be specified by several methods:

a. The last node can act as a heat sink as was assumed in the formulation of Equation 6.

b. The last node can act as an adiabatic wall as was formulated in Appendix II.

c. The heat conducted into the substrate can be subsequently convected into an interior environment.

$$-k \left(\frac{\partial T}{\partial x} \right)_{x=L_o} = \bar{h}_c A (T_N - T_{int})$$

d. The heat conducted into the substrate can be subsequently radiated into an interior environment.

$$-k \left(\frac{\partial T}{\partial x} \right)_{x=L_o} = \sigma \epsilon A (T_N^4 - T_{int}^4)$$

e. The heat conducted into the substrate can be subsequently carried away by a piped coolant (cooled structure).

$$-k \left(\frac{\partial T}{\partial x} \right)_{x=L_o} = C_{col} \dot{m}_{col} (T_n - T_{int})$$

where:

C_{col} is the heat capacity of the coolant

$\dot{m}_{col}$ is the rate of coolant consumption

f. Any combination of c, d, and e.

III. HEAT TRANSFER MECHANISMS

The heating rates to a re-entry vehicle are supplied primarily by aerodynamic heating, aerodynamic radiative heating, and combustion - both gas-phase and surface combustion. In ablation this heat input is not merely an exchange of mass for heat but rather involves several modes of heat dissipation mechanisms. These include transpiration, re-radiation, phase changes, and heat storage and insulation by both the char and virgin materials. It is the purpose of this section to discuss the various heat input and heat dissipation mechanisms.

There are many techniques for predicting convective heating rates; these vary from experimental to theoretical and predictions by correlation formulas. Several of these methods were investigated in (Ref. 18). Of the six stagnation point methods investigated, Lees' Approximate Method and the method due to Detra, Kemp, and Riddell were not only the simplest but also closest to the average of all six methods.

3.1 Convective Aerodynamic Heating

During re-entry a vehicle compresses the atmosphere in front of it by means of a bow shock wave causing a drastic increase in temperature and pressure. As the air flows over the surface of the high speed vehicle, fluid friction sets up shearing stress in the boundary layer creating additional heat. Forced convection is the predominant mode of aerodynamic heating for most of the flight regimes of current interest.

18. Hankey, W. L., Neumann, R. D., Flinn, E. H., "Design Procedures for Computing Aerodynamic Heating at Hypersonic Speeds," WADC-TR-59-610, Flight Dynamics Laboratory, Wright-Patterson AFB, Ohio, June 1960.

Lees' Approximate Method (Ref. 19) results in the stagnation point equation for laminar flow:

$$\left(\dot{q}_s\right)_L = 21.9 \left(\frac{\rho_\infty}{R_n}\right)^{0.5} \left(\frac{V_\infty}{1000}\right)^3 \left(\frac{h_s - h_w}{h_s}\right) \tag{45}$$

while the method of Detra, Kemp, and Riddell (Ref. 20) yields for laminar flow:

$$\left(\dot{q}_s\right)_L = \left(\frac{17600}{(R_n)^{0.5}}\right)\left(\frac{\rho_\infty}{\rho_{sL}}\right)^{0.5}\left(\frac{V_\infty}{V_c}\right)^{3.15}\left(\frac{h_s - h_w}{h_s - 3.2 \times 10^6}\right) \tag{46}$$

where:

R_n is the radius of the nose cap in feet

$h_s \approx \frac{1}{2} V_\infty^{\,2}$

$h_w = C_p\, T_w$

V_c = Circular orbital velocity = 26000 ft/sec.

The last term in Equations 45 and 46 can be usually neglected since the ratio of the enthalpy of the flow at the wall, h_w, to the enthalpy of the flow at the edge of the boundary layer, h_s, is small.

The stagnation point turbulent heating is given by:

$$\left(\dot{q}_s\right)_T = \left(\frac{5}{(R_n)^{0.2}}\right)\left(\frac{\rho_\infty}{\rho_{sL}}\right)^{0.8}\left(\frac{V_\infty}{1000}\right)^3 \tag{47}$$

All the heating on a re-entry vehicle can be given as some ratio of the stagnation point heating (Ref. 18). The following relations can

---

19. Lees, L., "Recovery Dynamics - Heat Transfer at Hypersonic Speed in a Planetary Atmosphere," Space Technology, ed. by H. Seifert, John Wiley and Sons Inc., New York.
20. Detra, R. W., Kemp, N. H., Riddell, F. R., "Addendum to Heat Transfer to Satellite Vehicles Re-entering the Atmosphere," Jet Propulsion, Dec. 1957.
18. Ibid.

be used to estimate the aerodynamic heating to a re-entry vehicle:

a. For a flat plate at an angle of attack, $\bar{\alpha}$:

$$\left(\frac{\dot{q}_{FP}}{\dot{q}_s}\right)_L = 0.0292 \left(\frac{R_n}{x}\right)^{0.5} (\bar{\alpha})^{0.667} \qquad \text{(laminar)}$$

$$\left(\frac{\dot{q}_{FP}}{\dot{q}_s}\right)_T = 0.0666 \left(\frac{R_n}{x}\right)^{0.2} \frac{\bar{\alpha}}{\left(1 + \frac{11}{3}\frac{h_w}{h_s}\right)} \qquad \text{(turbulent)}$$

b. For a wedge the heating equations are identical to those of a flat plate at an angle of attack equal to the wedge angle.

c. For a cone:

$$(\dot{q}_c)_L = (3)^{0.5} (\dot{q}_{FP})_L \qquad \text{(laminar)}$$

$$(\dot{q}_c)_T = (2)^{0.2} (\dot{q}_{FP})_T \qquad \text{(turbulent)}$$

d. Leading edge or fin:

$$\dot{q}_{LE,F} = \dot{q}_s \left(\frac{R_N}{2R_{LE}}\right)^{0.5} \cos \Lambda_e$$

where $\Lambda_e = \sin^{-1} (\sin \Lambda \ \cos \bar{\alpha})$ for leading edge

$\Lambda_e = \Lambda_F + \bar{\alpha}$ for fin

All the aforementioned equations, which were obtained from (Ref. 18) can be programmed, and the heating equation of interest can be selected to determine the amount of material required to protect a given location on a vehicle. If the actual trajectory equations are

---

18. Ibid.

programmed, the model can be made to switch the heating equation from laminar to turbulent when a given Reynolds number, N_{R_e}, is exceeded (i.e., when $N_{R_e} = 10^6$).

3.2 Aerodynamic Radiation Heating

A shock layer is formed at the stagnation region of blunt nosed vehicles moving at hypersonic speeds. This layer of gas is contained between the detached shock wave and the surface of the nose cone in the neighborhood of the stagnation region. Heat flux to a nose cone of a re-entry vehicle is transferred by convection from the hot gases and also by hot gas radiation from behind the shock wave. The latter form of heat transfer is also known as gas cap radiation. In some instances, the black body radiative heating from a shock layer exceeds convective heating from the boundary layer.

During re-entry the temperature of the gas behind the shock in the stagnation region may reach temperatures as high as $10{,}000^\circ$ R (Ref. 18). The black body radiation from such a source is of the order of 5000 BTU/ft^2 sec. However, the emissivity of the gas at high altitude is only of the order of 10^{-4} so that gas radiative heating is not excessive for many re-entry problems of interest.

Two semi-empirical radiation heat flux correlation formulas are in current use. One is due to Lees (Ref. 19):

$$\dot{q}_{rad} = 7.5\ R_n \left(\frac{\rho_\infty}{\rho_{SL}}\right)^{1.5} \left(\frac{V_\infty}{10000}\right)^{12.5} \tag{48}$$

---

18. Ibid.
19. Ibid.

The other is due to Detra and Hidalgo (Ref. 21):

$$\dot{q}_{rad} = 100\, R_n \left(\frac{\rho_\infty}{\rho_{SL}}\right)^{1.6} \left(\frac{V_\infty}{10000}\right)^{8.5} \tag{49}$$

The latter formula is more recent and was used in this analysis.

The hot gas radiation heat is only a major problem at the stagnation point. Since the distance from the shock wave increases toward the rear of the body, the effect of gas cap radiation diminishes. The actual radiation heating which reaches the body is given by:

$$\dot{q}_{rad\ in} = \alpha\, \dot{q}_{rad} \tag{50}$$

where α is the absorptivity of the material.

Equations 46 and 49 show that to reduce convective heating a blunt body is required, while to reduce radiant heating a sharp body is required. The solution as to what shape body is to be used requires an analysis based on the particular trajectory. Since the velocity ratio is raised to a rather high power in the radiation equation, this type of heating may be greater than convective aerodynamic heating for supercircular re-entry. Radiation heating can become significant when flight velocities approach orbital speed and higher. This problem may be especially acute since the transpiration effect inherent in ablators is able to block convective heating but not radiant heat. Work is currently in progress (Ref. 22) to develop

---

21. Detra, R. W., Hidalgo, H., "Generalized Heat Transfer Formulae and Graphs," AVCO Research Report 72, AVCO Research Laboratories, Everett, Mass., Mar. 1960.
22. Winkler, H. B., "Some Problems Associated with Re-entry After Planetary Exploration" Presented at the Joint ARS/IRE Meeting on Electronic Data Processing and Space Technology, April 12-13, 1961, Cincinnati, Ohio.

ablators whose products of ablation are opaque to radiation form the shock wave and thus absorb the radiant energy. This problem must be solved before re-entry from other planets becomes feasible.

Several recent papers by Hoshizaki (Ref. 23) suggest that the ablative gases which are injected into the region between the shock wave and the boundary layer may absorb some radiant heat. This topic is at the present of considerable interest and is only beginning to be explored. For this reason the self-absorption coefficients of the ablative species have been neglected.

3.3 Combustion Heating

Combustion of surface materials during ablation liberates heat and increases the surface heating rate. Also, oxidation of ablative species in the hot boundary layer increases the enthalpy of the environment and may increase heat to an ablating surface. Thus, combustion heating comes from two sources: the heterogeneous chemical reactions which occur at the surface, known as surface combustion, and the homogeneous chemical reactions which occur in the boundary layer, known as gas phase combustion. As a result of the increased heating due to combustion, the effect of these exothermic reactions is to produce an increase in the mass rate of ablation and a reduction in the material thermal efficiency. The fact that both types of combustion exist was shown experimentally by (Ref. 24). Further, the authors show that

---

23. Hoshizaki, H., Wilson, K. H., "Convective and Radiative Heat Transfer during Superorbital Entry," AIAA Journal, Jan. 1967.
24. Vojvodich, N. S., Pope, R. B., "An Investigation of the Effect of Gas Composition on the Ablation Behavior of a Charring Material," AIAA Conference on Physics of Entry into Planetary Atmospheres, Aug. 26-28, 1963, Cambridge, Mass. Also AIAA Journal, Mar. 1964.

surface reaction heating accounts for about one-third of the total combustion heating. The remaindor is attributed to gas-phase reaction heating.

a. Surface Combustion Heating

The effect of chemical reactions upon the behavior of a pure material, such as graphite, has been studied extensively. Scala (Ref. 25) treats the problem of graphite surfaces during atmospheric re-entry. Two regimes of oxidation are defined. One of those regimes is the rate controlled regime where the oxygen is supplied at a greater rate than it can be consumed, and thus the chemical reaction rate controls the process. For total pressures between zero and one atmospheres, this regime lasts until a surface temperature of 2000° R is reached. The diffusion controlled oxidation regime, which predominates from 2000° R to 4500° R, is defined as the regime where the oxygen can be consumed at a greater rate than the rate at which it is supplied to the surface and thus the oxygen diffusion through the boundary layer controls the process. Since the surface temperature on the ablators will be above 2000° R, the diffusion controlled regime will be considered to predominate.

The oxidation rate in the diffusion controlled regime is given by Scala (Ref. 25) as:

$$\dot{m}_d = 6.35 \times 10^{-3} \left(\frac{P_e}{R_n} \right)^{0.5} \qquad (51)$$

where $\dot{m}_d$ is the rate of weight loss of graphite in lb/ft^2 sec and $P_e \approx \rho_\infty V_\infty^2$ is the stagnation pressure in atmospheres.

25. Scala, S. M., "The Hypersonic Ablation of Graphite," Developments in Heat Transfer, ed. by W. M. Rohsenow, The M.I.T. Press, Cambridge, Mass.

Scala's theory assumes that the gases involved are principally carbon monoxide and carbon dioxide. At high temperatures the following reaction is likely to be predominant for charring ablators:

$$C + \tfrac{1}{2} O_2 \longrightarrow CO + 3960 \;\; \text{BTU/lb C} \tag{52}$$

The ratio of combustive heating to aerodynamic heating for an ICBM trajectory, which will be discussed in a later section, is shown for a nose cone of one foot radius in Table IIa. The values obtained by Scala's theory are approximately double the values obtained experimentally by Vojvodich and Pope in (Ref. 24). The latter authors suggest that a possible explanation lies in the fact that not only are the gases considered by Scala present, but many others as well. Scala's theory assumes that the gases injected into the boundary layer are principally CO and CO_2, which result from chemical reactions between the surface of the graphite and the hypersonic stream. However, for a charring material, light weight gases are produced by pyrolysis beneath the surface. These gases, some of which are chemically active (i.e., CH_4, C_2H_2, H and H_2) are subsequently diffused through the char layer and injected into the boundary layer where they react with the oxygen diffusing toward the surface. Thus, according to (Ref. 24), the unreacted oxygen at the surface which is available for reaction with char is less than that which would be available if the surface were nonporous graphite. From the foregoing and from Table IIa, the heating due to surface combustion was modeled as:

$$\dot{q}_{comb} = 0.5 \;\; (\psi \, \dot{q}_{aero}) \tag{53}$$

---

24. Ibid.

TABLE II. EFFECT OF COMBUSTION HEATING ON AN ICBM*

a. Surface Combustion Heating (Equation 51)

Time sec	P_e atmo	$\dot{m}_D$ lb/ft^2 sec	$\dot{q}$ aero BTU/ft^2 sec	$\dot{q}$ comb BTU/ft^2 sec	$\dot{q}$ comb/$\dot{q}$ aero
10	.067	.0016	140	6.5	.046
20	2.21	.0095	800	37	.047
30	38.1	.0392	2030	155	.076

b. Gas Phase Combustion Heating (Equation 55)

Time sec	$h_e - h_s$ BTU/lb	$\dot{q}$ comb/$\psi\dot{q}$ aero
10	5796	.180
20	5749	.183
30	3654	.286

c. Gas Phase Combustion Heating (Equation 57)

Time sec	P_e atmo	$\dot{m}_D$ lb/ft^2 sec	$\dot{q}$ aero BTU/ft^2 sec	$\dot{q}$ comb BTU/ft^2 sec	$\dot{q}$ comb/$\dot{q}$ aero
10	.067	.0022	140	13.1	.093
20	2.21	.0125	800	75.3	.094
30	38.1	.0521	2030	312	.15

*Initial conditions: $V = 24000$ ft/sec, $H = 300000$ ft, $\gamma = 2^{\circ}$,

$W/C_DA = 1000$.

Surface combustion heating produces only a small contribution to the total heat input to a re-entry vehicle.

b. <u>Gas Phase Combustion Heating</u>

Ablative gaseous species diffuse into the hot boundary layer, and if reactive, undergo exothermic oxidation. The heat liberated in the process serves to increase the total enthalpy of the environment. This leads to an additional heating rate to the ablating material.

The gas phase combustion produced by the homogeneous reactions has been studied by many groups (Ref. 24). Most of these authors used the similarity between the diffusion of mass and the transport of energy and obtained the result that the effect of combustion is to add a constant term to the boundary layer enthalpy potential. Swann (Ref. 5) gives an excellent derivation of the process and derives an expression of the ratio of rate of diffusion of oxygen to the surface to the heat transfer rate:

$$\frac{\dot{m}_d\ (O_2)}{\psi \dot{q}_{aero}} = \frac{C_{O_2}}{(h_e - h_s)}\ (N_{L_e})^{0.6} \tag{54}$$

where N_{L_e} is the Lewis number and C_{O_2} is the mass fraction of oxygen in the free stream.

Several authors (Ref. 2) calculate an upper bound of the effect of gas phase combustion. Assuming a Lewis number of unity (i.e., the molecular diffusivity is equal to the thermal diffusivity), and air containing twenty-one per cent oxygen, the increase in heating due to combustion can be calculated after multiplying both sides of Equation 54

---

24. Ibid.
5. Ibid.
2. Ibid.

---

by the heat of combustion for the combustible per pound of oxygen, h_c. The resulting equation is:

$$\dot{q}_{comb} = \frac{0.21\,(\psi \dot{q}_{aero})\,h_c}{h_e - h_s} \tag{55}$$

This equation gives the increase in heating due to gas phase combustion for air containing twenty-one per cent oxygen provided that all the oxygen diffusing into the boundary layer is completely reacted with combustible vapors. Equation 55 is in wide use and will be used in this analysis. An example of the ratio of the combustion heat to the net heat input is shown in Table IIb, assuming a value for the heat of combustion, h_c, of 5000 BTU/lb of oxygen.

Vojnodich and Pope's experiments (Ref. 24) indicated that Equation 55 may actually underestimate the magnitude of combustion heating. The authors feel that a possible reason for the difference may be due to the assumptions used in deriving Equation 55. These were: the reaction is controlled by the rate of oxygen diffusion, the diffusion coefficients of all species are equal, the frozen Lewis and Prandtl numbers are equal to unity, the reactions occur at a sharp flame front, the location of the flame front is determined by the dimensionless release rate, and the release rate was low.

It should also be possible to obtain an order of magnitude relation for the gas phase combustion using Scala's theory (Ref. 25) of the oxidation of graphite. Equation 51 defines an operating regime when the oxidation rate of the graphite is controlled by the rate of

---

24. Ibid.
25. Ibid.

---

oxygen diffusion through the boundary layer to the surface and assuming that all the oxygen is consumed. If we again assume that the important reaction is given by Equation 52, we can say that:

$$1 \text{ lb of Carbon requires } 1.33 \text{ lb of oxygen} \tag{56}$$

then,

$$\dot{m}_d (O_2) = 1.33 \dot{m}_d \tag{57}$$

Table IIc shows the ratio of the heat of combustion to the convective heating for the ICBM trajectory discussed earlier. The nose radius is assumed to be one foot and the heat of combustion, h_c, is assumed to be 5000 BTU/lb of oxygen.

Since both the boundary and surface combustion are limited by the diffusion rate of oxygen, a direct addition of the effects does not seem logical and the effects have to be considered separately or by fractional addition. Experimental data on the effects of combustions are inconsistent and additional work seems to be required in this area. Theories exist which have oxidation as the only char removal mechanism, while at the same time it is reported that good correlation of theory and flight test is obtained with combustion assumed negligible.

In our discussion it has been shown that the effect of combustion in ablative material is an area where more work effort is required since it is not completely understood. This area ties in directly with char removal mechanisms and due to the uncertainties involved a section will be devoted to the problem of char removal in a preliminary effort to grasp the problem. However, this analysis has pointed out that the gases that are evolved by the process of ablation are beneficial in that they produce the transpiration effect but are detrimental in that combustion of the gases may cause an additional heat input. One author (Ref. 26) even found that the combustion effect was greater than the transpiration effect causing a net gain in heating. The major heat dissipation mechanisms will be discussed in the subsequent paragraphs.

3.4 Transpiration Cooling

Organic components of ablative materials are depolymerized or pyrolyzed into gaseous products such as methane, ethyene, hydrogen, acetylene, and other hydrocarbons. The gaseous species upon being injected into the boundary layer produce a heat blockage of the aerodynamic heating. The blocking is achieved by the thickening of the boundary layer and reduction in the slope of the boundary layer temperature profile at the surface.

The transpiration cooling heat blockage parameter is defined (Ref. 2) as:

$$\frac{\dot{q}_{aero} - \dot{q}_{bl}}{\dot{q}_{aero}} = \frac{\dot{q}_{net}}{\dot{q}_{aero}} = \psi \tag{57}$$

where:

$\dot{q}_{aero}$ is the convective heat rate to a nonablating body at the surface ablation temperature

$\dot{q}_{bl}$ is the heat rate blocked by the transpiration effect.

The heat blockage parameter, ψ , is a function of mass injection rate, $\dot{m}_g$, the molecular weight of the vapor, the external flow Mach number and whether the boundary layer is laminar or turbulent.

---

26. Barber, E. A., "An Experimental Investigation of Stagnation Point Injection," AIAA Preprint 63-433, Aug. 1963.
2. Ibid.

Utilizing available experimental and theoretical transpiration results, several authors (Ref. 2) have obtained correlation formulas for the ψ function:

$$\psi \approx 1 - \beta \frac{\dot{m}_g}{\bar{h}_c} \approx 1 - \beta \frac{\dot{m}_g \, \Delta H}{\dot{q}_{aero}} \qquad (58)$$

where:

$\bar{h}_c$ is the convective heat transfer coefficient,

$\dot{q}_{aero} = \bar{h}_c \, (\Delta H)$ and

$\Delta H = h_e - h_s \approx \frac{1}{2} V_\infty^2$ is the enthalpy difference across the boundary layer.

The constant β is known as the transpiration factor and is reasonably well defined for a laminar boundary layer of air. From (Ref. 2) the laminar transpiration factor in air (molecular weight = 29) is:

$$\beta_L = N \left(\frac{29}{M_g} \right)^{\eta} \qquad (59)$$

where:

$0.67 \leq N \leq 0.72$

$0.25 \leq \eta \leq 0.40$

and M_g is the average molecular weight of the injected vapor.

The turbulent transpiration factor is not well defined. According to (Ref. 2), data for helium injection give values of β_t comparable with β_L. For ablating materials whose vapor molecular weight is comparable or heavier than air the following may be used:

$$\beta_T \approx \frac{1}{3} \beta_L \qquad (60)$$

---

2. Ibid.

The transpiration factor is a measured quantity and is frequently available as property data of the material.

Maximum heat blockage effect is obtained when the gasification ratio, Γ , is high and when the gaseous products of ablation are of low molecular weight. Organic ablators inject various gases in the boundary layer, including hydrogen which has the lowest molecular weight and thus has good heat absorbing characteristics.

The heat blockage parameter given by Equation 58 is in wide use even though several shortcomings are evident. Equation 58 is a straight line and if one plots ψ versus $\dot{m}_g \, \Delta H/\dot{q}_{aero}$, the x-axis will be intercepted at a value of $1/\beta$. Therefore, using the linear blocking term given by Equation 58, at a finite mass injection rate of

$$\dot{m}_g = \frac{\dot{q}_{aero}}{\beta \, \Delta H} \tag{61}$$

the aerodynamic heating is completely blocked and $\dot{q}_{net}$ will be reduced to zero. At higher mass injection rates Equation 58 will predict a negative blocking factor. Since this seems a physical impossibility, a lower limit of $\psi = 0.20$ was used in Equation 58 for use in our model. Thus:

$$\begin{aligned} \psi &= 1 - \beta \frac{\dot{m}_g \, \Delta H}{\dot{q}_{aero}} && \text{for} \quad \frac{1 - \beta \, \dot{m}_g \, \Delta H}{\dot{q}_{aero}} \geq 0.20 \\ \psi &= 0.20 && \text{for} \quad \frac{1 - \beta \, \dot{m}_g \, \Delta H}{\dot{q}_{aero}} < 0.20 \end{aligned} \tag{62}$$

It seems that Equation 58 would be in error at conditions of re-entry from supercircular orbits. In this case the aerodynamic heat input would consist of both convective and radiative heating. The transpiration effect reduces convective heating but not radiation heating, if we neglect the absorption coefficients of the gas species coming off the ablative material. The radiant heat would cause high mass transfer rates, $\dot{m}_g$, and Equation 58 is likely to predict total blockage of convective heating. For low and moderate mass-transfer rates Equation 58 has been experimentally verified (Ref 6). However, very little experimental data are available at high mass transfer rate.

Some authors (Ref. 27) imply that the blocking term is nonlinear. One possible relation would be an exponentially decaying function, such as:

$$\psi = e^{-\beta \dot{m}_g \Delta H / \dot{q}_{aero}} \tag{63}$$

An exact analysis of the heat blockage effect is found in (Ref. 28). The exact solution was obtained from the boundary layer solution for air-to-air injection. The results show that the usual linear approximation is not valid at a high mass transfer rate. Swann (Ref. 6) used a second degree approximation to fit Roberts' (Ref. 28) results. At very high transfer rates, however, Swann's curve-fit predicted total blockage and Swann was forced to use a cut-off minimum value of ψ . Using a minimum value of ψ is conservative, since it seems unlikely that sufficient vapor can be injected to reduce the slope of the temperature profile, in the boundary layer, without first resulting in separated flow.

Determining the molecular weight of the injected vapors is a problem when analyzing transpiration cooling effects. For a simple

---

6. Ibid.
27. Fledderman, R. G., "Heat Transfer to a Vaporizing Ablating Surface," Journal of the Aerospace Sciences, Sept. 1959.
28. Roberts, L., "A Theoretical Study of Stagnation Point Ablation," NASA TR R-9, 1959.

subliming material, such as Teflon, the only vapor product of decomposition is assumed to be the C_2F_4 monomer with a molecular weight of 100. The problem is more complex when one considers cross-linked plastic material such as phenolic nylon or carbon phenolic which liberate numerous species.

Figure 6 shows a plot of the heat blockage parameter, ψ , versus the dimensionless release rate, $\dot{m}_g \Delta H/\dot{q}_{aero}$. Equations 62 and 63 are plotted for a molecular weight of the gases equal to 15 and a transpiration factor, β, of 0.714. The second-order approximation for ψ developed by Swann-Pittman-Smith (Ref. 6) for charring ablators is also shown for a molecular weight of 15. If the curve were continued to a dimensionless release rate, $\dot{m}_g \Delta H/\dot{q}_{aero} = 2.5$, the Swann-Pittman-Smith approximation would predict total blockage (i.e., $\psi = 0$). Equation 62 was used in the model due to its simplicity and the fact that it reasonably approximates more exact theories.

3.5 Reradiation

Total thermal emission from an ablating surface is given by the Stefan-Boltzman radiation law:

$$\dot{q}_{re-rad} = A \epsilon \sigma T_s^4 \tag{64}$$

Equation 64 indicates that energy dissipation by radiative emission becomes appreciable at high values of emissivity, ϵ , especially at high surface temperatures. The amount of heat rejected by radiation for an organic plastic such as Teflon is small due to the fact that this material sublimes at a temperature in the neighborhood of 1000° F.

---

6. Ibid.

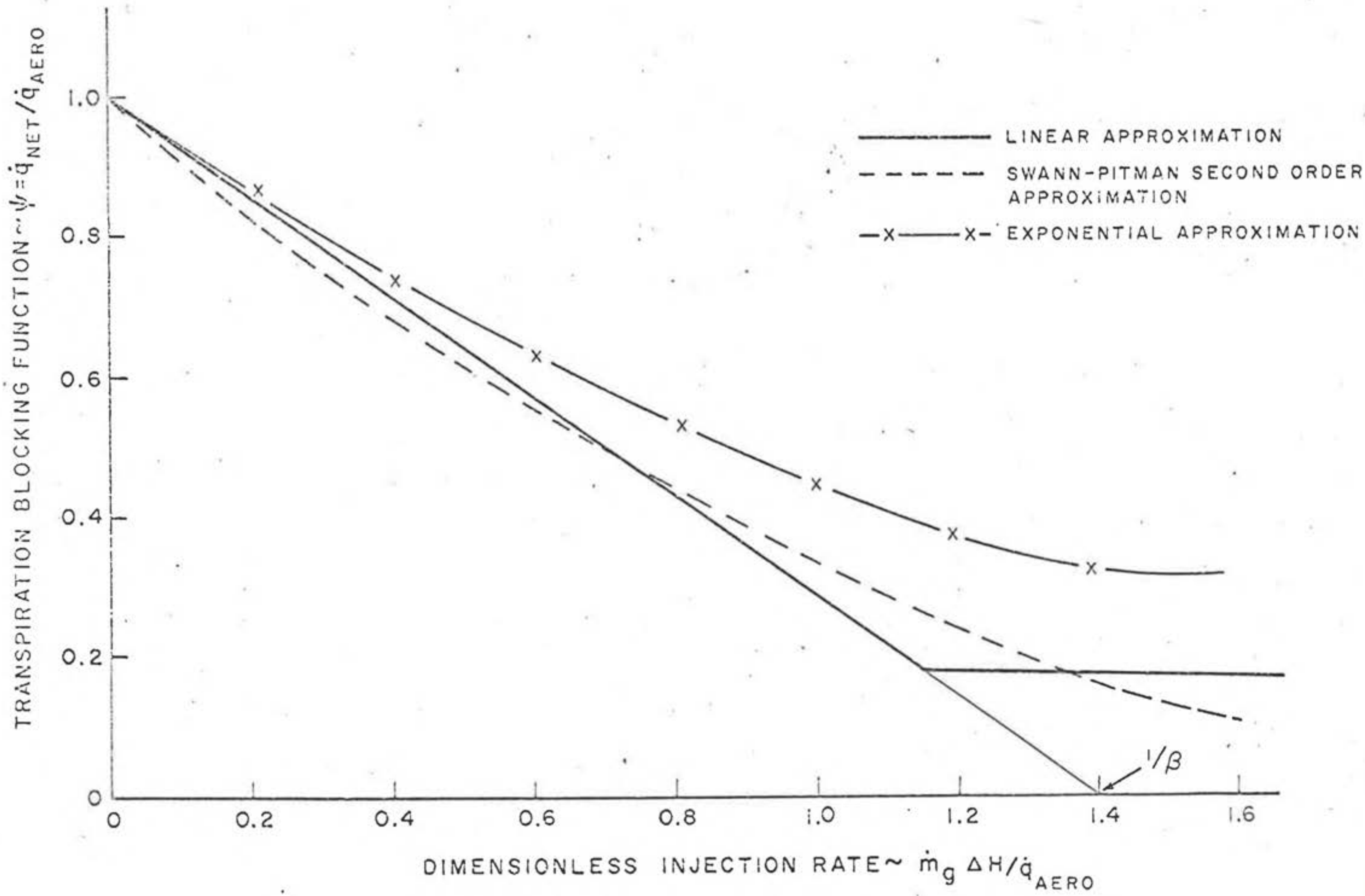

Figure 6. Ratio of Heat Transfer with and without Mass Injection as a Function of Dimensionless Injection Rate.

Composite plastics, such as Carbon Phenolic, produce a carbonous char which not only has a high emissivity but sustains temperatures up to the sublimation temperature of carbon (i.e., 6600° F). For many moderate heating and long exposure time trajectories most of the heat input to an ablating body is rejected by reradiation. Reradiation is the principal mode of energy transport in many ablative plastics, especially composites. Because of its heat blockage capability, reradiation produces an apparent increase in the material's thermal efficiency.

High surface temperatures in ablative plastics reduce the enthalpy potential across the boundary layer and thus reduce the aerodynamic heat to the exposed surface and hence reduce the loss rate of the material.

In our analysis we have assumed the material to be opaque to internal radiation. Materials which are transparent to radiation are normally not desired since they allow energy to flow into the virgin material and thus increase temperature causing the ablator to degrade.

3.6 Char Layer

The effect of having char on an ablator not only produces a reradiation effect but also an insulation effect. The effect of char thickness on the amount of material lost can be seen from Equation 28. A simple steady state analysis shows that a large char thickness, δ_c, is important as a heat transfer mechanism as evidenced by:

$$\dot{q}_{char} = \frac{k_c A}{\delta_c} (T_s - T_a) \tag{65}$$

The presence of a porous char layer, through which the gases formed by pyrolysis escape are partially responsible for the transpiration effect. The heat absorbed by the gases, for steady state, during passage through the char layer can be given by:

$$\dot{m}_g C_g (T_s - T_a) \tag{66}$$

3.7 Heat Absorbed by Pyrolysis or Phase Change

As an ablative material is heated, the material undergoes decomposition by fusion, vaporization and sublimation and depolymerization. As a result energy is absorbed as evidenced from Table I. The importance of using materials which sublime as opposed to materials which melt has been discussed in Section I. An effective heat of pyrolysis, H_p, will be defined as such that the heat absorbed by phase changes is given by:

$$\dot{q}_{pyr} = \dot{m}_p H_p \tag{67}$$

The importance of this term can be seen from Equation 27. A high heat of pyrolysis means a high heat absorption capability before degradation of the material takes place.

The formulation of the effective heat of pyrolysis utilizing the degradation of Teflon as an example (Ref. 1) will be briefly reviewed. Teflon remains an essentially solid material until a temperature of approximately 1000° F is reached. When Teflon, a highly crystalline linear polymer, is heated several order-disorder transitions occur. The first transitions can occur at temperatures as low as room temperatures with the absorption of small quantities of heat (approximately 4 BTU/ft^2 sec). As the temperature approaches 620° F, the polymer changes into an amorphous, transparent, rubbery substance. At this

1. Ibid.

point Teflon is said to be melting, although a liquid phase is not apparent. The energy absorbed during this process is the heat of fusion, h_f, and the value is 37 BTU/lb. As the temperature is further increased to 750° F, the polymer slowly depolymerizes into its monomer C_2F_4 and other fluorine-containing compounds. The energy absorbed by this phase change is the heat of depolymerization, h_d. The heat of depolymerization is approximately 680 BTU/lb. Then the total heat required to vaporize Teflon under steady state conditions is:

$$h_{tot} = C_p \Delta T + h_f + h_d \tag{68}$$

Since the first term of Equation 68 is already taken care of in the ablation model the effective heat of pyrolysis for Teflon will be defined as:

$$H_p = h_f + h_d \tag{69}$$

Similar analogies hold true when obtaining the effective heat of pyrolysis for other materials.

3.8 Heat Conducted and Stored in the Virgin Material

In ablative materials a low thermal conductivity (i.e., diffusivity) is required in order to raise the surface to a high temperature quickly and thus benefit from the heat dissipation of reradiation and phase changes, while at the same time keep the substructure and virgin material relatively cool. Table I shows that magnesium oxide and graphite have great potential as heat absorbing materials. However, the high thermal conductivity of these materials would result in a low surface temperature and high substrate temperature. In addition, the difference between the boundary layer gas temperature and the surface temperature remains high, thus increasing the aerodynamic heating while the substrate structure remains insufficiently insulated. The heat of vaporization can also never be realized, resulting in the material being used as a heat sink.

In order to obtain an order of magnitude analysis as to how much heat is conducted into an ablating material a simplified analysis will be discussed. Assuming an ablating semi-infinite plate having an ablation velocity, V_w, the energy equation, Equation 13, can be written as:

$$\frac{\partial}{\partial x}\left(k\frac{\partial T}{\partial x}\right) = -V_w \rho c \frac{\partial T}{\partial x} + \rho c \frac{\partial T}{\partial t} \tag{70}$$

If the steady state ablation velocity, V_w, has been reached, the temperature distribution can be assumed to be nearly steady provided that the thermal conductivity is extremely low (Ref. 29). Then Equation 70 reduces to:

$$\frac{d}{dx}\left(k\frac{dT}{dx}\right) = -V_w \rho c \frac{dT}{dx} \tag{71}$$

subject to boundary conditions:

at $x = 0$; $T = T_a$

at $x = \infty$; $dt/dx = 0$

at $x = \infty$; $T = T_i$

If the thermal conductivity is small, $x = L_o$ may be assumed as $x = \infty$. In other words, under these conditions, the finite slab acts as a semi-infinite slab. Upon integrating Equation 71 the following temperature distribution results:

$$T_x = T_i + (T_a - T_i)\, e^{-(V_w x/\alpha)} \tag{72}$$

---

29. Rohsenow, W. M., Choi, H., Heat, Mass, and Momentum Transfer. Prentice-Hall, Inc., Englewood Cliffs, New Jersey, 1961.

Again, assuming steady state conditions, an energy balance for the ablating material results in:

$$\dot{q}_{in} - \rho V_w H_p = - k \left(\frac{\partial T}{\partial x}\right)_{x=0} = \rho V_w c (T_a - T_i) \tag{73}$$

The total amount of heat conducted into the solid:

$$Q_{cond} = \rho c \int_{x=0}^{\infty} (T_x - T_i) \, dx = \frac{k(T_a - T_i)}{V_w} \tag{74}$$

The total heat transferred to the surface in time t is:

$$Q_{in} = \dot{q}_{in} \, t \tag{75}$$

Then the fraction of the total heat transferred which is conducted into the solid is:

$$\frac{Q_{cond}}{Q_{in}} = \frac{\rho k (T_a - T_i) \left[H_p + c (T_a - T_i)\right]}{\dot{q}_{in}^2 \, t} \tag{76}$$

From Equations 76 and 73 one sees that a large magnitude of $H_p + c (T_a - T_i)$ is desired in order to reduce the amount ablated, but a small magnitude is desirable to reduce the fraction of Q_{in} which is conducted into the virgin material. This conflict is the subject of compromises.

The heat storage capability of ablators is not utilized. The heat storage of a solid will be appreciable only at high values of specific heat, density, ablation velocity, and temperature rise. These requirements are not compatible with the thermal insulation and weight restrictions imposed upon ablative materials.

IV. MODEL VALIDATION

Several approximations and assumptions were made in formulating a model to predict the transient response of thermal protection systems. It is hoped that the simplifying assumptions and approximations, which were introduced to obtain fast and hopefully accurate solution, will introduce only minor errors. The intended purpose of this section is to validate the analysis and resultant accuracy by:

a. comparison with exact theoretical solutions,

b. comparison with other approximate numerical solutions and models,

c. comparison with simplified solutions,

d. comparison with experimental and flight test data.

Various examples have been selected for the purpose of comparing this proposed model with exact theoretical solutions and test data, as well as with some approximate analytical machine solutions. These examples will be covered in the subsequent paragraphs of this section.

4.1 Comparison with Exact Theoretical Solutions

The accuracy of the numerical analysis model is best determined by comparing its results with an exact solution that is available. A simple transient heating example was chosen to demonstrate the accuracy and numerical stability of our model. The case under consideration is a homogeneous nonablating heat sink material, with a constant initial temperature distribution, one side of which is subjected to a suddenly applied constant heating rate and the other side is assumed thermally insulated. If the thermal properties are assumed constant, an analytical solution can be found (Ref. 30):

$$T_x - T_i = \frac{\dot{q}_{in}}{\rho c L_o} + \frac{\dot{q}_{in} L_o}{k} \left\{ \frac{3\bar{x}^2 - L_o^2}{6 L_o^2} - \frac{2}{\pi^2} \sum_{n=1}^{\infty} \frac{(-1)^n}{n^2} e^{-\alpha n^2 \pi^2 t / L_o} \cos \frac{n\pi\bar{x}}{L_o} \right\} \tag{77}$$

where: $\bar{x} = L_o - x$

A steel slab six inches thick was selected and assumed to be at a uniform initial temperature of 460° R. The front surface was subject to a heating rate of 75 BTU/ft^2 sec. The thermophysical properties for steel were obtained from standard handbooks. Reradiation from the surface is not considered. In order to make the ablation program discussed in Section II function as a heat sink, all that is required is to set the ablation temperature, T_a, at an extremely high value. In this way ablation never starts and thus the recession and combustion equations yield values of zero. Also, since there is no mass loss, the transpiration blocking function, ψ , is unity and thus all the heat input is allowed to enter the surface. The system of equation which results is identical to Equation 7. Forty-eight nodes were used to simulate this problem.

Equation 77 does not readily lend itself to hand calculations due to the slowly converging series term. This equation was programmed on a digital computer and one hundred terms of the series were used.

Figure 7 shows a comparison of the in-depth temperature distribution as a function of time obtained from this model, with the exact

---

30. Carslaw, H. S., Jaeger, J. C., Conduction of Heat in Solids, Clarendon Press, Oxford, 1959.

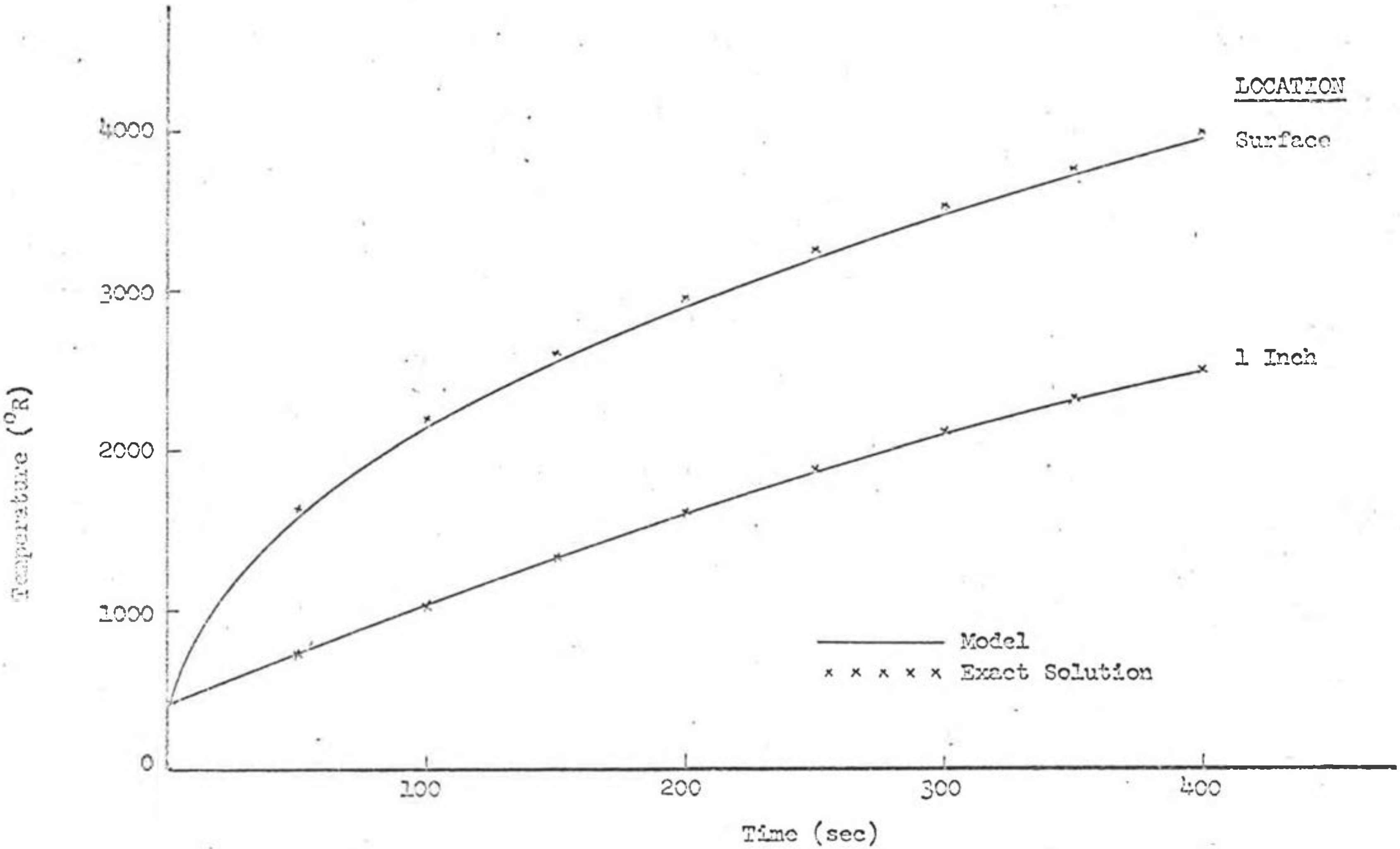

Figure 7. Comparison of Temperature Histories for Non-ablating Steel Slab (Pure Conduction).

solution obtained from Equation 77. The comparison is seen to be adequate. Note that the solution obtained from this model is always somewhat lower than that obtained by the exact solution. The reason for this is that the true surface temperature is not really obtainable from this model. Even though the first node was made extremely small, one-tenth of the other nodes, the surface temperature obtained from this model is still some finite amount below the surface.

Other exact heat sink solutions obtained from (Ref. 30) could have been compared with this analysis, however, this was not deemed necessary since similar results to Figure 7 would apply.

Figure 7 presents the model solution using 48 nodes. Each node was 0.125 of an inch and gave very good results. The model was run using only ten nodes, each being 0.6 of an inch, and the results showed that the lesser nodes gave five per cent lower temperatures than the higher node model.

4.2 Comparison with Other Approximate Numerical Solutions and Models

The electric analog computer with its continuous variable, time, has long been in use in the solution of transient problems. It is of interest to check a simple problem on the electric analog computer and by this model. A slab, similar to the one shown in Appendix II, is divided into five nodes and it is desired to find the variation of temperature, T_1 through T_5, as a function of time for a given heat rate input. Before the heat is applied, the slab will be considered to be at a uniform temperature of 100° F. The back surface will be assumed insulated. The physical properties of the slab and the heat

30. Ibid.

rate inputs as well as the electric analog solution were obtained from (Ref. 31). The physical properties of the slab are as follows:

L_o = 1 inch

Δx = 1/60 ft.

α = 1.1661×10^{-4} ft^2/sec

k = 3.056×10^{-3} BTU/ft sec F

The heat rate input $\dot{q}$ is:

$$\dot{q} = 18.3 \text{ BTU/ft}^2 \text{ sec} \qquad 0 < t \leq 50 \text{ sec}$$

$$\dot{q} = 0 \qquad t > 50 \text{ sec}$$

The solution to this problem is presented in Figure 8. The plot was obtained from the MIMIC computer program using a Stromberg-Carlson 4020 Plotter. Comparing the results of Figure 8 with those presented in (Ref. 31) shows the results to be virtually identical.

As a further check the steady state temperature that would result after the application of heat for 50 seconds can be computed analytically. The steady state temperature at all five points will be the same, just as the initial temperatures were. If the five temperature equations given in Appendix II are integrated from zero to infinity, added and divided by five, the following will result in the steady state temperature:

$$T_{ss} = T_i + \frac{1}{5}\int_0^{\infty} \frac{\alpha}{k\Delta x}\,\dot{q}\,dt = T_i + \frac{1}{5}\int_0^{50} \frac{\alpha}{k\Delta x}\,(18.3)\,dt$$

$$T_{ss} = 100 + \frac{1}{5}\,(41.897)\,(50) = 518.97^{\circ}\text{ F}$$

31. Analog Indoctrination Program, Analog Computation Facility, WPAFB, Ohio, April 1965.

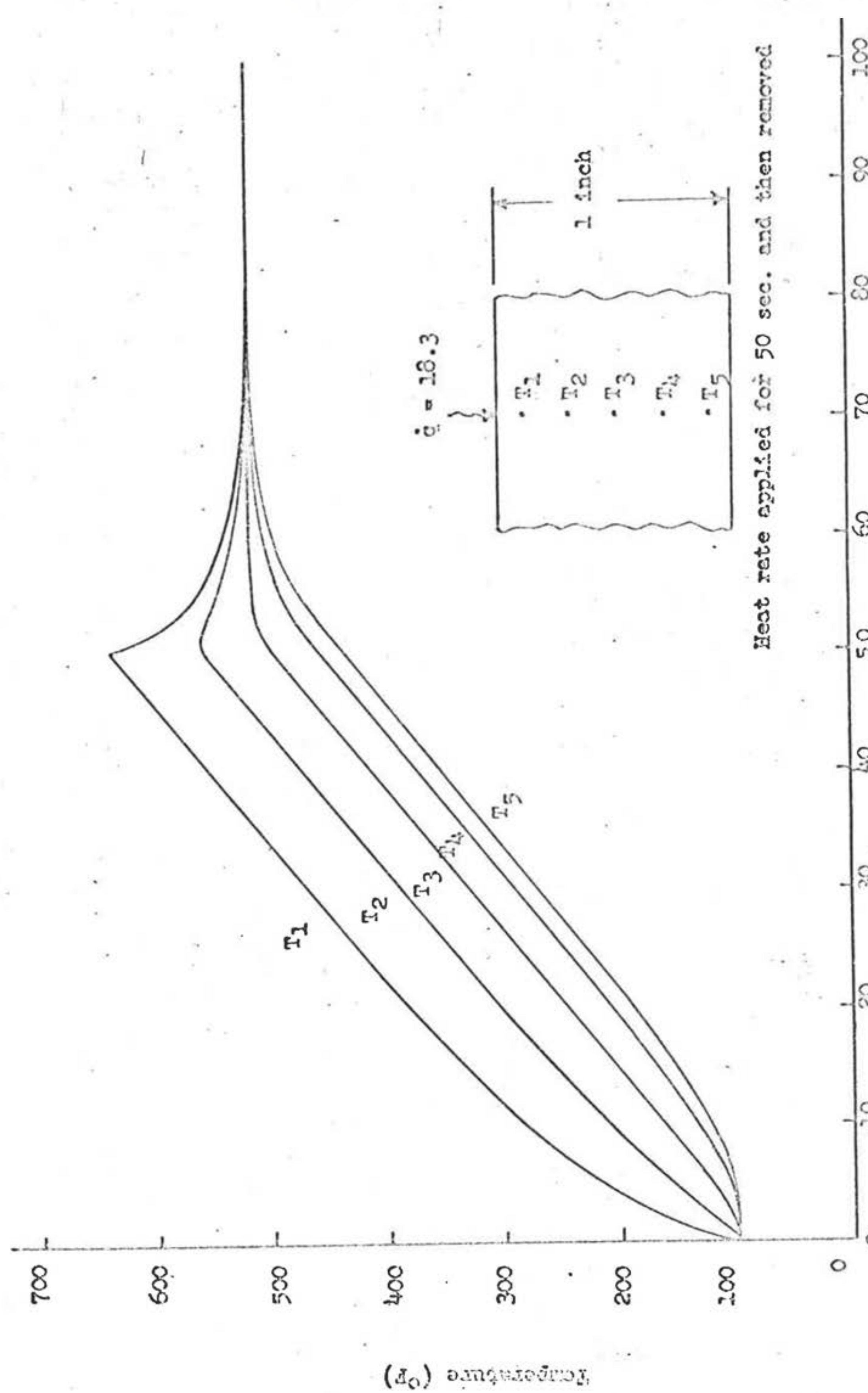

Figure 8. Steady State Temperature in a Slab.

Figure 8 shows that steady state conditions have essentially been reached at time equal to 100 seconds. At $t = 100$ seconds, the following temperature distribution was obtained from the model:

$T_1 = 519.008$

$T_2 = 518.996$

$T_3 = 518.977$

$T_4 = 518.957$

$T_5 = 518.946$

This is an indication that the model is valid for solving heat conduction problems.

In order to illustrate the validity of the model in solving heat transfer problems with a moving boundary we will presently solve a one-dimensional melting problem. The solution which is obtained for a typical problem will then be compared to the solutions reported in Landau's classic paper on the subject of heat conduction in a melting solid (Ref. 32). The material which will be considered is ice. The properties of this substance are well defined and if it is assumed that the liquid is removed immediately after formation, ice can be thought of as an ablating material. Ice melts to water at a constant temperature, T_m, and with the absorption of a constant quantity of heat (i.e., the heat of fusion, F). The behavior of an ablator, such as Teflon, can be studied in a similar manner upon the substitution of the thermochemical heat of ablation for the heat of fusion.

---

32. Landau, H. G., "Heat Conduction in a Melting Solid," Quart. Appl. Math., Jan. 1950.

Landau treats the heat conduction problem in which one material is transformed into another with the generation or absorption of heat. To make the problem tractable, Landau assumed a one-dimensional semi-infinite melting solid with constant properties and with its surface heated at a constant rate. For this case an exact steady state solution can be derived. The proposed analysis is not limited by Landau's assumptions; that is, a finite solid with variable thermochemical properties and heat input as a function of time can be considered. The problem can be formulated in two or three dimensions and in cylindrical or spherical coordinates.

The problem will be formulated for a one-dimensional flat plate and thus Equation 2 applies, subject to the following initial and boundary conditions:

$$\text{at } t = 0; \qquad T = T_i$$

$$\text{at } x = 0; \qquad -k\frac{\partial T}{\partial x} = \dot{q}$$

$$\text{at } x = L_o; \qquad -k\frac{\partial T}{\partial x} = 0$$

where $\dot{q}$ represents the heat flux prior to melting. When the surface temperature, T_s, reaches the melting temperature, T_m, the second boundary condition must account for the heat of fusion of ice. If $\dot{\delta}$ is the velocity with which the surface of the ice recedes and F is the heat of fusion, then the second boundary condition becomes:

$$-k\frac{\partial T}{\partial x} = -\dot{q} - \rho F \dot{\delta} \tag{78}$$

In the formulation of our analysis, Section II, the quasi steady state value of $\dot{\delta}$ was formulated and used as an input to the model. In the formulation that follows the transient value of $\dot{\delta}$ will result directly from the model formulation.

The region $0 \leq x \leq L_o$ can be divided into N sections, each of width Δx, where $N \Delta x = L_o$ in the same manner as was done in Section II. The resulting system of equations is the same as Equation 7. As soon as the first cell reaches the melting temperature, T_m, it is assumed that the entire first cell is instantaneously at this temperature. At this point a specific amount of heat is required to melt the cell. This quantity of heat is $\Delta x \rho F$. If t_1 is the time at which the first cell reaches T_m, then the first cell is completely ablated at time t_2, when:

$$\int_{t_1}^{t_2} (\dot{q} - \dot{q}_{cond\ 1-2})\, dt = \Delta x \rho F \tag{79}$$

Then the first cell is removed by switching the heat flux $\dot{q}$, at time t_2, to the face of the second cell. There are now (N-1) cells in the system and the operation of heating to the melting temperature and delay time, due to the heat of fusion, continues from cell to cell until ablation is terminated or the model stopped. Each successive cell, in a finite plate, will melt faster than the preceding cell since it is at a higher temperature when the heat flux, $\dot{q}$, is switched to its face. In this manner the melting proceeds in discrete steps by melting Δx of the material at a time. If Δx is made small enough, a good approximation to the melting problem results. This method was simulated for the one-dimensional melting of ice and the results were found to be excellent.

The following problem was simulated assuming constant properties:

material :	ice
initial temperature:	$T_i = -5^o$ F
melting temperature:	$T_m = 32^o$ F
heat of fusion :	$F = 144$ BTU/lb

material thickness: $L_o = 4$ in.

heat flux : $\dot{q} = 5$ BTU/ft^2 sec

number of nodes : $N = 40$

thickness of node : $\Delta x = 0.1$ in.

The ice was subjected to a heat rate of 5 BTU/ft^2 sec for 300 seconds and the following results were obtained:

number of nodes which were totally melted: 19

partially melted nodes: $\frac{18.60}{68.39}$

thickness which melted: $s = 0.1606$ ft.

material remaining after melting: $L_o - S = 0.1727$ ft.

The twentieth node was only partially melted. The thickness of material which melted in the twentieth node was determined from:

$$\int_{t_1}^{t_x} (\dot{q} - \dot{q}_{cond\ 20\text{-}21})\, dt \,/\, \Delta x\, \rho\, F \tag{80}$$

In order to determine if our original partial differential equation is correctly represented by the set of finite difference equations, one can determine how closely the steady-state heat balance was satisfied. This is said to always be a critical check that can be applied to the set of equations which approximate the partial differential equation.

Thus, let the heat flux $\dot{q}$ be equal to 5 BTU/ft^2 sec for 300 sec and zero otherwise. If only a fraction of the initial length L_o melts, then the remaining length, $L_{ss} = L_o - s_{ss}$, will eventually assume some steady-state temperature, T_{ss}. Here s_{ss} is the steady state value of s where s is the total melted length or the distance that the surface has receded from its initial boundary. The value of s is given by:

$$s = \int \dot{\delta}\, dt \tag{81}$$

The steady state criteria states that the total heat entering the bar,

$$Q_{tot} = \int_{o}^{t_{ss}} \dot{q}\, dt$$

must be equal to the heat consumed by melting plus the heat content, in steady state, of the remaining bar. The steady state temperature of the unmelted material was determined by running the model for 10,000 seconds after the heat rate was removed. The steady state temperature was found to be $T_s = 1.03314^{o}$ F.

Thus, the equation describing the steady state heat balance is:

$$\int_{o}^{t_{ss}} \dot{q}\, dt = \rho c\, s_{ss} (T_m - T_i) + \rho F\, s_{ss} + \rho c\, L_{ss} (T_{ss} - T_i) \tag{82}$$

total heat input	=	heat required to raise the melted portion to the melting temperature T_m	+	heat required to melt the material once the melting temperature has been reached	+	heat content of remaining material

1505 = 57(0.46)(1.1606)(37) + 57(144)(0.1606) + 57(0.46)(0.1727)(6.033)

Finally:

$$1505 \approx 1501.3$$

The steady state heat balance shows that the approximation to the melting problem yielded results which were in error by less than 0.25 per cent.

At the time at which the heat rate was removed, at t = 300 sec, the temperature of the last node of the ice was: $T_f = -4.95^{o}$ F. The initial temperature distribution of the ice was minus five degrees Fahrenheit. This indicates that the ice slab essentially behaved as a semi-infinite body. Thus, we should expect to obtain good correlation with Landau's (Ref. 32) solution which was obtained for a semi-infinite plate. A check comparing this solution with Landau's solution revealed that the recession rate, and thus the amount of material melted, were virtually identical. The average recession rate obtained from this analysis was found to be 5.35 x 10^{-4} ft/sec. Landau develops a steady state recession rate, V_w, for a semi-infinite plate. The relation is:

$$V_w = \frac{\dot{q}}{\rho\left[F + c\ (T_m - T_i)\right]} \tag{83}$$

Note that this relation could have been obtained from Equation 73. Upon substituting numerical values in Equation 83 the steady state recession rate is found to be 5.44 x 10^{-4} ft/sec which agrees closely with the value predicted from this analysis.

Landau's analysis assumed a semi-infinite plate subject to a constant heating rate. Prior to the melting the temperature distribution in the semi-infinite plate is from (Ref. 30):

$$T_x = T_i + 2\ \dot{q}\ \left(\frac{t}{k\ c\ \rho}\right)^{0.5}\ \text{ierfc}\ \left(\frac{x}{2\alpha t^{0.5}}\right) \tag{84}$$

The time when the semi-infinite plate starts to melt, t_m, can be found from Equation 84. Thus, at x = 0:

$$t_m = \frac{\Pi}{4}\ \frac{k\ c\ \rho}{\dot{q}^2}\ (T_m - T_i)^2 \tag{85}$$

The time for the surface temperature of ice to reach 32° F, for a semi-infinite, can be obtained from Equation 85 and is found to be 0.4007 sec.

32. Ibid.
30. Ibid

The time for the surface temperature to reach 32° F for a finite plate is obtained by numerically solving Equation 77. This was done on a digital computer and the result was found to be 0.4005 seconds. This shows that for this particular example the finite plate can be replaced by a semi-infinite plate and yield acceptable results. The reason is that due to the low melting temperature of ice, heat does not penetrate very deeply into the body. Since it is frequently easier to obtain analytical solutions for a semi-infinite plate, the assumption is frequently made that the temperature distribution of an ablating finite solid is merely the temperature distribution of a semi-infinite plate. This is an erroneous assumption but is approximately true when the material in question is of very low thermal conductivity, the surface temperature is low and a constant ablation velocity has been established. This topic will be discussed more fully in the ensuing paragraphs.

The model which has been presented for the melting of the ice problem allows for discrete removal of the melted material (i.e., the melting proceeds in steps). A more sophisticated, but more difficult technique, exists which allows for continuous recession of the melting or ablating surface. The method of continuous recession closely resembles the physical problem and is therefore more accurate. The method of continuous recession is based on the introduction of a new nondimensional space variable in place of x. The transformation is due to Landau and takes the form:

$$\xi = \frac{x - s}{L_o - s} \tag{86}$$

It should be noted that since this transforms the region $s \leq x \leq L_o$ into $0 \leq \xi \leq 1$, the front boundary condition is applied continuously at $\xi = 0$. The coordinates thus shrink with time. For a fixed number of nodes, the nodes move closer together and the special representation becomes more accurate. It is conceivable that fewer nodes are required in the continuous recession method to obtain the same degree of accuracy as was obtained in the discrete ablation method.

If Equation 2 is transformed according to Equation 86, and noting that s is a function of time, the following results:

$$\frac{\partial T'}{\partial t} = \frac{\alpha}{(L_o - s)^2} \frac{\partial^2 T'}{\partial \xi^2} + (1 - \xi) \frac{\dot{\delta}}{(L_o - s)} \frac{\partial T'}{\partial \xi} \tag{87}$$

where the primes indicate the new coordinate system.

The boundary conditions for the ice problem become:

$$\text{at } \xi = 0; \qquad -k \frac{\partial T'}{\partial \xi} = (L_o - s)\,(\dot{q} - \rho F \dot{\delta})$$

$$\xi = 1; \qquad -k \frac{\partial T'}{\partial \xi} = 0$$

Equation 87 can be reduced to a system of ordinary differential equations by the methods outlined in Section II and Appendix II. This method of solving the ablation problem was not evaluated in this analysis, but its advantages are evident. This method is not too different from the method of receding coordinates presented in Section II where the transformation used was $x' = x - \delta$. However, the resulting finite difference equations are more complex. A typical result is illustrated below for the second node:

$$\frac{dT_2'}{dt} = \frac{\alpha\,(T_3' - 2T_2' + T_1')}{(L_o - s)^2\,(\Delta\xi)^2} + \frac{(1 - \xi)\,\dot{\delta}\,(T_2' - T_1')}{(L_o - s)\,(\Delta\xi)} \tag{88}$$

The advantages of this method, compared to the continuous recession model presented in Section II, is that this method gives the solution in non-dimensional form and thus the solution can be obtained for a class of problems as opposed to a specific problem.

4.3 Comparison with Simplified Solutions

No exact solutions are available for heat conduction problems involving phase changes and a finite plate. In view of this most approximate solutions rely on the work of Neumann, Goodman, and Grosh. Neumann (Ref. 30) obtained a solution of a heat-transfer problem with phase change for semi-infinite plate and a constant surface temperature. The solution obtained by Neumann for the recession rate was:

$$X_n(t) = 2 \dot{\lambda} (\alpha t)^{0.5} \tag{89}$$

where λ is a constant of proportionality satisfying a transcendental equation. Goodman's (Ref. 33) work involves the use of the heat balance integral and in order to obtain a solution a temperature distribution must be assumed. Grosh (Ref. 34) also resorts to a semi-infinite plate in order to obtain the temperature distribution with phase change.

Apart from the few exact solutions, all problems involving phase changes have to be solved numerically usually with the aid of a computer. Because of the expense involved in obtaining these solutions, many approximate solutions are reported in the literature. A few of

---

30. Ibid.
33. Goodman, T. R., "Application of Integral Methods to Transient Nonlinear Heat Transfer," Advances in Heat Transfer, ed. by T. F. Irvine and J. P. Hartnett, Academic Press Inc., New York, 1964.
34. Grosh, R. J., "Transient Temperature in a Semi-infinite Porous Solid with Phase Change and Transpiration Effects," Wright Air Development Division TR 60-105, WPAFB, Ohio, Jan. 1960.

these solutions will be covered in the ensuing paragraphs. A partial list of these approximate solutions will be listed in the bibliography. Approximate solutions are useful to obtain trends and order of magnitude results. However, numerical methods have the advantage that the variation in thermal properties with temperature, which is usually considerable over the ranges of temperature involved in ablation problems, can be taken into account.

The most popular temperature distribution assumed for ablating materials is Equation 72. In the derivation of this equation it was assumed that the body is a semi-infinite, homogeneous material, with constant thermal properties whose ablation velocity has reached steady state conditions and is therefore a constant. Assuming zero initial temperature, Equation 72 can be written as:

$$T_x = T_a \, e^{-(V_w \, x \, \rho c/k)} \tag{90}$$

The validity of this equation, which is independent of time, is predicated on the assumption that the temperature gradient at the surface is so steep so that the boundary condition $x = L_o$ can be considered as $x = \infty$ (i.e., the finite plate acts as a semi-infinite plate). In order for this to be true, the material should have a very low thermal conductivity and high specific heat. Also, Equation 90 will not give correct results for ablators which are subjected to long exposure time, since the heat will penetrate to the interior of the material. Due to its higher initial temperature the interior material will ablate at a faster rate, and the ablation velocity will be changing, thus the temperature profile, different than that predicted by Equation 90, is also likely to occur because ablators are subjected to temperature variations in the thousands of degrees. Clearly the thermophysical properties are not likely to remain constant.

Schneider (Ref. 35) attempts to obtain the transient temperature distribution in a semi-infinite body with a receding surface and initial temperature, T_i. In Schneider's analysis a plane heat source, $\dot{q}$, is moving, parallel to the x-axis, with a uniform velocity, V_w, with respect to a stationary coordinate system. With this scheme a stationary observer on the x-axis would notice a change in the temperature of his surroundings as the source moved along, while if the observer were stationed at a point on the moving ξ-axis, he would notice no such change in temperature. This condition of apparent steady state uses essentially the same logic which was used in deriving Equation 90. This state is represented mathematically by assuming $\frac{\partial T}{\partial t} = 0$ in the moving coordinate system. Equation 2 is transformed from a stationary to a moving coordinate system by the transformation:

$$\xi = x - V_w t \tag{91}$$

The resulting total differential equation in one-dimension is:

$$-\frac{d^2T}{d\xi^2} = \frac{V_w}{\alpha} \frac{dT}{d\xi} \tag{92}$$

This equation and the form of its solution are the same as Equation 71.

The boundary condition applicable to Equation 92 is:

$$\text{as } \xi \longrightarrow \pm\infty; \quad \frac{dT}{d\xi} = 0$$

$$\text{as } \xi \longrightarrow 0 \quad ; \quad -k\frac{dT}{d\xi} = \dot{q}$$

$$\text{at} \quad t = 0 \quad ; \quad T = T_i$$

35. Schneider, P. J., Conduction Heat Transfer, Addison-Wesley Publishing Co., Inc., New York, 1955.

The resulting solution, for an infinite solid initially at T_i through which passes a uniform plane source $\dot{q}$ at a constant velocity V_w is given in two parts:

$$\text{for} \quad \xi < 0; \qquad T = T_i + \dot{q}\,\frac{\alpha}{k\,V_w} = \text{constant}$$

$$\text{for} \quad \xi > 0; \qquad T = T_i + \frac{\dot{q}\,\alpha}{kV_w}\; e^{-(V_w/\alpha)\xi} \tag{93}$$

A discontinuity exists at time zero, violating the initial condition.

Equation 93 resembles an ablating material in that the temperature remains constant in the region behind the heat source and this is the maximum temperature attainable (i.e., this maximum temperature is also attained at the surface). The same shortcomings which were discussed for Equation 90 are applicable for this analysis. The temperature distribution obtained by Equation 93 is applicable only for materials with low conductivity and high specific heat.

In order to compare the results obtained from Equation 93 with those obtained from this model, a slab with constant properties, uniform initial temperature, front surface moving with a constant velocity, and a constant heat rate was programmed. Equation 93 predicts a constant surface temperature which is applied instantaneously, since no provisions are inherent in Equation 93 for the transient heating period. The model was modified to accept a constant ablation velocity and the surface temperature predicted by Equation 93. In order to determine the temperature distribution within the solid the discrete node removal method was used with no reradiation. The following conditions were selected for the analysis:

material : 1.2 inches of Teflon

heat source: $\dot{q}$ = 10 BTU/ft^2 sec recession rate : $\dot{\delta} = 0.00025$ ft/sec

initial temperature: 460° R

Teflon was chosen because it is a material with low thermal conductivity ($k \approx 6.9 \times 10^{-6}$ BTU/ft sec $^{\circ}$R) and diffusivity. The heat rate and recession rate were chosen to give a surface temperature of approximately 1000° F, which is approximately the sublimation temperature of Teflon.

Figure 9 presents a comparison of this model's temperature response with that obtained from Equation 93. As can be seen from this figure, the two solutions are not in agreement, especially for the nodes which are closest to the surface. The disagreement is especially pronounced during the early phase of heating (i.e., the transient heating up phase). This disagreement is the result of the quasi steady state assumption made in the derivation of Equation 29.

Several approximate solutions are available in the literature which take kinetics into account. Two methods, one due to Newman (Ref. 36) and the other due to Newman and Rigdon (Ref. 37), will be briefly discussed and compared. Newman ignores the question of heat transfer entirely by assuming Equation 90 as his temperature distribution, and develops a model for the chemical reactions occurring in the ablating model and thus computes a recession rate. He used the Arrhenius expression to calculate the rate of the decomposition reactions and uses this recession rate to obtain his temperature profile

---

36. Newman, R. L., "A Kinematic Treatment of Ablation," Journal of Spacecraft and Rockets, May-June 1965.

37. Newman, R. L., Rigdon, W. S., "Temperature Distribution in an Ablating Solid," Journal of Heat Transfer, Trans. ASME, Aug. 1966.

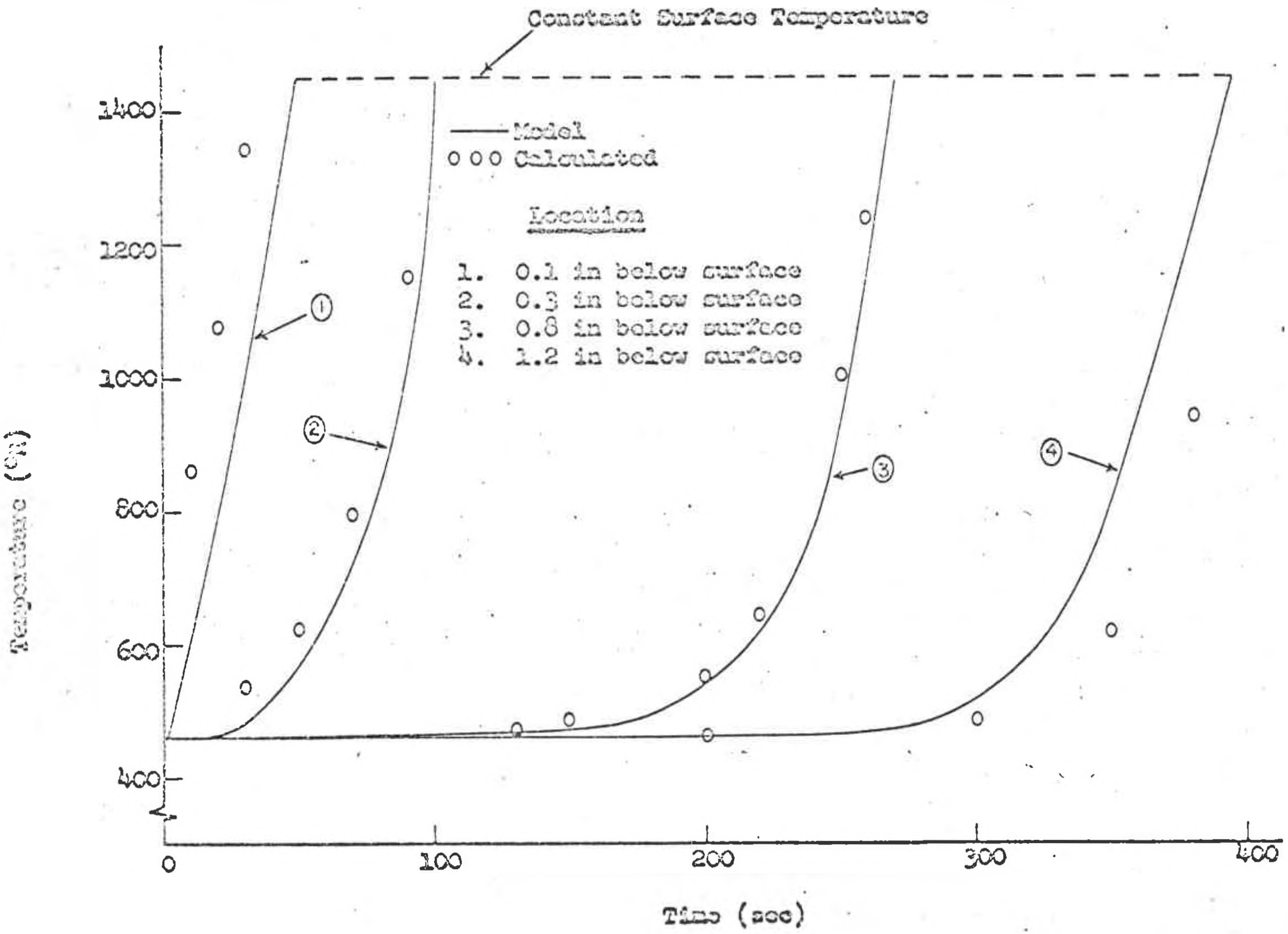

Figure 9. Comparison of Temperature History with Moving Heat Source Solution.

from Equation 90, which is assumed as the temperature distribution. Newman's model is a semi-infinite slab of polymeric material with a heat-flux input at the surface. The physical model is a reacting material moving through the thermal profile, and being completely decomposed into gas at the surface. The reaction is followed with reference to the fraction of bonds in the polymer chain which remain unbroken. Newman and Rigdon extend Newman's original model by keeping the model on the degradation of the bonds and deriving a temperature distribution. The temperature distribution obtained by both methods suffers from the fact that the distribution is a function of distance and not time.

Figure 10 shows a comparison of this model's predicted temperature distribution with those of Newman, Newman and Rigdon, Equation 90 and the experimental data of Hanst (Ref. 38). The distribution obtained from this model is shown for two time periods. Since ablation and its temperature response is a dynamic process, the temperature profiles change with time. It was not possible to obtain temperature distribution for larger time periods with this model due to the small distances involved (i.e., 2×10^{-3} inches). In obtaining the data for Figure 10 the values reported in (Ref. 36) were used.

A simple but interesting expression for the recession rate, taking into account kinetic considerations, is reported in (Ref. 39).

---

38. Hanst, P. L., "Surface Temperature Measurements on Ablating Missile and Satellite Heat Shields Materials," Temperature - Its Measurement and Control in Science and Industry, Reinhold Publishing Co., New York, 1962.
36. Ibid.
39. Freedman, S. I., "Heat Transfer with Chemical Reactions," Developments in Heat Transfer, ed. by W. M. Rohsenow, The M.I.T. Press, Cambridge, Mass.

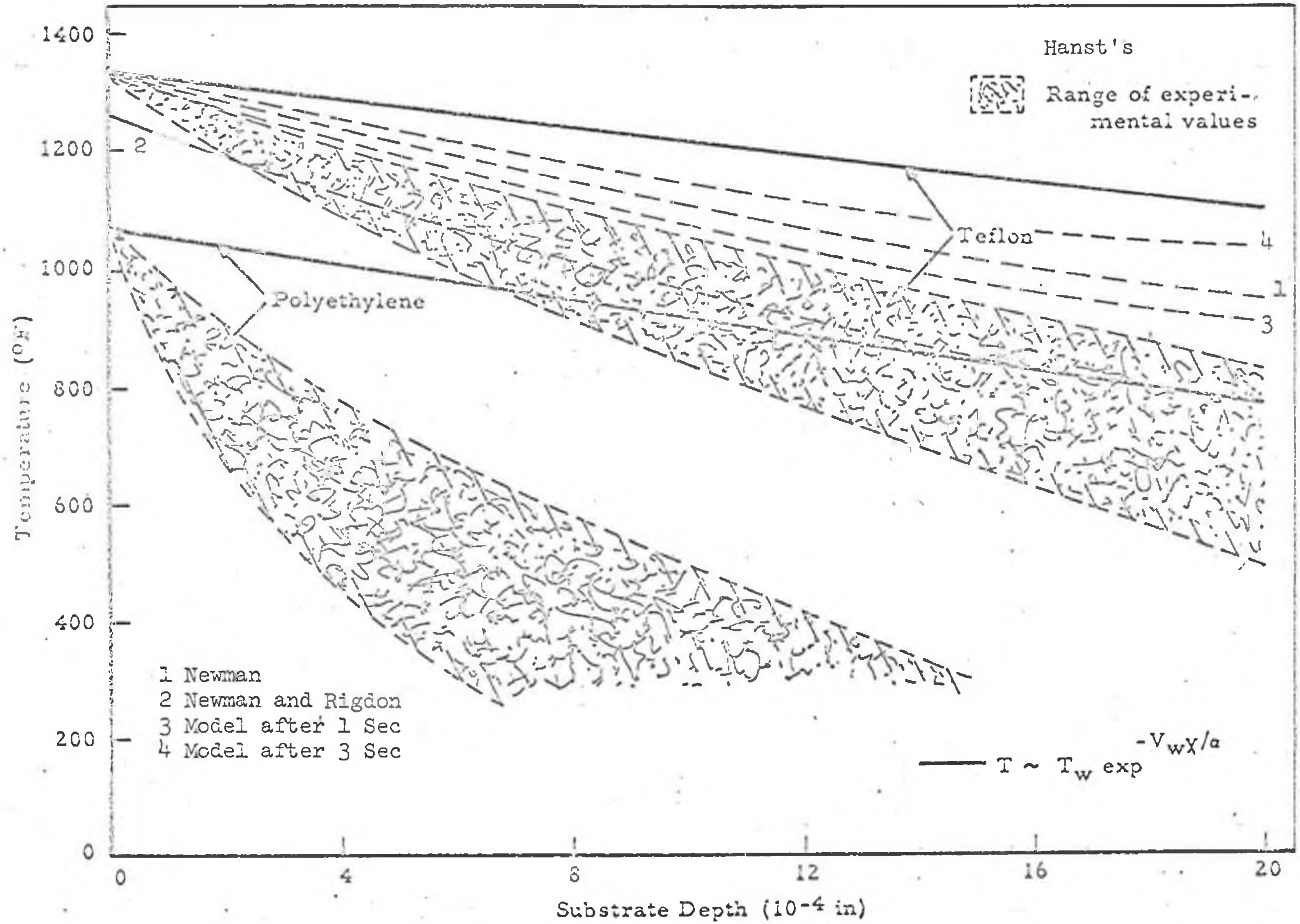

Figure 10. Comparison of Temperature Distribution by Several Methods.

According to this reference an ablating substance which is a solid under ordinary conditions partially decomposed into a gas at elevated temperatures, according to the relationship based on a first-order decomposition reaction rate:

$$\dot{m}_g = \frac{dm}{dt} = \quad \Gamma m B e^{-E/RT} \tag{94}$$

which is essentially Equation 11. Dividing by the density and integrating over the entire volume being heated, one obtains:

$$\dot{s} = \int_0^\infty B e^{-E/RT} dx \tag{95}$$

where $\dot{s} = - V_w$ is the rate at which the surface is receding. The gasification ratio for a sublimer, such as Teflon, is unity and will be omitted for clarity. If the temperature distribution, given by Equation 90 with its exponent linearlized, is substituted into Equation 95, the recession rate becomes:

$$\dot{s} = \left[\frac{B e^{-E/RT_s}}{\left(\frac{E}{\alpha RT_s}\right)\left(1 - \frac{T_i}{T_s}\right)} \right]^{\frac{1}{2}} \tag{96}$$

For Teflon the following parameters are reported (Ref. 39):

activation energy: $E = 81{,}400$ cal/mole

collision frequency factor: $B = 9.4 \times 10^{18}$ 1/sec

For an assumed surface temperature of 1250° F an ablation rate of 0.0001 ft/sec is predicted by Equation 96.

Equation 96 has several shortcomings. Linearizing the exponent $\dot{s}x/\alpha$ can only be justified if this term is small; the kinetic constants,

---

39. Ibid.

B and E, are experimentally determined and the data is subject to much scatter, and finally the surface temperature of the ablating material must be known. The surface temperature is obtainable only from an energy balance since usually the heat flux is known but not the surface temperature.

A simple expression for the mass loss rate of the virgin plastic of a charring ablator can be formulated (Ref. 40) by considering a steady state energy balance for a control volume which encloses the char. Thus,

$$\psi \dot{q}_{aero} - \epsilon \sigma T_s = \dot{m}_p H_p + \dot{m}_p \Gamma c_g (T_s - T_a) + \dot{q}_k \quad (97)$$

convective heat to char surface	-	heat reradiated from char surface	=	heat absorbed by pyrolysis	+	heat absorbed by gases during passage through char layer	+	heat conducted into virgin plastic

reduces to:

$$\dot{m}_p = \frac{\psi \dot{q}_{aero} - \epsilon \sigma T_s^4 - \dot{q}_k}{H_p + \Gamma c_g (T_s - T_a)} \quad (98)$$

or:

$$\dot{m}_g = \Gamma \dot{m}_p$$

Equation 98 is compared with Equations 28 and 30 in Table III. The data is for nylon phenolic during a portion of a re-entry trajectory in which the heating rate was approximately constant and had a value of 20 BTU/ft^2 sec. Table III shows that the steady state equation underestimates the rate of mass loss and that for small mass loss rates Equation 30 as a good approximation of Equation 28.

---

40. Reinikka, E. A., Wells, P. B., "Charring Ablators in Lifting Entry Vehicles," Journal of Spacecraft, Jan. 1964.

TABLE III. COMPARISON OF SEVERAL METHODS OF CALCULATING $\dot{m}_g$

$\dot{m}_g$ (lbs/ft^2 sec)	Equation 98	Equation 30	Equation 28
	0.00165	0.00261	0.00262

4.4 Comparison with Experimental and Flight Test Data

Ablative materials have been used as thermal protection system in a great number of flight tests. However, due to the classified nature of this work much of this data is not available to the general public. A free flight investigation of an ablating body is reported in (Ref. 41). A five-stage rocket propelled research vehicle system was flown to a maximum Mach number of 13.1 at an altitude of approximately 78,000 feet to determine the ablation characteristics of Teflon in free flight. The six inch radius Teflon nose cone was fixed to the fifth stage. The launch vehicle consisted of five stages with an Honest John M6 rocket motor as the first stage. The second and third stages were Nike M5 motors. The fourth stage was an XM19 Recruit motor, and the fifth stage sustainer was a T55 rocket motor. Continuous in-flight measurements were made of the ablating nose cone using sensors developed by the National Aeronautics and Space Administration. One of the sensors was located at the stagnation point. The stagnation point aerodynamic heating was computed using Equation 46. The trajectory and stagnation point aerodynamic heating were used as inputs to the model, obtained from (Ref. 41). The five-stage trajectory lasted for approximately 100 seconds. Severe aerodynamic heating ranging from 90 BTU/ft^2 sec to 530 BTU/ft^2 sec was encountered for approximately two seconds.

41. Winters, C. W., et al, "A Free-Flight Investigation of Ablation of a Blunt Body to a Mach Number of 13.1," NASA TN D-1500.

Figure 11 compares the ablated length predicted by this model with that obtained from the flight test. The agreement between the calculated curve and the measured data is quite good.

In order to verify the fully charring ablation model, an example of a typical charring material was obtained from (Ref. 42). This reference presents test results and results predicted with a digital charring ablation model. The charring ablation material under consideration is Phenolic Nylon, initially 1.6 inches thick with an adiabatic back surface and a constant heat flux of 95 BTU/ft^2 sec applied to the front surface. The surface is assumed to recede at a constant velocity of 0.0009 in/sec. The recession rate, $\dot{\delta}$, was determined from actual test results obtained in an arc tunnel operating in a nitrogen environment. The properties used for Phenolic Nylon were obtained from (Ref. 42).

Two runs were made with our model in order to simulate this problem. The object of the first computer run was to obtain the in-depth temperature distribution to see how well these correlate with the measured values. For this case the discrete recession model was used with the recession rate of 0.0009 in/sec as an input. The second computer run was used to see if our computer model could actually predict the recession rate, given the heating rates and material properties. For this situation the continuous recession model described in Section II was used.

---

42. Curry, D. M., "An Analysis of a Charring Ablation Thermal Protection System," NASA TN D-3150, Dec. 1965.

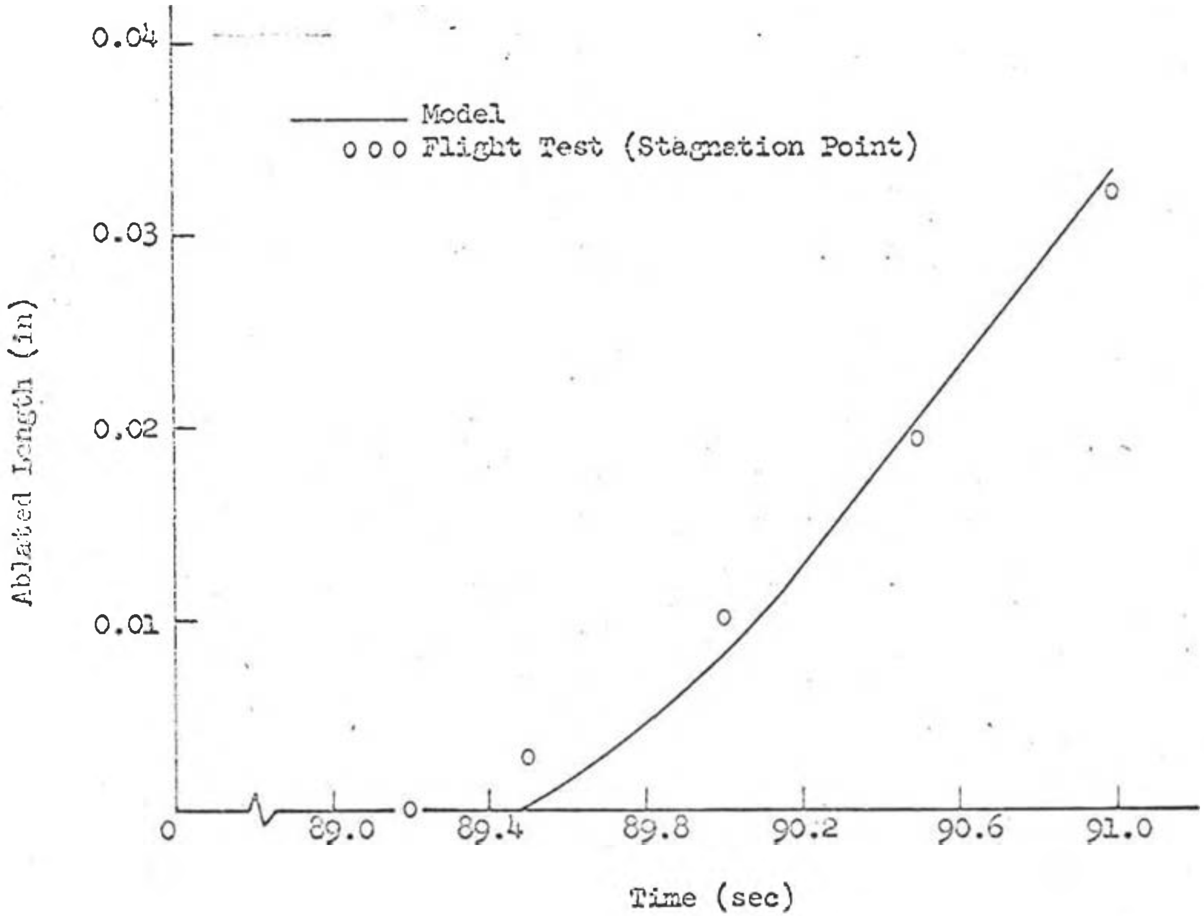

Figure 11. Comparison of Ablated Length with Flight Test Data.

Figure 12 presents a comparison of the in-depth temperature with the actual test results obtained in an arc tunnel as reported in (Ref. 42). The arc tunnel test temperature distribution was obtained by thermocouples instrumented within the Phenolic Nylon sample. The results between the predicted and test results are in fair agreement. The disagreement could be attributed to several possible errors: thermal property values, incorrect location of thermocouples, the fact that the thermocouples' instrumentation wires could act as heat conductors, and the fact that the surface recession rate was probably not really a constant, but merely an average value obtained from test conditions.

Figure 13 shows the surface recession obtained from the given constant recession rate and the surface recession predicted by this model. The figure shows that the model predicted the surface recession rate fairly well.

The following section will present the results of an experimental investigation. In this experimental study specimen of Teflon and Carbon Phenolic were subjected to various heating rates and the time to burn through was determined. The experimental results will be correlated with those obtained from exercising the ablation model.

---

42. Ibid.

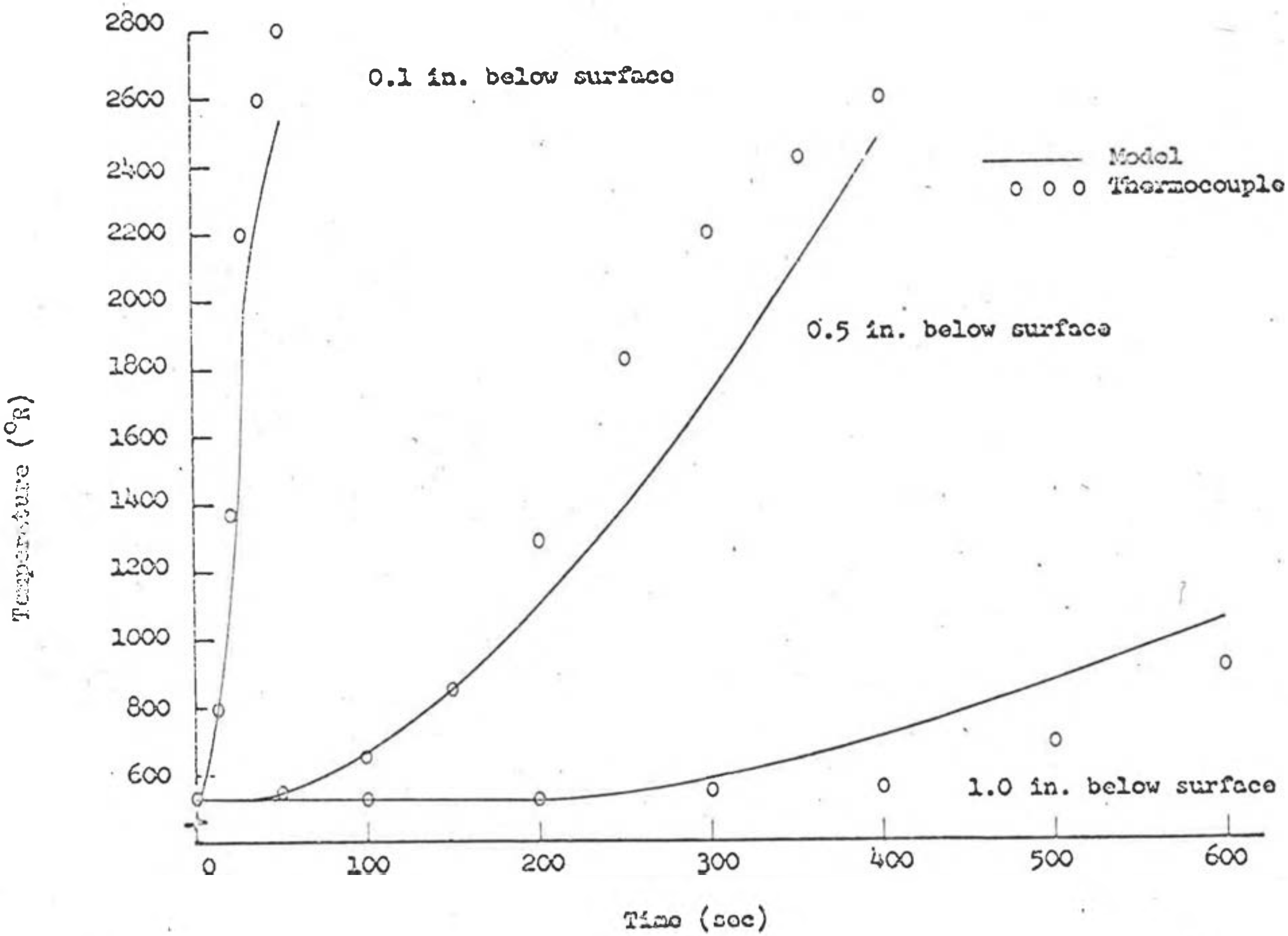

Figure 12. Comparison of Temperature Distribution with Typical Arc Tunnel Test Results.

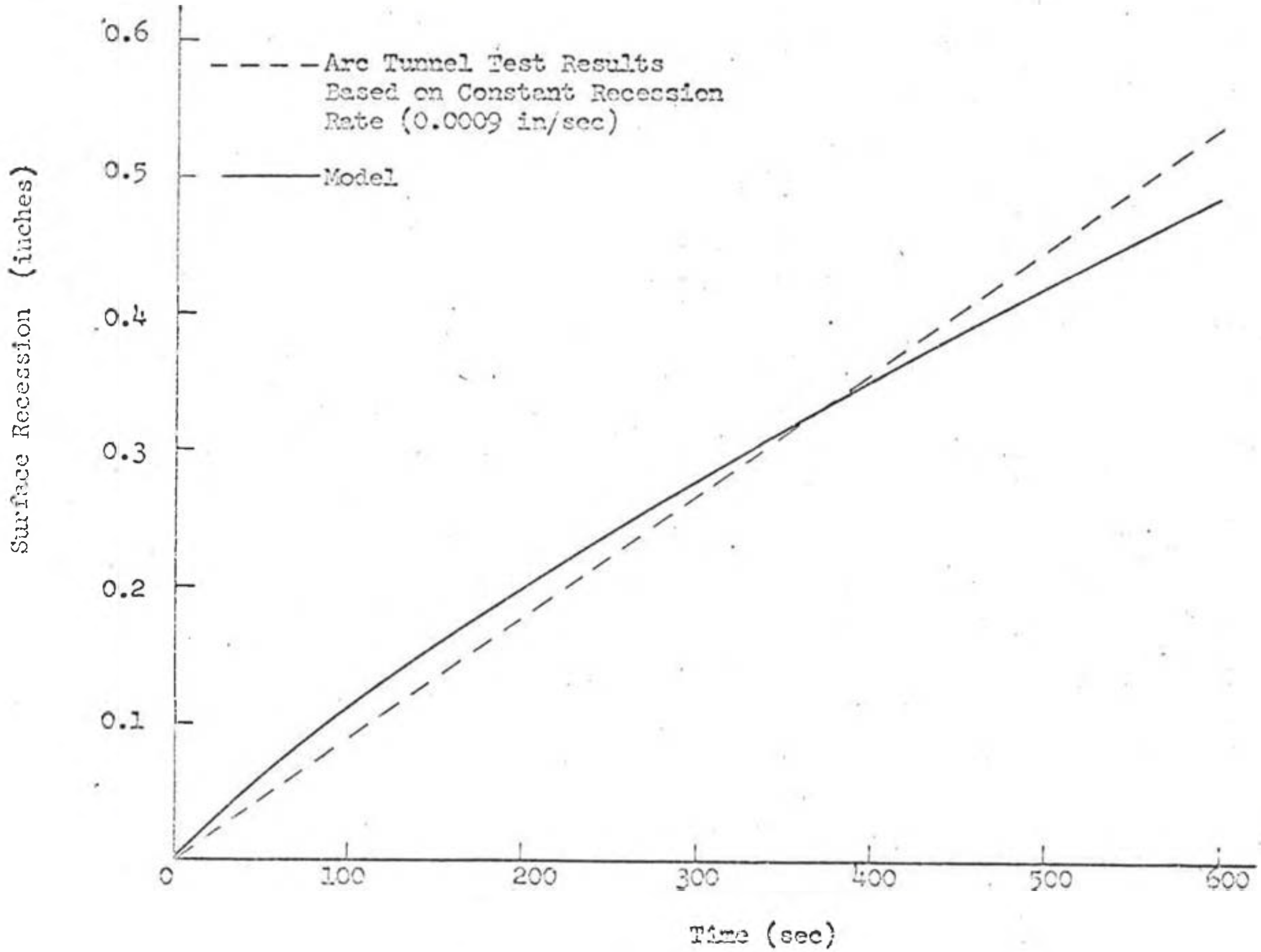

Figure 13. Comparison of Surface Recession with Typical Arc Tunnel Test Results.

V. EXPERIMENTAL INVESTIGATION

The arc-plasma-jet heater has successfully been used as a tool for testing, screening, and studying the behavior of ablating materials. In order to obtain some experimental ablation data to compare with the model results, several ablative material specimens were tested in the University of Dayton arc-plasma-jet facility. This facility, shown in Figure 14, is a modified Plasmadyne M-4 plasma jet nominally rated for 100 KW operation. The plasma jet can simulate thermal environment up to 1000 BTU/ft^2 sec but not high shear pressure environment.

The arc-plasma-jet heater discharges a one-half inch effluent, consisting of simulated air (i.e., twenty-one per cent O_2 and seventy-nine per cent N_2) to the atmosphere. A fixture employing a rotating plate, pivoted on a roller bearing located below and to the rear of the plasma torch, is used to introduce specimens and instrument probes into the plasma effluent. The facility features a combined pitot-tube-calorimeter shown in Figure 15. In this configuration the pitot tube is located in the water cooled guard ring of the probe, directly below the centerline of the calorimeter face. To obtain a pressure measurement the calorimeter portion of the probe assembly is centered in the flow and then the entire probe lifted a preset distance by a mechanical lever to position the pitot tube orifice. Heat flux is determined with the water-cooled calorimeter at ninety degrees to the arc effluent.

The arc-plasma-jet facility is instrumented for the continuous measurement of temperature-time histories of both front and back surfaces of specimens during tests. A pair of Leeds and Northrop total

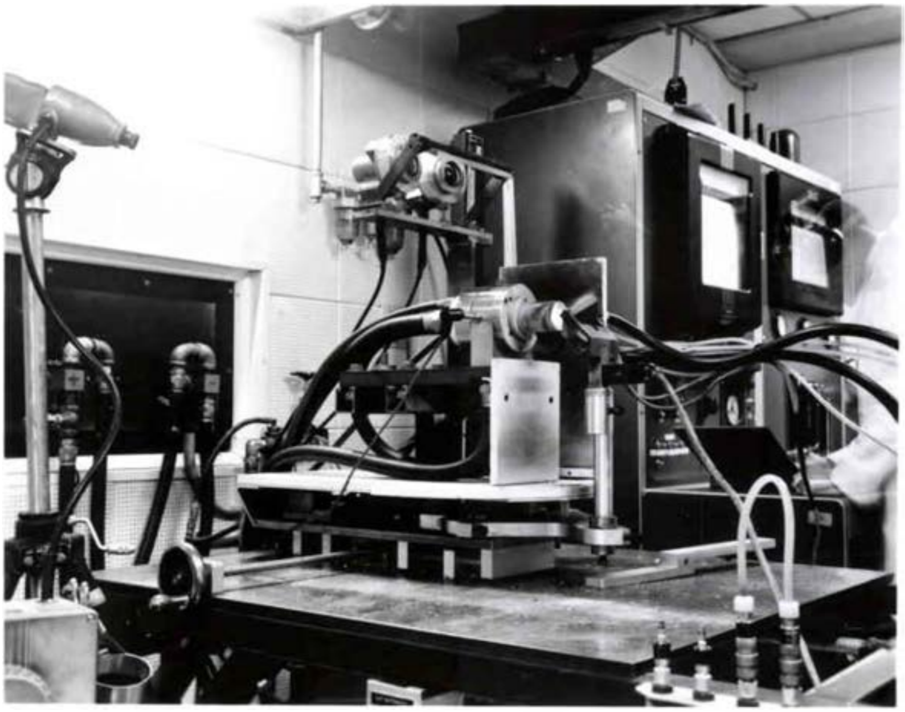

Figure 14. The 100 KW Arc Plasma Jet Testing Facility

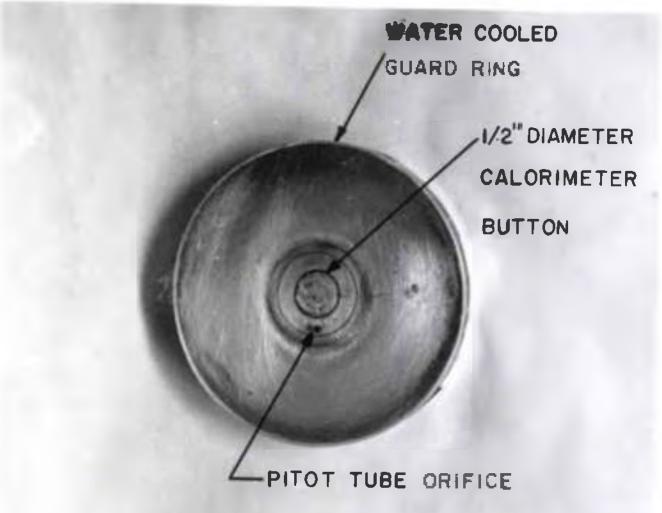

Figure 15. Front View of Calorimeter-Pitot-Tube Assembly

radiation pyrometers with ranges of 1380° F to 2970° F, and 2700° F to 5950° F, are employed for front surface temperature measurement. The output of one instrument is recorded by a Leeds and Northrop Speedomax recorder which by means of a cam actuated mechanism, switches the recorder from the low range pyrometer to the high range pyrometer whenever specimen temperatures exceed 2800° F. Front surface temperatures can also be measured with an IR radiation pyrometer. This pyrometer is used to measure ablators, such as Teflon, which have a low surface temperature. A hand held optical radiation pyrometer can also be used to measure surface temperature. However, this method was found to be unreliable at low surface temperatures.

Spring loaded Pt + Pt 13% Rh contact thermocouples referenced to 32° F are used, in conjunction with a Brown millivolt recorder, for the measurement of the specimen's back surface temperature.

Electric power to the plasma head is measured with a voltmeter and ammeter. All specimens are tested at a sample distance of 1-1/8 inches from the torch exit, with the desired heat flux at the sample obtained by varying the electrical power to the arc. The arc-plasma-jet facility can be used to evaluate flat plate, rod, or disc specimens. The operating conditions of the plasma jet prior to actual testing are determined from the following measurements: nitrogen and oxygen flow rate, input power to the arc, plasma jet coolant losses, heat flux at the sample location, and stagnation pressure of the stream at the sample location. The following effluent properties can then be calculated: gas enthalpy at the nozzle exit, gas velocity at the sample, and gas temperature at the nozzle exit.

Prior to running a group of test specimens at a given heat flux level, the following procedure is used to define the properties of the environment. With the combined calorimeter-pitot tube probe inserted on a rotating fixture so that the probe's face is at an angle of 90° to the discharge effluent, the fixture is positioned axially to locate the face of the probe at the desired specimen location. With the probe clear of the discharge path, the arc is initiated and nitrogen and oxygen gas flow rates are adjusted to the desired values and the power to the arc regulated to obtain a stable effluent. The calorimeter is centered in the effluent and power to the arc is adjusted until the desired heat flux level is achieved. This power level is maintained during the remainder of the calibration, and throughout the test. Then, the entire probe is lifted by a mechanical lever to position the pitot tube orifice and obtain the pressure.

The water flow rate through each section of the arc chamber and nozzle assembly is determined by the stop watch-weight tank method, and the inlet and outlet water temperature of each section is recorded to determine heat losses to the coolant.

Immediately after completing the calibration procedure, specimens which had been previously measured and clamped into holders are introduced into the effluent for test. In testing a number of specimens at the same heat flux level, the colorimeter is re-inserted into the discharge prior to the exposure of each specimen to recheck the initial calibration.

Prior to testing, the weight, density and physical dimensions of each specimen are determined. The samples are cleaned, their face dimensions determined by scale measurement and their thickness determined by use of a micrometer. Moderately porous specimens are sprayed with Krylon to seal the pores. From measurement of specimen weight in air and in water, volume and density are calculated.

During the actual test exposure, the front and back surface temperatures of the specimens are continuously recorded as a function of time, and the front surface temperature is measured periodically with an optical pyrometer.

After a test exposure, the specimen is photographed to show the effects of the environment upon it. Depth of erosion is determined with a standard ball micrometer by measuring the minimum distance from the bottom of the eroded area to the back face of the specimen. The sample is then sprayed with Krylon, the weight in air and water is determined and thus the post test volume and density is calculated. Volume of erosion and weight loss during test are calculated by difference.

Glass bead displacement is employed for erosion volume determinations when the conditions of the sample after test do not permit water immersion. However, this method is not particularly reproducible nor accurate.

The methods and equations needed for reducing the experimental data were obtained from (Ref. 43, 44) and will not be repeated here.

The environment in which an ablative material must ultimately perform is too complex to be simulated in simple laboratory tests.

---

43. Wurst, J. C., Gerdeman, D. A., "Arc Heater Screening of Ablative Plastics," AFML-TR-65-110, Air Force Materials Laboratory, WPAFB, Ohio.
44. Wurst, J. C., Gerdeman, D. A., "Instructions for Reduction of Plasma Jet Test Data," University of Dayton Bulletin.

The subsonic plasma jet adequately simulates thermal environment but does not simulate high mass flow and high velocity pressure. Thus, this facility is primarily used to screen materials, and for ranking the thermal endurance of ablative materials.

Two types of material specimens were tested in the plasma jet facility. Teflon, which sublimes and has well defined thermophysical properties, and Carbon Phenolic, a modern charring ablator. Specimen geometry was a 2 in. x 2 in. x 3/8 in. plate for Teflon and 2 in. x 2 in. x 1/2 in. plate for Carbon Phenolic. The specimen was oriented at 45 degrees in the subsonic plasma effluent in order to simulate flow over an aerodynamic surface. Both materials were tested, to burn-through, at heat fluxes of 100, 300, 500, and 1000 BTU/ft^2 sec. The measured and calculated parameters for these tests are shown in Table IV for the Carbon Phenolic specimens and in Table V for the Teflon specimens.

An attempt was made to correlate the experimental data with that obtained from our model. The model was run with 10 nodes with and without combustion effects using the continuous recession model. The time to burnthrough, which is a measure of thermal endurance, is shown in Figure 16 for Carbon Phenolic. It is interesting to note that the experimental results were bracketed by the model results. The model results are shown with and without the effects of combustion. A possible explanation for this may be the fact that our gas phase combustion equation, Equation 55, is too conservative. However, the fact that the experimental results are also in disagreement with the no combustion case points to the fact that some combustion must have been present.

TABLE IV SUMMARY OF CARBON PHENOLIC TESTS

Specimen Number	1	2	3	4
Test Duration (sec.)	284	185	143	108
Heat Flux (BTU/ft^2 sec)	100	300	500	1000
Peak Stag. Press. (in. H_2O)	7.6	15.1	19.9	31.7
Input Power Volts/amp	116/143	129/290	139/355	146/502
Outlet H_2O Temp (^oF)	72.2	77.2	81.4	87.2
Inlet H_2O Temp (^oF)	68.2	68.2	68.2	68.2
Coolant Flow (lb/sec)	1.16	1.16	1.16	1.16
Final Optical Temp. (^oC)	1665	2200	2600	2560
Pre Test Mass (gr)	45.23	45.23	45.23	45.23
Input Energy (BTU/sec)	15.69	35.39	46.68	69.33
Coolant Losses (BTU/sec)	4.64	10.44	15.31	22.04
Enthalpy (BTU/sec)	1347	3042	3825	5767
Gas Temp. (^oF)	4132	6392	7495	9825
Gas Exit Velocity (ft/sec)	422	839	1106	1762
Post Test Mass (gr)	12.25	14.13	15.48	16.62

TABLE V SUMMARY OF TEFLON TESTS

Specimen Number	5	6	7	8
Test Duration (sec.)	89	29	24	20
Heat Flux (BTU/ft^2 sec)	100	300	500	1000
Peak Stag. Press. (in. H_2O)	7.5	15.5	20.1	31.5
Input Power Volts/amp	115/145	132/295	140/357	145/500
Outlet H_2O Temp (^oF)	72.4	78.5	82.4	86.8
Inlet H_2O Temp (^oF)	68.2	68.2	68.2	68.2
Coolant Flow (lb.sec)	1.16	1.16	1.16	1.16
Final Optical Temp. (^oC)	1195	1340	1425	1470
Pre Test Mass (gr)	53.09	53.09	53.09	53.09
Input Energy (BTU/sec)	15.77	36.83	47.28	68.58
Coolant Losses (BTU/sec)	4.87	11.95	16.47	21.58
Enthalpy (BTU/sec)	1329	3035	3757	5732
Gas Temp (^oF)	4088	6385	7380	9800
Gas Exit Velocity (ft/sec)	417	861	1117	1751
Post Test Mass (gr)	25.14	25.81	26.08	26.27

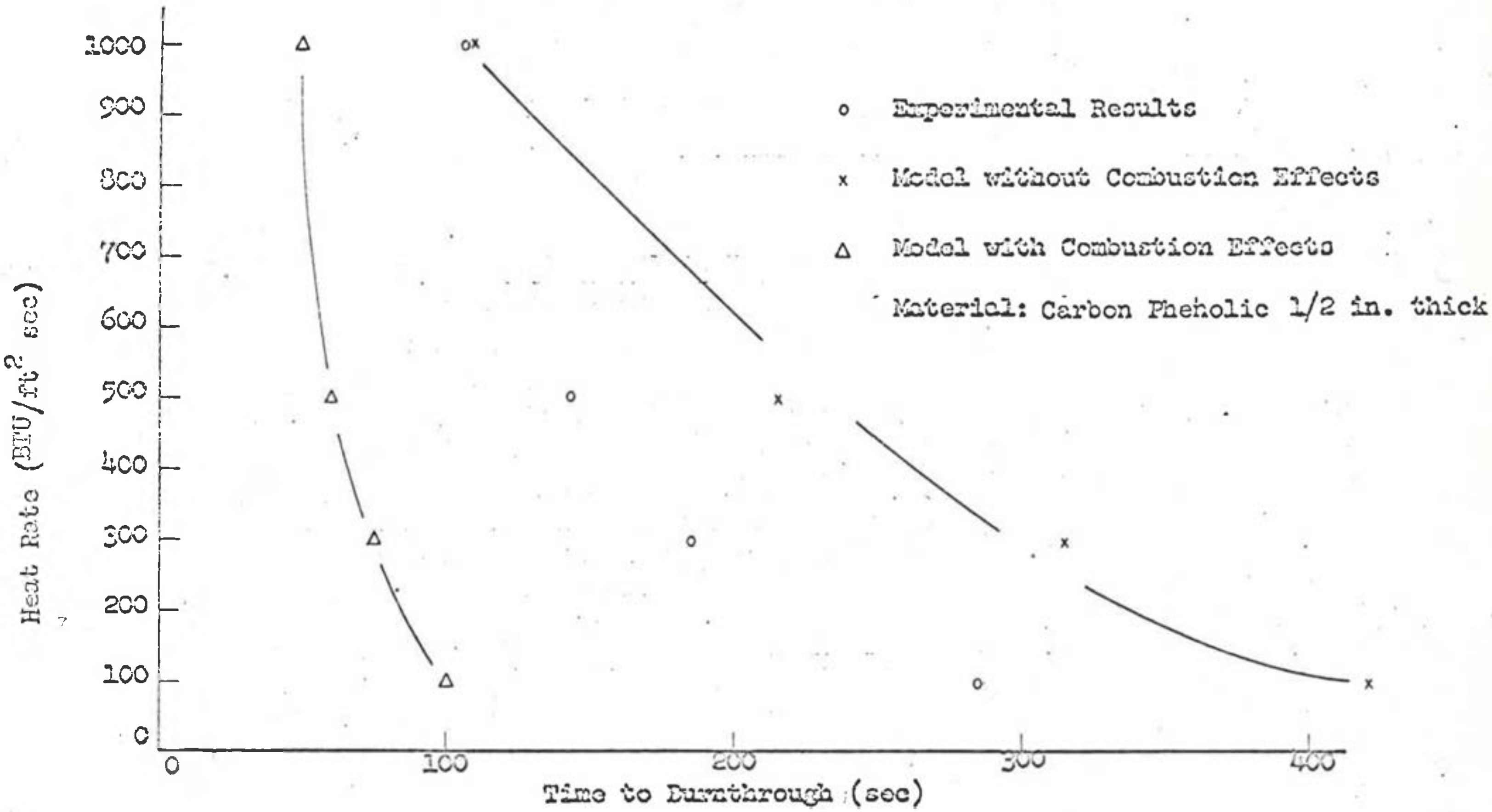

Figure 16. Thermal Endurance of Carbon Phenolic.

Figure 17 presents the time to burnthrough for Teflon. Again, the test results are bracketed by the model results, with the exception of the specimen which was subjected to 1000 BTU/ft^2 sec. In addition, Figure 17 shows a shaded area which is the calculated time to burnthrough using curves for the thermochemical heat of ablation for Teflon. The method utilized in generating this curve is outlined in Appendix I. The left hand portion of the shaded area accounts for combustion effects, while the right hand side of the shaded area neglects combustion effect. The thermochemical heat of ablation for Teflon has been studied extensively and the reported values are thought of as reliable and usable for the preliminary design of heat shields. Thus, data points falling near the shaded area can be thought of as being correct.

Figure 18 shows the average recession rate, which was obtained experimentally, for Teflon and Carbon Phenolic. Since the model results would bracket the experimental results, shown in Figure 18, in the same manner as Figures 16 and 17, they have been omitted from this figure.

Post test photographs of Carbon Phenolic and Teflon are shown in Figures 19 and 20, respectively. Both figures show the respective specimens after being tested at heat fluxes of 100 and 1000 BTU/ft^2 sec. The delamination of Carbon Phenolic can be clearly seen. This may result from thermal stress or internal pressure buildup. The Carbon Phenolic specimen tested at 1000 BTU/ft^2 sec, seemed more charred and warped than the specimen which was tested at a heat flux of 100 BTU/ft^2 sec. The carbon cloth reinforcement is clearly seen in Figure 19. However, Teflon, Figure 20, ablated very cleanly and no warpage was noticed. The severity of the heating did not drastically affect the

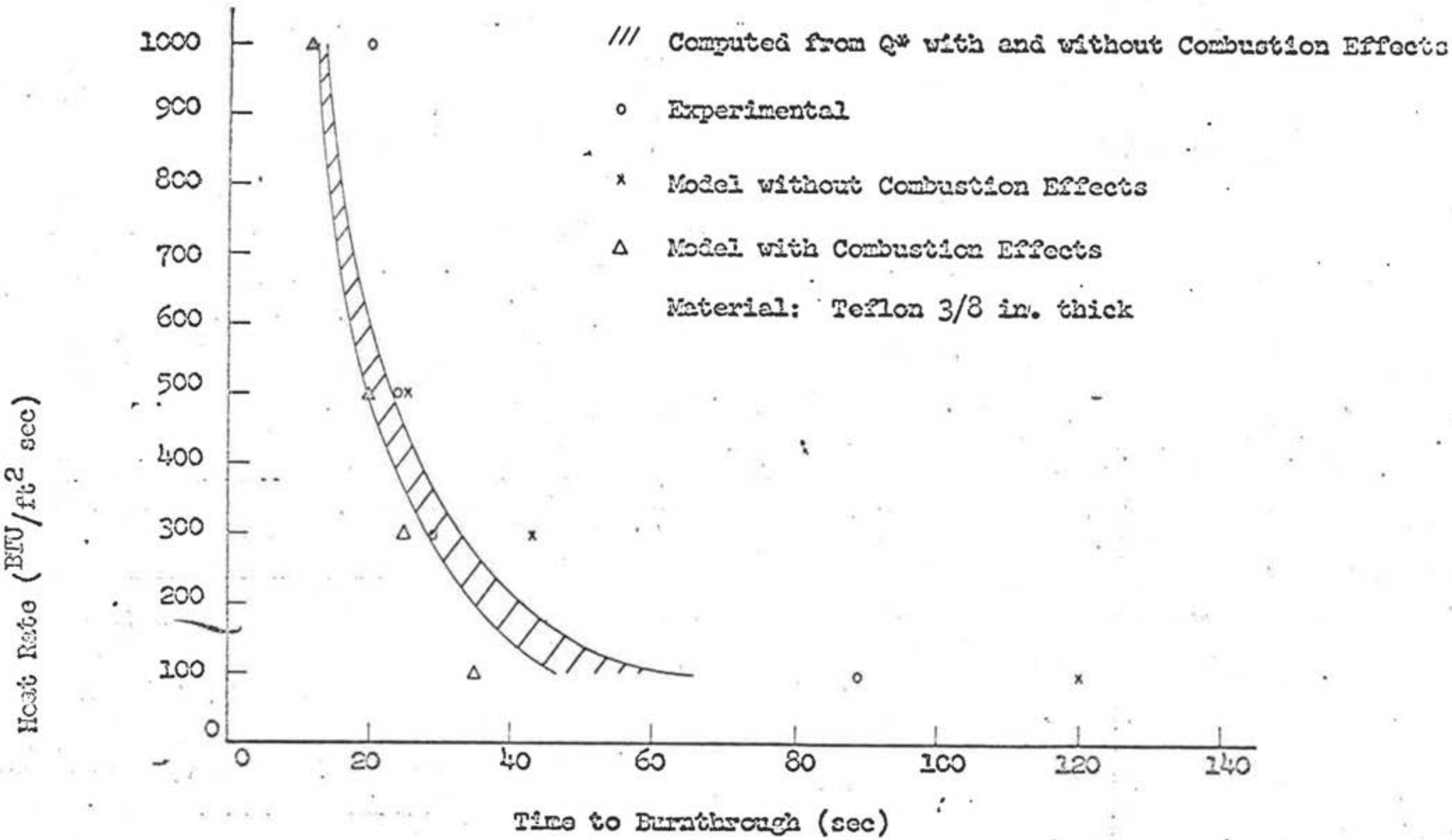

Figure 17. Thermal Endurance of Teflon.

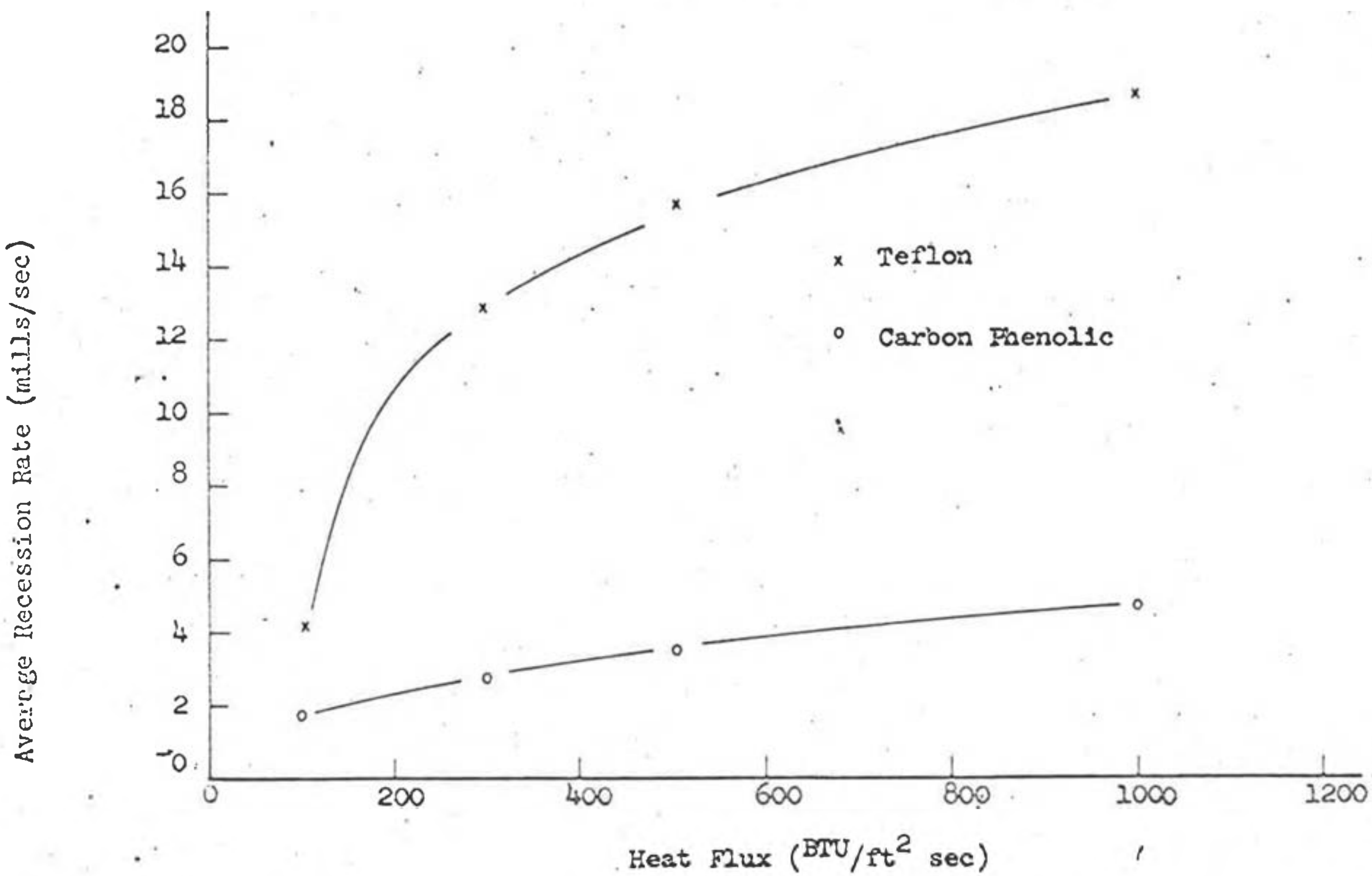

Figure 18. Experimentally Determined Average Recession Rate for Teflon and Carbon Phenolic.

Test at Heat Flux of 100 BTU/ft^2 sec.

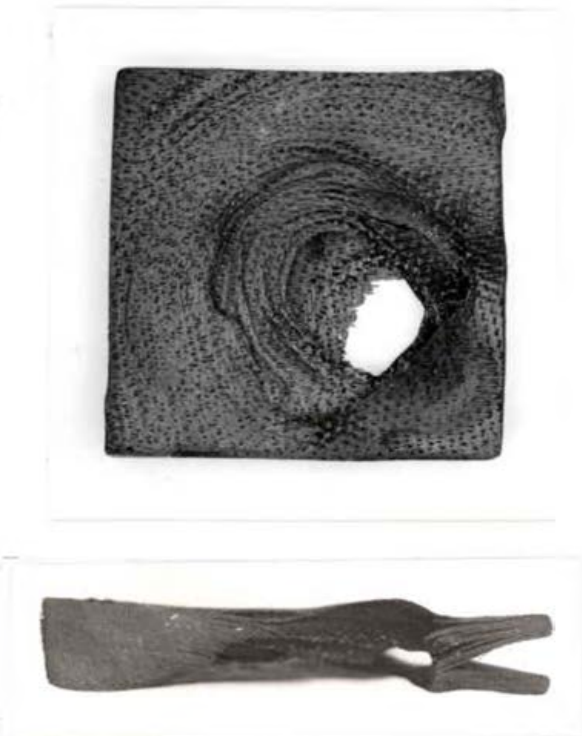

Test at Heat Flux of 1000 BTU/ft^2 sec.

Figure 19. Post Test Photographs of Carbon Phenolic Showing the Effects of Thermal Environment.

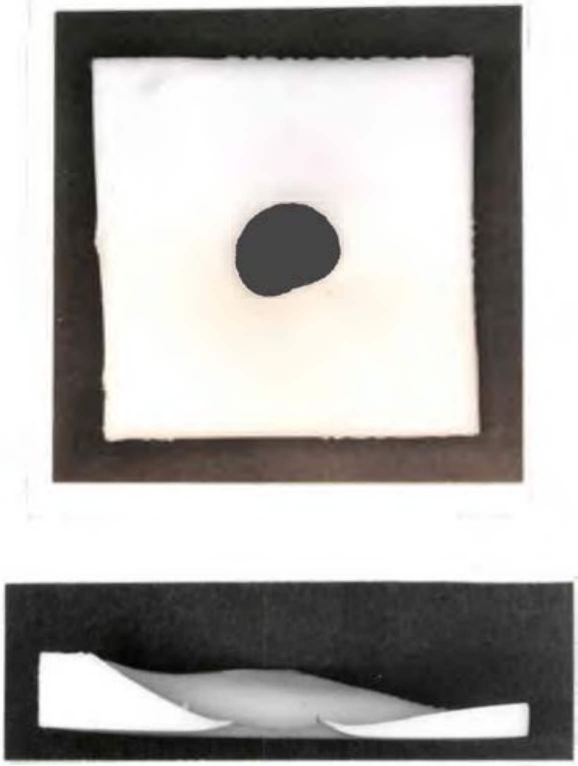

Test at Heat Flux of 100 BTU/ft^2 sec.

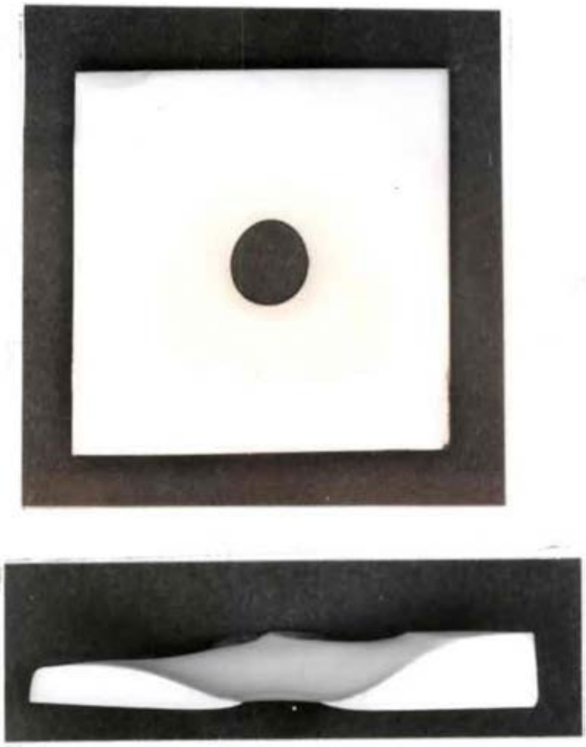

Test at Heat Flux of 1000 BTU/ft^2 sec.

Figure 20. Post Test Photographs of Teflon Showing the Effects of Thermal Environment.

appearance of Teflon at post test inspection. A possible explanation for this is that Teflon ablates at a nearly constant surface temperature which is rather low (i.e., circa 800° F) and has no reinforcements. On the other hand, Carbon Phenolic is a charring ablator and its surface supports high temperature, up to 5000° F, which enhances the possibility of delamination and warpage due to the great temperature differences which may exist.

It has been stated previously that the plasma-jet test facility is equipped to record the surface and substrate temperature continuously. Figure 21 compares the measured substrate temperature with that obtained from the model. The agreement is not very good. Part of the explanation may lie in the fact that a spring loaded contact thermocouple was used to experimentally measure the substrate temperature. Contact thermocouples are believed to be somewhat limited in their ability to predict true substrate temperature. Another possible limitation may be that the thermophysical properties which were inputed to the model were in error.

In the modeling of the ablator Teflon it was assumed that this ablator sublimed at a constant temperature of 800° F. It was interesting to note that the measured surface temperature of Teflon was insensitive to heat flux. The recorded surface temperature of Teflon seemed to vary between 650° F and 750° F for all the thermal environments used in this analysis.

Figure 22 compares the experimentally determined backface temperature of Carbon Phenolic with the backface temperature determined for by the model. The case shown is for Carbon Phenolic specimen number four which was subjected to 1000 BTU/ft^2 sec. The explanation for the

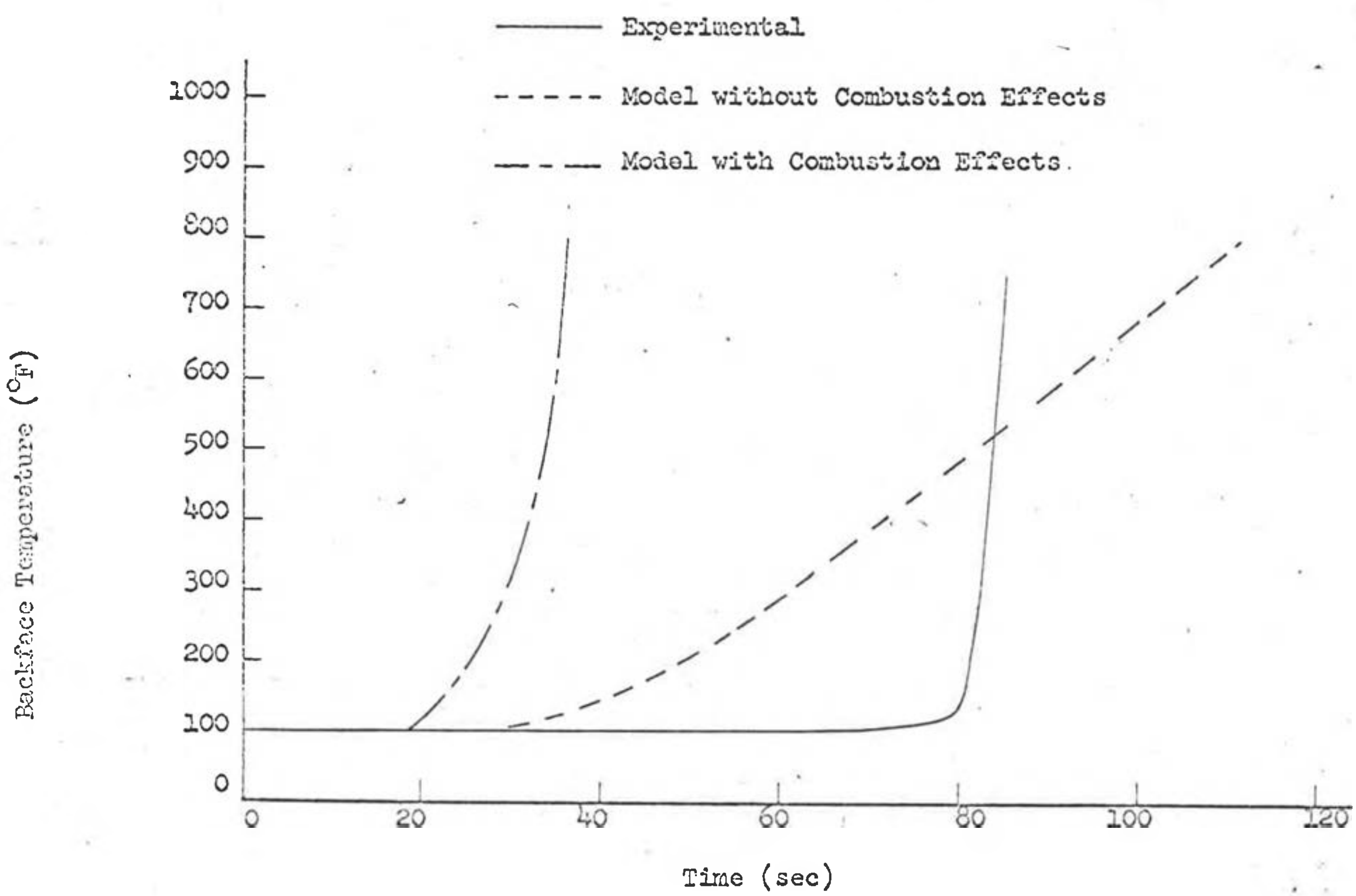

Figure 21. Backface Temperature for 3/8 inches of Teflon Subjected to 100 BTU/ft^2 sec.

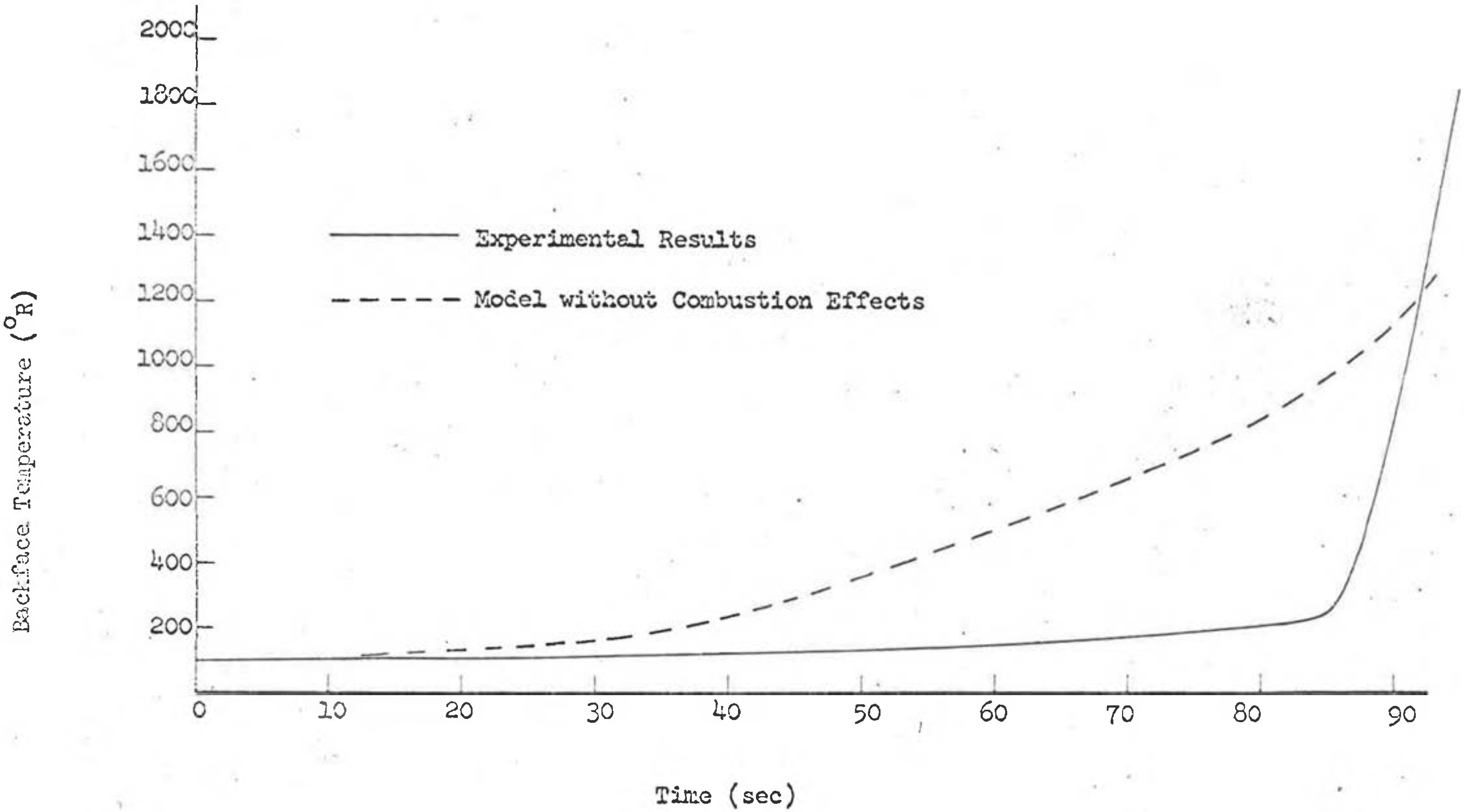

Figure 22. Backface Temperature for 1/2 inches of Carbon Phenolic Subjected to 1000 BTU/ft^2 sec.

disagreement can be attributed to several sources. Among them are the limitations of the contact thermocouple and the fact that the thermophysical property data that was used in the model analysis is not well defined and subject to errors.

The surface temperature of Carbon Nylon specimen four is illustrated in Figure 23. Approximately a twenty per cent error between the experimental and model results is evident. A total radiation pyrometer was used to experimentally measure surface temperature. This pyrometer is subject to errors such as the reflection of the arc from the surface of the specimen and calibration errors.

The model predicts a temperature of approximately 6000° F with a slight rise in temperature as the run progresses. The high temperatures supported by Carbon Phenolic are an indication that much of the incident heat is rejected by radiation.

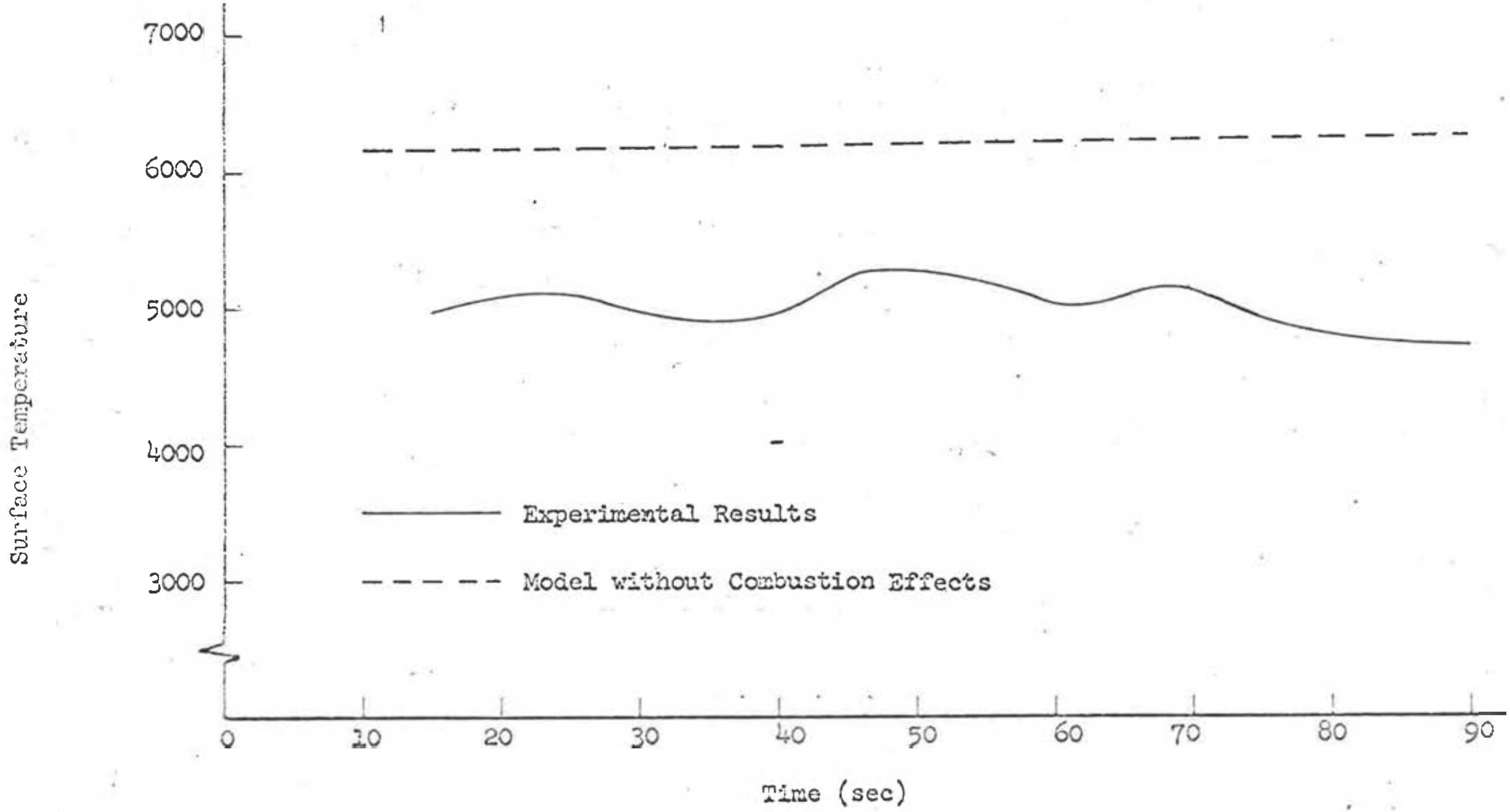

Figure 23. Surface Temperature for ½ inches of Carbon Phenolic Subjected to 1000 BTU/ft^2 sec.

VI. CHAR REMOVAL MECHANISMS

It has been stated in a previous section that the char removal or surface recession problem can be an enormous problem to handle analytically. Thermal stresses, pressure gradient shear, aerodynamic shear, and surface thermochemistry all can contribute to char removal and mass loss. All these char removal mechanisms can contribute in varying degrees under proper environmental conditions. Under some flight conditions, the prediction of surface recession is complicated because of the simultaneous application of aerodynamic shear, pressure gradient shear, thermal stress, and high temperatures. In a high shear environment, understanding material response to this high shear environment is difficult since the high temperature aerodynamic shear can not be measured and must be inferred from heat transfer measurements. The pressure gradient shear can only be calculated or inferred from mass loss measurements, and the thermal stresses in the char layer can only be estimated or guessed since the thermophysical properties are not well defined and the char layer thickness may be only a few hundredths of an inch thick. The complexity of surface thermochemistry has already been pointed out in Section III when combustion was discussed. According to (Ref. 45) at least seventy-six reactions are required to describe the kinetics for the system carbon-ethane-oxygen. While some thermodynamic and kinetic data are available, the problem is so complex that

---

45. Slaughter, J. I., "Performance of Re-entry Thermal Protection Materials," International Symposium on High Temperature Technology, 1967.

one must resort to some approximate solution. One such expedient is suggested by Scala (Ref. 25) who proposed that the gases injected into the boundary layer are principally CO and CO_2, which result from chemical reactions between the surface of the graphite in the hypersonic stream.

The purpose of this section is to present a survey of the current state of the art on char removal mechanisms. Any or all of the methods, which will be subsequently discussed, can be included in the proposed ablation model. The principal mechanisms of char removal which will be covered in this section are: thermochemical effects (i.e., removal of char by reaction or diffusion controlled oxidation or sublimation); intermittent spallation caused by thermal stresses, surface shear forces, and the internal stresses due to the gas pressure build-up within the char; and several empirical formulations which predict a maximum char thickness based on selected experimental results.

6.1 Char Removal by Thermochemical Effects

A series of tests were conducted by Lundell, Dickey, and Jones and reported in (Refs. 46 and 47). In these series of experiments, spherical samples of phenolic nylon were subjected to a series of tests at moderate pressures and high heat flux in both an inert nitrogen environment and in an air environment. In the nitrogen environment very little char loss was apparent until a surface temperature of 6000° R

25. Ibid.
46. Lundell, J. H., Wakefield, R. M., Jones, J. W., "Experimental Investigation of a Charring Ablative Material Exposed to Combined Convective and Radiative Heating, AIAA Journal, Nov. 1965.
47. Lundell, J. H., Dickey, R. R., Jones, J. W., "Performance of Charring Ablative Materials in the Diffusion Controlled Surface Combustion," presented at AIAA Thermophysics Specialist Conference, New Orleans, La., April 17-20, 1967.

was reached. After the surface temperature reached 6000° R a vast increase in char recession rate was apparent. The theoretical work of Scala and Gilbert (Ref. 25) on the ablation of graphite indicates that sublimation occurs at this temperature.

The series of tests were then repeated in an air environment. The results below 6000° R correlated very well with Scala's theory on diffusion controlled surface combustion for graphite. Thus, the mechanism of char removal was thought to be due to diffusion controlled oxidation. When the same tests were conducted at high pressures, the char removal rate was greater than that predicted by the diffusion controlled rate. This indicates that other mechanisms of char removal, beside diffusion, were now present.

The work of Scala and Gilbert (Ref. 25) on the ablation of graphite is in wide use and will be briefly discussed in the ensuing paragraphs.

In accordance with the work of Scala and Gilbert, the performance of char in char forming ablative materials is greatly dependent on its surface temperature and to a lesser extent on pressure as evidenced from Figure 24. The surface temperature controls the mechanism of char removal which may include reaction-rate-controlled oxidation, transition oxidation, diffusion-controlled oxidation, and sublimation regimes. The oxidation rate of carbonaceous materials in these regimes is dependent on surface temperature, the reactivity of the carbon, and the diffusion processes in the gaseous boundary layer. At higher surface temperatures the nitrogen reactions must be accounted for as well as the homogeneous and heterogeneous chemical reactions occurring between

---

25. Ibid.

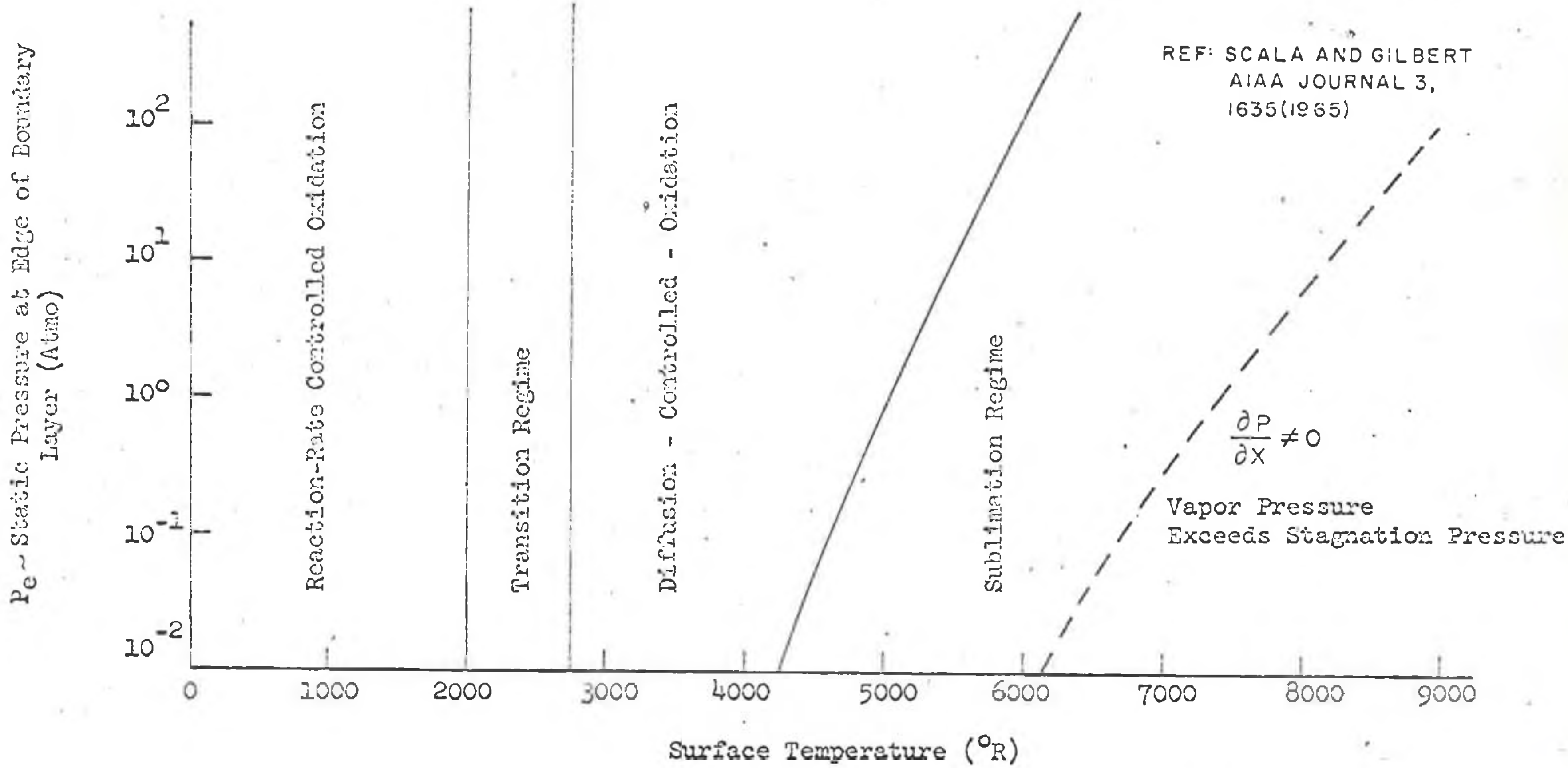

Figure 24. Mass Transfer Regimes for Ablating Carbon (Char)

the oxygen present in the boundary layer and carbon. In this ultra-high surface-temperature regime, sublimation of the graphite is the mode of char mass loss.

6.2 Rate Controlled Oxidation

The rate controlled regime is defined as the regime where the oxygen is supplied at a greater rate than it can be consumed, and thus the chemical reaction rate controls the process of oxidation at surface temperatures below 2000° R. At these low surface temperatures both CO and CO_2 can be detected adjacent to the surface, although there is still some disagreement as to the sequence of the steps in the chemical reactions. Consequently, Scala introduces the following empirical Arrhenius representation for the oxidation rate in the reaction-rate-controlled oxidation regime:

$$\dot{m}_r = k \, (P_{O_2})_w^n \tag{99}$$

where k is the specific reaction rate given by:

$$k = B \, e^{-E/R \, T_w} \tag{100}$$

$(P_{O_2})_w$ is the partial pressure of molecular oxygen near the surface, n is the order of the reaction, E is the activation energy, and B is the effective collision frequency. The chemical kinetic data is experimentally determined and subject to much scatter. Scala (Ref. 25) gives the following bounds on the chemical kinetic properties:

$0 < n < 1$

$8 < E < 60$ kcal/mole

$1 < B < 10^9$ lb/ft^2 sec

---

25. Ibid.

This extremely wide range in chemical kinetic data for char is due to the fact that these properties depend critically on the way in which the charring ablator is manufactured.

It is noted that, in the rate-controlled regime, the rate of oxygen consumption adjacent to the surface is low and that, therefore, the mass fraction of the element oxygen is essentially the same as the undisturbed stream. Also, the atomic species recombines in the low temperature regime adjacent to the surface and thus the mole fraction of molecular oxygen at the wall is very nearly equal to its value in the undissociated air. Further, the static pressure gradient in the reaction zone in a direction normal to the surface is negligible. These considerations enable us to write the partial pressure of oxygen at the surface as:

$$(P_{O_2})_w = X_{O_2} \; P_e \tag{101}$$

Thus, if we assume a reaction rate, n, of one-half, Equation 99 becomes:

$$\dot{m}_r = B \; (X_{O_2} \; P_e)^{0.5} \; e^{-E/R \; T_w}$$

where the mole fraction of oxygen at the wall, $X_{O_2} = 0.21$ in undissociated air.

6.3 Diffusion Controlled Oxidation

The diffusion controlled regime, which is predominant at temperature ranges of 2500° to 5000° R, is defined as the regime where the oxygen can be consumed at a greater rate than the rate at which it is supplied to the surface and thus the oxygen diffusion through the boundary layer controls the process. In this regime the temperature is sufficiently high that carbon dioxide is no longer stable and carbon monoxide is the only product formed at the surface boundary layer, Equation 52. Carbon dioxide is formed only as the carbon monoxide diffuses away from the graphite surface. Since the surface temperature of the ablators of interest fall primarily in this regime, the diffusion controlled regime is probably the most understood and verified.

Swann (Ref. 5) derives equations which can be used in the diffusion controlled oxidation regime. He shows that the maximum rate at which oxygen diffuses to the surface, $\dot{m}_d\ (O_2)$, is given by Equation 54.

The rate of char removal in the diffusion controlled regime, according to Swann, is:

$$\dot{m}_d = \lambda\ \dot{m}_D\ (O_2) \quad \text{or,}$$

$$\dot{m}_d = \frac{\psi\, \dot{q}_{aero}}{h_e - h_s}\ C_e\ (L_e)^{0.6}\ \lambda \qquad (102)$$

where λ, the weight of char removed per unit weight of oxygen, is proportional to the relative amounts of carbon monoxide and carbon dioxide produced. The analytic determination of λ is very complex and can be determined only by a detailed aerothermochemical analysis (Ref. 48). If the assumed reaction at the surface is Equation 52, then $\lambda = 3/4$ if all the available oxygen reacts with the char. However, if only one-half of the available oxygen reacts with the char, $\lambda = 3/8$ instead of 3/4.

---

5. Ibid.
48. Dow, M. B., Swann, T. R., "Determination of Effects of Oxidation on Performance of Charring Ablators," NASA TR R-196, June 1964.

A correlation formula derived by Scala can be used to estimate the mass loss at the stagnation point. This equation has been presented as Equation 51. In deriving this equation the effects of yaw have been disregarded and axially symmetric flow is assumed:

$$\dot{m}_d = 6.35 \times 10^{-3} \left(\frac{P_e}{R_n} \right)^{0.5} \tag{51}$$

where the units of $\dot{m}_d$ are lb/ft^2-sec, P_e in atmospheres and R_n in feet. The total pressure, P_e, can be obtained from the Newtonian pressure law:

$$P_e = P_\infty + \rho_\infty V_\infty^2 \cos^2 \theta \tag{103}$$

which reduces at the stagnation point to:

$$P_e = P_\infty + \rho_\infty V_\infty^2 \tag{104}$$

In (Ref. 49) effective radii for use with shapes other than spherical are discussed.

At this point it is worthy to note that the rate-controlled char loss at the stagnation point is independent of vehicle geometry while the diffusion-controlled mass loss is not.

6.4 Transition Regime

In the transition regime between the rate-controlled regime and the diffusion-controlled regime, the total rate of mass loss of the char is controlled by a combination of diffusion and reaction rate control. In this regime the overall chemical process is limited by the presence of two resistances in series, one chemical (reaction

---

49. Metzger, J. W., Engel, M. J., Diaconis, N. S., "The Oxidation and Sublimation of Graphite in Simulated Re-entry Environment," AIAA Paper No. 65-643, AIAA Thermophysics Specialist Conference, Monterey, Calif., Sept. 13-15, 1965.

control kinetics) and the second gas dynamic (diffusion control effects). Thus, Scala (Ref. 25) treats the transition regime by making use of the electrical analogy of the sum of resistances in parallel:

$$\dot{m}_{tra} = \frac{1}{\left(\frac{1}{\dot{m}_d} + \frac{1}{\dot{m}_r}\right)} \tag{105}$$

A modified form of this equation is suggested by Scala to account for the order of reaction $n = \frac{1}{2}$.

$$\dot{m}_{tra} = \frac{1}{\left(\frac{1}{\dot{m}_d^{\,2}} + \frac{1}{\dot{m}_r^{\,2}}\right)^{0.5}} \tag{106}$$

6.5 Sublimation Regime

When the surface temperature exceeds 5000° R, diffusion controlled oxidation is of less significance as a char removal mechanism and sublimation becomes important. In the sublimation regime, it is necessary to include the presence of the atomic and molecular species, which are present in the boundary layer, as a consequence of vaporization at the surface. The chemical interaction between the injected species and the products of dissociated air should also be included. Scala has constructed a theoretical model for the response of graphite char to high surface temperatures during flight at hypersonic speeds. A nine component gas model was chosen to represent the aerothermal-chemical interactions, including O, O_2, N, N_2, CO, CO_2, C, C_3, and CN. This model depends upon the validity of the boundary layer approximation which states that the static pressure gradient in the reaction zone in a direction normal to the surface is negligible (i.e., $\frac{\partial P}{\partial x} = 0$).

25. Ibid.

Since the sum of the partial pressures of the vaporizing species increases exponentially with surface temperature, this model will become invalid at extremely high temperatures. It is further assumed that "equilibrium vaporization" applies. This means that the net mass loss due to diffusion and convection is small compared to the forward rate of vaporization, and the sum of the partial pressures within a mean free path of the surface is nearly equal to the equilibrium vapor pressure. The concept of "equilibrium vaporization" is only approximately true when we have finite mass ablation rate. In this high temperature regime not only do chemical reactions between carbon and oxygen occur, but those of nitrogen and carbon as well. Both homogeneous and heterogeneous reactions occur within the boundary layer. Above a surface temperature of 5000° R the vaporization rate of carbon increases exponentially with temperature. However, the increase does not become appreciable until surface temperatures go beyond 6000° R.

A number of boundary layer solutions covering a wide range of stagnation enthalpies, stagnation pressures, and surface temperature yield the following formula (Ref. 50) for the char removal by sublimation:

$$\dot{m}_s = 6.67\, \dot{m}_d\, C_w \tag{107}$$

where:

$$C_w = 0.15 + 2.4 \times 10^6\, P_e^{-0.67}\, e^{-(11.1 \times 10^4/T_w)}$$

P_e is in atmospheres and T_w in degrees Rankine. When C_w approaches unity, a normal pressure gradient is induced in the flow and the theory

50. Scala, S. M., Gilbert, L. M., "Sublimation of Graphite at Hypersonic Speeds," AIAA Journal, Sept. 1965.

is no longer applicable. Combining Equations 107 and 51 yields:

$$\dot{m}_s = 0.04235\ C_W\ (P_e/R_n)^{0.5} \tag{108}$$

which can be used to predict the mass ablation rate of char at the stagnation point, neglecting the pyrolysis mass rate. Scala (Ref. 50) gives the mass ablation rate at stations on the re-entry vehicle other than the stagnation point.

In all cases where the mass loss rate, $\dot{m}$, has been given, the char recession rate can be obtained from:

$$V_c = \dot{m}/\rho_c \tag{109}$$

where ρ_c is the density of the char.

6.6 Char Removal by Spallation

Spallation is defined as the intermittent removal of char. This process can be caused by stresses associated with the pressure drop through the char material due to internal pressure build-up of the degradation gases, external pressures, thermal stresses, and surface shear stresses which can play an important role in high shear environments.

6.7 Effects of Internal Pressures

Results of high pressure tests reported by (Ref. 51) in a high Nitrogen environment, which precluded oxidation as a char removing mechanism, showed that mechanical removal of the char was observed. In some cases, no mechanical removal of char was observed, while in

---

50. Ibid.
51. Swann, R. T., Brewer, W. D., Clar, R. K., "Effect of Composition and Density on the Ablative Performance of Phenolic Nylon," Presented at VIII National Meeting of the Society of Aerospace Materials and Process Engineers, San Francisco, Calif., May 25-28, 1968.

others a char of appreciable thickness was built up and then periodically removed at an interval of several seconds. The periodic spallation which was observed in these tests consisted of complete local removal of the char at the interface between char and uncharred material. This type of char removal might result from tensile failure at the interface caused by the internal pressure built up by gaseous products of pyrolysis. The tests reported in (Ref. 51) indicated that spallation increased with increasing nylon content in phenolic nylon. This is consistent with the hypothesis that spallation is caused by tensile failure resulting from internal pressures, since increasing the nylon content also increases the amount of gases formed. The tensile strength of phenolic nylon char as a function of temperature is reported in (Ref. 51). At 700° F the ultimate tensile strength of the phenolic nylon char used by Swann is less than 50 psi. Thus, relative low internal pressures could result in a mechanical failure of the char. In the following paragraphs an approximate analytical expression for the stress at the char-virgin material interface of a charring ablator will be formulated. It will be shown that more realistic results can be obtained with the aid of the MIMIC computer program.

It has been assumed in Section II that our model of a charring ablator consists of a porous char layer and an impermeable layer of virgin material. The gases of pyrolysis are generated at the interface of these layers at a rate $\dot{m}_g$.

The pressure distribution through a porous material subjected to internal gas flow is obtained from the momentum equation and known

---

51. Ibid.

as Darcy's Law (Ref. 52):

$$\frac{dP}{dx} = - \frac{\dot{m}_g \mu_g}{k_p \rho_g} \tag{110}$$

where μ_g is the viscosity of the gas, ρ_g is the density of the gas and k_p is the proportionality factor and is defined as the permeability. Assuming the ideal gas law to be applicable:

$$P = \frac{\rho_g RT}{M} \tag{111}$$

and assuming that the viscosity is a function of temperature:

$$\mu_g = \mu_o \left(\frac{T}{T_a}\right) \tag{112}$$

and the average molecular weight of the gases is a constant:

$$M_{av} = \text{constant} \tag{113}$$

where μ_o is a reference value, the following results:

$$P\,dP = - \frac{\dot{m}_g \mu_o R}{k_p M T_a} T_x^2\,dx \tag{114}$$

Upon substituting the temperature distribution in the char layer Equation 39, the above equation can be integrated across the char thickness to yield:

$$\frac{P_s^2 - P_w^2}{2} = \frac{K_1}{K_2^2} \left\{ e^{-2K_3\delta_c} \left(T_s^2 \delta_c + \frac{3 T_s^2}{2 K_3} - \frac{T_a T_s}{K_3} - \frac{T_a^2}{2K_3} \right) - e^{-K_3 \delta_c} \left(2 T_a T_s \delta_c + \frac{2 T_s^2}{K_3} - \frac{2 T_a^2}{K_3} \right) + \left(T_a^2 \delta_c + \frac{T_s T_a}{K_3} - \frac{3 T_a^2}{2 K_3} + \frac{T_s^2}{2K_3} \right) \right\} \tag{115}$$

52. Koh, J. C. Y., Casal, del, E., "Heat and Mass Flow through Porous Matrices for Transpiration Cooling," Proceeding of the 1965 Heat Transfer & Fluid Mechanics Institute, Stanford Press, Stanford, Calif.

where: $K_1 = \dfrac{\mu_o R}{k_p M T_a}$

$$K_2 = 1 - e^{-K_3 \delta_c}$$

$$K_3 = \dot{m}_g C_g / k_c$$

and where $\dot{m}_g$ is given by Equation 28. From Equation 115 the pressure at the char virgin material interface, P_p, can be obtained. The pressure at the surface, P_s, can be approximated from Equation 104.

Note that in deriving Equation 115 we used simplified relations for the viscosity and a constant average molecular weight for the escaping gases. This expediency was necessary in order to integrate Equation 114 and obtain an analytical solution. If the MIMIC computer program were used, more sophisticated relations such as Sutherland's law of viscosity could be used. Since the MIMIC computer program solves the integral numerically, a solution to nearly any integral form of Equation 114 is possible.

As time progresses, the char layer thickness, δ_c, will increase and $\dot{m}_g$ will change, then failure should occur when the stress, σ_s, reaches the ultimate tensile strength of the char. The stress at the interface is given by:

$$\sigma_s = \frac{f P_p - P_s}{1 - f} \tag{116}$$

where f is the porosity of the material and is defined as the ratio of the void volume, occupied by the gas, to the total volume of the char.

6.8 Thermal Stresses

In (Ref. 3) mechanical removal of char was assumed to occur as a result of internal pressure and radial thermal stresses. The resulting equations were solved on a computer and predicted a periodic removal of char. Some authors (Ref. 51) contend that in some charring ablators thermal stress presents no problems since the thermal stresses can be relieved by plastic yielding in the reaction zone.

The thermal stress distribution of a finite plate with constant heat flux applied on one surface is obtained from (Ref. 53). This reference also gives some useful charts for computing thermal stresses in flat plates. Schneider, Dalton, and Reed (Ref. 54) have performed an analysis of carbon phenolic and interpret the results in terms of a combination of a thermal stress fracture in the char in conjunction with thermochemical combustion. Equations are given for computing radial and tangential thermal stresses cylindrical in char layers. The tangential components were found to be greater than the radial components and to exceed the ultimate tensile and compressive strength of the char.

6.9 Surface Shear and Pressure

At very high stagnation pressures and shear stresses, all polymeric materials and their surface residues are extensively damaged.

---

3. Ibid.
51. Ibid.
53. Brooks, W. A., "Temperature and Thermal-Stress Distributions in Some Structural Elements Heated at a Constant Rate," NACA TN 4306, Aug. 1958.
54. Schneider, P. J., Dalton, T. A., and Reed, G. W., "Char-Layer Structural Response in High Performance Ballistic Re-entry," AIAA Paper No. 66-424, Presented at AIAA 4th Aerospace Science Meeting, Los Angeles, Calif., June 27-29, 1966.

As the stagnation pressure increases, the char may be compressively crushed. Graves (Ref. 55) shows that char forming ablators exhibit high efficiency up to some critical pressure region and then greatly reduced efficiency at higher pressures. However, subliming materials, such as Teflon, were not drastically affected by the high shear environment. This indicates that Teflon is not affected by pressures.

The pressure exerted at the stagnation point of a vehicle traveling at hypersonic speeds can be estimated from Equation 104. The shear stress can be estimated from:

$$\tau = C_f\, q \tag{117}$$

where C_f is the skin friction coefficient which is related to the Stanton number and is of the order of 0.002 to 0.004 at hypersonic speeds and q is the dynamic pressure:

$$q = \tfrac{1}{2}\, \rho_\infty V_\infty^{2} \tag{118}$$

6.10 Empirical Char Removal Formulations

Bishop and Di Cristina (Ref. 56) analyzed silica phenolic and carbon phenolic wedges and cones, tested in the Cornell Aeronautical Laboratory Wave Superheater Facility, and developed a theory based on pressure gradient shear to explain the increased recession which occurs at high pressure test conditions. From the tests a maximum char thickness is derived which is consistent with observed char thickness and correlates the data for extrapolation to high pressure flight conditions.

---

55. Graves, K. W., "Ablation in a High Shear Environment," AIAA Journal, May 1966.
56. Bishop, W. M., Di Cristina, V., "A Prediction Technique for Ablative Material Performance Under High Shear Re-entry Conditions," AIAA/ASME 8th Structures, Structural Dynamics and Materials Conference, Palm Springs, Calif., Mar. 29-31, 1967.

Their results for silica phenolic and for carbon phenolic indicate the sensitivity of these materials to high pressure, high shear environment.

The maximum char layer thickness, δ_{max}, as a function of pressure for a Carbon Phenolic wedge was found to be:

$$(P - 0.456)\ (\delta_{max} + 2.260 \times 10^{-3}) = 0.285 \qquad (119)$$

where P is the pressure in atmospheres.

Mathieu (Ref. 11) neglects chemical erosion and thermal stress and works with a two spall-failure criteria. In the first case char spallation was assumed to occur when the maximum gas stress reached the ultimate char strength, referred to as a "failure stress" (i.e., an equation similar to Equation 116). The second case attempted to draw in the effect of surface shear by specifying that repetitive spalling takes place when either the failure stress or a "critical" char thickness develops, whichever occurs first. The critical char thickness was governed by a purely empirical equation that included the effect of surface gasdynamic shear. The equation for the critical char thickness δ_{CR} is:

$$\delta_{CR} = \frac{a}{(b + \tau)} \qquad (120)$$

where a and b are determined from tests for each material and τ is the shear stress. Actually, the author claims that this relation includes the effects of thermal and gas pressure stresses, since these effects must have been present when the empirical results were obtained.

---

11. Ibid.

Thus, we can conclude that internal pressures, thermal stresses, pressure gradient shear, aerodynamic shear, and surface thermochemistry all contribute to char mass loss. The precise mechanism of char removal is still not understood quantitatively. This means that extra margins of safety must be provided in designs of heat shields which may be subject to unknown forms of char removal.

VII. DESIGNING HEAT SHIELDS

The first process which must be accomplished in the design of heat shields for re-entry vehicles is to select candidate heat shield materials. In this section of the report we will state a criterion for sizing or determining the actual design thickness of the ablative material that is required to protect a re-entry vehicle from the thermal environment. Examples of the sizing process for two ablative materials, Teflon and Carbon Phenolic, will be shown for two re-entry missions at the stagnation point of a one foot radius nose cap.

The primary purpose of the ablative heat shields is to keep the load carrying substructure at a temperature consistent with its load carrying capability. Generally, vehicle design must be accomplished with the lowest possible combined heat shield and substructure weight compatible with the anticipated thermal and structural environment. Conventionally, a maximum allowable substructure temperature is defined for the purpose of heat shield design. A typical maximum temperature for a 2024-T3 structural aluminum alloy is 400° F. This criterion can be obtained from a stress-strain curve of the alloy at different temperatures.

In many re-entry vehicles, the heat shield is bonded to the substructure. Thus, the bonding agent's performance should also be a design criterion. The bond integrity must be maintained over the complete flight trajectory. In order to insure this, the traditional approach has been to restrict the bondline temperatures to low temperature levels, where it can be demonstrated that the bond possesses sufficient strength to maintain the heat shield material firmly attached to the structure. For conventional resin-based materials this temperature level coincides with that at which resin degradation becomes significant. With epoxy bonds a value of 600^{o} F is normally employed (Ref. 6). Either constraint, the substructure temperature or the bondline temperature may determine the heat shield thickness. With re-entry vehicles which have a high ballistic coefficient (W/C_dA) heating rates are significant until impact and the temperature gradients through the heat shield and substructure composite are of sufficient magnitude that the bond temperature is a limiting factor. For low ballistic parameter trajectories where the vehicle experiences long periods of low aerodynamic heating prior to mission termination, thermal equilibrium through the composite will be approached during the flight, and the substructure temperature will be the critical factor.

Since in modern re-entry vehicles, the load carrying substructure is made of high temperature materials such as Titanium, Tungsten, or Molybdenum, the bondline temperature will be assumed to be the designing criterion in our model.

The ablation model was modified to include the option of generating a re-entry trajectory for the purpose of computing aerodynamic heating, enthalpies, pressures, etc. In order to obtain the minimum ablation thickness required, an initial ablation thickness is guessed and is used as an input to the program. If the substrate temperature, which is taken as the temperature of the heat sink material, is below 550^{o} F the ablator thickness is decreased some predetermined amount.

---

6. Ibid.

If the substrate temperature exceeds 650° F, the ablator thickness is increased by some incremental thickness. The program will continue to iterate in this fashion until a substrate temperature, T_w, between 550° F and 650° F is obtained. Thus, when $550 \leq T_w \leq 650^{\circ}$ F the desired ablator thickness has been obtained and the model stops. A schematic of the ablation design model is shown in Figure 25.

In order to determine the trajectory, for different classes of re-entry vehicles, the equations of motion, Appendix IV, were programmed into the ablation model. All that is required to obtain a re-entry trajectory is for the following to be specified: initial velocity, V_o, initial altitude, H_o, initial flight path angle, γ_o, ballistic parameter, W/C_dA, and for lifting re-entry vehicles the lift to drag ratio, L/D. Simplified equations of motion for polar entry and for a spherical non-rotating earth, which are described in Appendix IV, have been programmed into the ablation heat shield design model. The effect of assuming polar entry is shown to be negligible (Ref. 40) in computing total re-entry time. The rotation of the earth should be included if we were interested in an accurate ground range calculation. Since this calculation had no effect on the results of this analysis, the assumption of a non-rotating earth is justified.

The most important part of a re-entry trajectory is the portion over which the re-entry vehicle undergoes the severest heating and aerodynamic loads. This portion of the trajectory is achieved during that portion of the trajectory in which the vehicle actually re-enters the earth's atmosphere. An altitude of 300,000 feet is generally considered as the initial re-entry altitude for circular orbit re-entry

---

40. Ibid.

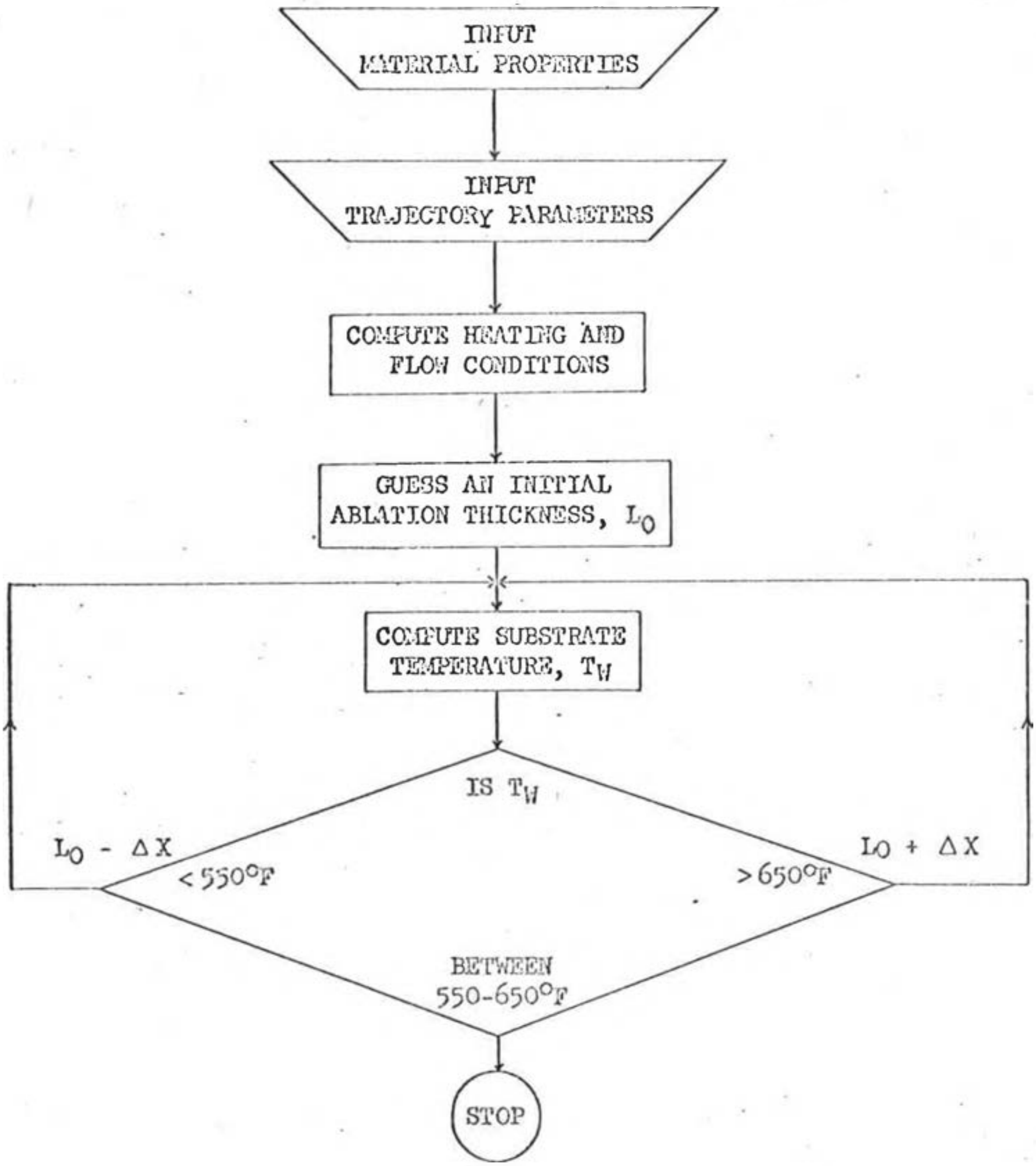

Figure 25. Schematic of the Ablation Heat Shield Design Model.

vehicles (i.e., satellite re-entry where re-entry speed is below 26,000 ft/sec). For supercircular re-entry vehicle the re-entry altitude is higher and values in the neighborhood of 400,000 feet are chosen. This is because the re-entry speed exceeds the circular velocity, 26,000 ft/sec, and heating may become appreciable at higher altitudes. Thus, a re-entry altitude between 300,000 and 400,000 feet is chosen because it represents the point at which aerodynamic heating starts to become significant. It is an arbitrary value selected on the basis of heating calculations at re-entry speeds.

In order to study the ablator's behavior to different re-entry environments two re-entry missions will be briefly discussed. The re-entry portion of a re-entry vehicle trajectory is generally divided into three regions for the purpose of analysis. The first region is at an extremely high altitude, usually between 300,000 to 400,000 feet, where the re-entry vehicle is first affected by the atmosphere. The second region is that where the vehicle experiences extremely high heating and deceleration. The third region, depending on the ballistic parameter and lift to drag ratio, may include a subsonic "slow fall" where the aerodynamic forces are comparable to the forces of gravity and surface cooling may occur.

The ballistic parameter, BP, plays a strong role in determining the heating of a re-entry vehicle. From the equations of motion, Appendix IV, we can note that by varying the ballistic parameter simply varies the altitude or atmospheric density at which a particular fraction of re-entry occurs. However, the time to go from one velocity to another is not affected by the ballistic coefficient (Ref. 45). Thus,

45. Ibid.

if the ballistic parameter is halved, deceleration starts at densities which are half as large and the vehicle subsequently goes through the same deceleration pattern but at a higher altitude. Maximum deceleration for ballistic re-entry, having a high ballistic parameter, is of the order of 60 g's. For manned systems, the g's must be kept below 10 g's. This low g constraint may be met by incorporating a "skip" or lift component in the vehicle design.

Allen and Eggers (Ref. 57) noted that re-entry heat absorbed by the vehicle may be minimized by either very high or very low ballistic parameters. In the former case, the vehicle impacts the ground with a large fraction of its initial kinetic energy and in this way minimizes heat transferred to the vehicle. While in the later case, maximum kinetic energy is transferred to the atmosphere, thus minimizing heat transfer to the vehicle's surface.

It is important in assessing heat shield performance for a specific re-entry mission to know what part of the re-entry will be laminar and turbulent since heating and recession in turbulent flow may be increased by a factor of two or more. From Equations 46 and 47, for a given heat shield geometry, the local laminar and turbulent heat rates at a particular point on the surface vary approximately, according to:

$$(\dot{q}_s)_L \sim V^3 \rho^{0.5} \tag{121}$$

and

$$(\dot{q}_s)_T \sim V^{3.15} \rho^{0.8} \tag{122}$$

---

57. Allen, H. J., and Eggers, A. J., "A Study of the Motion and Aerodynamic Heating of Ballistic Missiles Entering the Earth's Atmosphere at High Supersonic Speeds," NACA Report 1381, 1958.

If the density associated with a particular velocity can be lowered arbitrarily by changing the ballistic parameter, then we should be able to lower the heating to some acceptable level, especially since it was stated that the total time of heating is unaffected by the changes in the ballistic parameter. The time to re-enter is affected, however, by re-entry angle and initial velocity. If the heating rate over the period of re-entry is integrated, the total amount of heat, Q, added per unit area to the surface of the heat shield can be obtained. The total heat, Q, is found to depend on the ballistic parameter, W/C_dA. From (Ref. 45) the total heat for laminar and turbulent flow is proportional to:

$$Q_L \sim (BP)^{0.5} \frac{V_o^2}{\sin^{0.5} \gamma_o} \qquad (123)$$

$$Q_T \sim (BP)^{0.8} \frac{V_o^{2.48}}{\sin^{0.2} \gamma_o} \qquad (124)$$

where V_o and γ_o are the re-entry velocity and flight path angle, respectively.

Equations 123 and 124 show why bodies with low ballistic parameter are used for manned and for instrumented research re-entry vehicles. The total heat varies directly with the ballistic parameter. Also, for a ballistic parameter of 1000 lb/ft^2 the impact is very nearly at sonic speeds. For ballistic parameters of 100 lb/ft^2 sonic velocity occurs at about 45,000 ft and almost 90 seconds are required for the free-fall to the earth. This time is adequate for a drogue or parachute to be deployed in order to meet the deceleration constraints necessary for recovery.

45. Ibid.

Two re-entry missions will be considered in this analysis and the heat shield will be designed, with Teflon and Carbon Phenolic, for the stagnation point of a one foot radius nose cap. One re-entry mission will be representative of a 5500 nautical mile ICBM having a ballistic coefficient of 1000 lb/ft^2 and the other will be a manned re-entry vehicle having a ballistic coefficient of 100 lb/ft^2 and a lift to drag ratio of 0.5. The initial conditions and environments to which these two re-entry vehicles are subjected are shown in Table VI.

7.1 ICBM Ballistic Re-entry

ICBM re-entry is characterized by re-entry velocities which range from 24,000 ft/sec to 16,000 ft/sec and relatively high re-entry angles which range between 15-30 degrees. As a result of high re-entry angles the vehicle descends rapidly and the majority of the heating occurs at low altitudes or at a high Reynolds number. Consequently, over most of the re-entry vehicle there is a turbulent aerodynamic boundary layer during the high re-entry heating phase of the trajectory and only near the stagnation point is there a laminar boundary layer. From Table VI we can see that ICBM re-entry is characterized by high heating rates, high pressures, and high decelerations. Since the majority of the re-entry body is subjected to turbulent flow, we would also expect high shear forces. However, due to the high re-entry angle, the duration of flight is short and rarely exceeds a minute. Most of the heating is due to aerodynamic convective heating with a lesser amount of radiation heating due to emission from the hot gas behind the bow shock wave. In our ballistic trajectory approximately eleven per cent of the total heating was due to radiation heating.

TABLE VI. ENVIRONMENT OF ATMOSPHERIC RE-ENTRY VEHICLES

	5500 nm Ballistic Re-entry	Lifting Body Re-entry from Satellite Speeds
Re-entry Altitude (ft)	300000	350000
Re-entry Velocity (ft/sec)	24000	25000
Re-entry Angle (deg.)	20	2
Ballistic Parameter, W/C_dA (lb/ft^2)	1000	100
Lift to Drag Ratio	0	0.5
Speed at 45000 ft Altitude (ft/sec)	3330	740
Speed at Impact (ft/sec)	2193	270
Time of Re-entry Flight (sec)	50	875
Max. Aero. Heating Rate (BTU/ft^2 sec)	2130	195
Max. Rad. Heating Rate (BTU/ft^2 sec)	577	negligible $\approx$ 0.25
Occurrence of Max. Heating (alt/vel)	63276/ 20316	185435/ 21607
Ratio of Aero. to Rad. Heating	29835/ 4139	40580/ 20
Total Heating (BTU/ft^2)	33975	40600
Max. Deceleration (g's)	53	2.2
Max. Stag. Press. (atmo.)	48	0.2
Max. Dynamic Press. (atmo.)	23	0.1

7.2 Lifting Body Re-entry

Lifting body re-entry from satellite orbits are characterized by re-entry velocities in the neighborhood of 25000 ft/sec and shallow re-entry angles which range from a fraction of a degree to three degrees. One of the major reasons for shallow re-entry angles is to keep the decelerations within human tolerance limits for manned re-entry. Maximum deceleration for ballistic re-entry is about 60 g's. For manned systems the deceleration must be kept below 10 g's. By incorporating some lift by means of wings or very blunt shapes, the deceleration will be kept to a reasonable value as shown in Table VI. Manned re-entry vehicles should also have low ballistic parameters to lower the amount of heating to which the vehicle is subjected. Because of the shallow re-entry angles, lift and low ballistic parameters, deceleration and heating occur at high altitudes or at a low Reynolds number. Thus, the re-entry heating is laminar with low heat transfer rates. However, due to the low re-entry angles the flight time and hence duration of heating for lifting body re-entry is greater than that for the ICBM by at least an order of magnitude, as evidenced from Table VI. By increasing the lift to drag ratio the peak heating will be reduced, but the time of flight will be increased. Practically all the heating is due to aerodynamic heating with only negligible amounts of radiation heating.

The lifting trajectory shown in Table VI was chosen in order to give approximately the same total heating as the ballistic case. In this fashion the effects of longer exposure time on material behavior can be studied.

7.3 Results

The results of designing a heat shield for a typical ICBM and lifting body re-entry vehicle using Teflon and Carbon Phenolic ablators are summarized in Tables VII and VIII. The ablation temperature for Teflon and Carbon Phenolic was assumed to be 1000° F and a maximum char thickness of 0.05 inches was assumed for Carbon Phenolic.

For the case of ballistic re-entry, with a WC_d/A of 1000 lb/ft^2, the aerodynamic heating rates were so intense and the duration of heating of such a short duration that extremely steep temperature gradients were produced. Consequently, the material required to keep the substrate temperature in the neighborhood of 600° F consisted primarily of the amount of material ablated, Table VII. Thus, very little material was required for insulation. However, the fact that some material was required for insulation points to the fact that in the design of heat shields both the ablated material and the material needed for insulation must be accounted for. The problem can rarely be uncoupled. Thus, the combined insulation and ablation requirements must be considered together for a particular heat shield design.

The results for the lifting body trajectory heat shield design are shown in Table VIII. Due to the prolonged time spent in re-entry, lifting body re-entry may require more thermal protection in an insulative sense rather than by ablation processes. This is evidenced from Table VIII. The amount of insulation required would be still greater if the lift to drag ratio were increased. The feasibility of using ablators in lifting body re-entry, which is characterized by low heat fluxes over longer times and with long soak times before final recovery, could be enhanced if the insulation requirement could be

TABLE VII. RESULTS OF HEAT SHIELD DESIGN FOR BALLISTIC RE-ENTRY

Material: TEFLON

Total Material Required (in.)	2.125
Amount of Material Ablated (in.)	1.378
Amount of Material Required for Insulation (in.)	0.747
Substrate Temperature (^{o} F)	633

Material: CARBON PHENOLIC

Total Material Required (in.)	1.125
Amount of Material Ablated (in.)	0.774
Amount of Material Required for Insulation (in.)	0.451
Char Layer Thickness (in.) (assumed)	0.05
Substrate Temperature (^{o} F)	650

TABLE VIII. RESULTS OF HEAT SHIELD DESIGN FOR LIFTING BODY RE-ENTRY

Material: TEFLON

Total Material Required (in.)	3.000
Amount of Material Ablated (in.)	1.759
Amount of Material Required for Insulation (in.)	1.241
Substrate Temperature (^{o} F)	600

Material: CARBON PHENOLIC

Total Material Required (in.)	1.750
Amount of Material Ablated (in.)	0.683
Amount of Material Required for Insulation (in.)	1.067
Char Layer Thickness (assumed)	0.05
Substrate Temperature (^{o} F)	570

reduced by using mechanical attachments instead of adhesives to bond ablators to the substructure. Then the temperature capability of the substrate material could be used in lieu of the adhesives.

The superiority of Carbon Phenolic over Teflon is readily apparent from Tables VII and VIII. The difference lies in the fact that Carbon Phenolic forms a char. A char not only possesses insulative properties and allows for more efficient transpiration effects but also supports high surface temperatures, thereby expelling much of the heat by reradiation. Teflon is representative of the class of ablators known as low-surface-temperature sublimers. Carbon Phenolic, on the other hand, is representative of the high surface-temperature class. For a given re-entry mission one of these materials can be shown to be superior to the other. For the two re-entry missions which were selected for analysis, Carbon Phenolic is shown to provide the best thermal protection per unit weight. Other factors such as cost, ease of fabrication, etc., may actually dictate which ablator is chosen.

Thus, it should be emphasized that the choice of an ablating material for a specific re-entry mission is largely determined by the re-entry mission itself. Consequently, different missions, in general, require different types of ablating material for the construction of the most efficient heat shield. Furthermore, for any given mission it is necessary to consider the heat conduction problem in conjunction with the ablation problem. For example, a material with the largest heat of ablation is not necessarily the best ablator for a specific mission. Graphite has a very high heat of ablation as evidenced from Table I. Yet, because of its high thermal conductivity, 3×10^{-2} BTU/ft sec ^{o} F, graphite will act as a heat sink in many re-entry missions and will not absorb much heat by ablation. As evidenced from Table VIII, depending upon the physical properties of a particular material, the heat transfer rate and the heating time, the insulation weight may be either more or less than the ablated weight.

The proposed ablation model can be used to study the thermal response of ablators under varying thermal environments. How much heat is expended by the various heat dissipation mechanisms can be readily obtained. The model can also be used as a tool for examining the material's ablative behavior by parametrically varying the thermophysical properties. By varying each property individually it can be determined which property or properties will effect material ablative-insulative performance the most. The errors introduced by assuming constant thermophysical properties, as opposed to temperature dependent properties, can also be studied. Heating rates to a re-entry vehicle are not known precisely. The model can thus be used to determine the ablators response if the heating rates are varied about a mean value.

VIII. CONCLUDING REMARKS

In this report equations are derived for calculating the thermal response of charring ablators to re-entry heating conditions. The analysis was developed primarily for charring ablators but is also applicable to impregnated ceramic, subliming, and heat-sink thermal protection systems. The theoretical analysis of charring ablator systems is very complex, and many approximations and assumptions must be made to obtain solutions. In this analysis the details of the chemical kinetics of the reactions through the depth of the material have not been considered. A simplifying expedient has been assumed in that the decomposition process is assumed to occur in a single plane at a temperature which may be fixed or a function of the rate of decomposition. Since it has been shown (Ref. 13) that the thickness of the decomposition zone is very small compared with the total thickness of the material, this simplifying assumption appears to be justified.

The most difficult problem encountered in the analysis of the performance of charring ablators is the formulation of a quantitative expression for the rate of char removal. It appears that the char may be removed chemically by oxidation, thermally by sublimation, mechanically by spalling and aerodynamic shear, or by a combination of these methods. All these methods have been discussed and, depending on the material involved, can be incorporated into the program.

---

13. Ibid.

In the investigation of charring ablators one encounters moving boundaries, reradiation, time dependent heat flux, and thermophysical properties which are functions of temperature and possibly pressure. All these factors lead to nonlinear differential equations. Thus, explicit or implicit numerical methods must be used which may be difficult to program and an extensive computer time is required to obtain solutions. In this report a different approach has been suggested for numerically solving nonlinear partial differential equations. The proposed method is to reduce the partial differential equation to a system of ordinary differential equations which can then be solved numerically. The use of the MIMIC computer program employs a fourth-order variable step Runge-Kutta technique to integrate the resulting set of ordinary differential equations. Programming the MIMIC computer program is extremely simple and extensive computer time does not seem to be required. Good agreement was obtained between the numerical solution, using the MIMIC computer program, and exact solutions. In addition results which were obtained with the computer model were compared to other models, test data and flight test data. The results were found to be acceptable.

Finally, the model was exercised by using it to determine the ablation thermal protective thickness required to protect a nose cap on several important re-entry missions. There are several heat transfer mechanisms which interact in the re-entry ablation process. The heat input mechanisms included convective heating, radiation heating, and combustion heating. The heat dissipation mechanisms include transpiration, changes of phase, heat conduction, and reradiation. The degree to which the heat dissipation mechanisms contribute to the total energy absorbed depends upon the physical characteristics of the specific ablation material and the interaction of these characteristics with the aerodynamic environment to which the material is exposed. The environment varies greatly for different re-entry conditions. To assess the behavior of materials under diverse re-entry conditions, Teflon and Carbon Phenolic were subjected to re-entry missions which were representative of ballistic re-entry and lifting body re-entry. It was observed that organic plastics, such as Carbon Phenolic, which tend to char at the ablating surface, perform significantly better when exposed to extreme heat sources than those such as Teflon which act as pure sublimers. The explanation lies in the fact that char forming plastics not only incorporate the basic principles of cooling by ablation, but also much of the heat dissipated by the process of reradiation.

In order to minimize weight heat shield designers seek ablators which have a low density. By exercising the model the following ablators parameters are desired in ablators: low conductivity and diffusivity, high heat of vaporization, large volume of low molecular weight gases which give high transpiration factor, a thick stable char layer, a relatively high surface temperature, and a high specific heat.

The charring ablators constitute one of the most important classes of materials, because these materials provide a relatively efficient heat-protection system through a variety of heat-absorbing mechanisms, which occur during the overall ablation process. Initially, the material absorbs the heat it is exposed to, and the temperature rises. As the temperature continues to increase, the material undergoes thermal degradation. Gases are formed and a porous carbonaceous char remains. As the process continues, the degradation zone moves into the material.

The degradation gases flow through the porous char to the surface and tend to cool the surface. At the same time, the gases interact with the external flow, reducing the heat flux and shear stresses at the surface because of the mass addition effects. The char layer also has an insulating effect, and as it becomes thicker the heat flux to the undegraded material is reduced. Thus, the flow of gases decreases as the degradation process slows down allowing the surface temperature to rise again. At the higher temperatures, much heat is reradiated from the surface. The char is finally removed by one or several erosion mechanisms such as oxidation, sublimation, or spallation due to mechanical or thermal stresses. Much is to be gained by improving reinforcements in char forming ablators and thus keep a strong stable char.

BIBLIOGRAPHY

1. Ning, C. H., "Simplified Solutions for Ablation in a Finite Slab," AIAA Journal, June 1965.

2. Brogan, J. J., "A Simple Numerical Solution for a Heat Conduction in a Solid with a Receding Surface," Journal of Spacecraft and Rockets, January-February 1965.

3. Sharma, O. P., et al, "Phase-Change Problems with Variable Surface Temperatures," AIAA Journal, April 1967.

4. Adarkar, D. B., Hartsook, L. B., "An Integral Approach to Transient Charring Ablator Problems," AIAA Journal, December 1966.

5. Boehringer, J. C., Spindler, R. J., "Radiant Heating of Semitransparent Materials," AIAA Journal, January 1963.

6. Kendall, R. M., et al, "A Multicomponent Boundary Layer Chemically Coupled to an Ablating Surface," AIAA Journal, June 1967.

7. Roberts, L., "Mass Transfer Cooling Near the Stagnation Point," NASA TR-R-8, 1959.

8. Roberts, L., "Stagnation Point Shielding by Melting and Vaporization," NASA TR-R-10, 1959.

9. Scala, S. M., "Sublimation in a Hypersonic Environment," Journal of Aerospace Sciences, January 1960.

10. Bethe, H. A., Adams, Mac C., "A Theory for the Ablation of Glassy Materials," Journal of the Aero Space Sciences, June 1959.

11. Scala, S. M., "Vaporization into a Hypersonic Laminar Boundary Layer," Journal of the Aerospace Sciences, October 1958.

12. Steg, L., Lew, H. G., "Hypersonic Ablation," AGARD Hypersonic Conference, TCEA Rhode-St. Genese, Belgium, April 3-6, 1962.

13. Hurwicz, H., "Aerothermochemistry Studies in Ablation," Fifth AGARD Combustion and Propulsion Colloquium, Brunswick, Germany, April 9-13, 1962.

14. Munson, T. A., Spindler, R. J., "Transient Thermal Behavior of Decomposing Materials, Part I, General Theory and Application to Convective Heating," IAS Paper 62-30, January 1962.

15. Swann, R. T., et al, "Analysis of the Effects of Environmental Conditions on the Performance of Charring Ablators," Journal of Spacecraft and Rockets, January 1966.

16. Truitt, R. W., Fundamentals of Aerodynamic Heating, The Ronald Press, New York, 1960.

17. Wilson, R. J., "Thermophysical Properties of Six Charring Ablators from 140° to 700° K, and Two Chars from 800° to 3000° K," NASA TN D-2991, October 1965.

18. Swann, R. T., et al, "Analysis of the Effects of Environmental Conditions on the Performance of Charring Ablators," AIAA Entry Technology Conference, Williamsburg and Hampton, Va., October 12-14, 1964.

19. Brazel, J. P., et al, "Determination of the Thermal Performance of Char Under Heating Conditions Simulating Atmospheric Entry," AIAA Paper No. 65-640, September 1965.

APPENDIX I

Heat of Ablation

In the early days of re-entry materials performance evaluation, heat shield designers depended heavily on determining the heat of ablation, Q, which is defined as the amount of heat absorbed by a pound of ablative material and has the units BTU/lb:

$$Q = \frac{\dot{q}_{conv}\, t}{W} \tag{I-1}$$

where $\dot{q}_{conv}$ is the convective heating rate applied to non-ablating wall and W is the weight of heat shield required in lb/ft^2. In order to use the heat ablation concept a designer should have heat of ablation data which exactly match those encountered by re-entry vehicles. The heat of ablation data obtained in one environment cannot be extrapolated to new re-entry environments, particularly to higher temperatures and higher pressures. Since existing arc heater facilities only partially simulate a re-entry environment encountered, recent trends have been toward developing computer models which extrapolate test data according to recognized laws governing heat and mass transfer. However, the heat of ablation concept is still in wide usage for use in preliminary designs.

In presenting steady state ablation results it is found convenient to define the "heat of ablation" in a number of different forms. Three of the most common definitions are listed below.

Cold wall heat of ablation:

$$Q_c = \frac{\dot{q}_c}{\dot{m}} \tag{I-2}$$

where $\dot{q}_c$ is the cold-wall heat input rate and $\dot{m} = \rho V_w$.

Hot wall heat of ablation:

$$Q_h = \frac{\dot{q}_h}{\dot{m}} \quad \frac{h_s - h_w}{h_s} \; \frac{\dot{q}_c}{\dot{m}} \tag{I-3}$$

where $\dot{q}_h$ is the hot-wall heat input to nonablating surface at the same surface temperature as the ablating surface, h_s is the total free stream gas enthalpy and h_w is the total wall gas enthalpy.

Thermochemical heat of ablation:

$$Q^* = \frac{\dot{q}_h - \dot{q}_{re\text{-}rad}}{\dot{m}} = \frac{\dot{q}_{net}}{\dot{m}} \tag{I-4}$$

A thermochemical heat of ablation curve for Teflon is shown in Figure I-1.

Figure I-1 shows that the thermochemical heat of ablation of Teflon is a linear function of the enthalpy difference. For a low temperature ablator, such as Teflon, the hot wall correction, $(h_\infty - h_w)/h_\infty$, and the net surface reradiation, $\dot{q}_{re\text{-}rad}$, are negligible. Thus Equation I-4 becomes (Ref. I-1):

$$Q^* = \frac{\dot{q}_c}{\rho V_w} \tag{I-5}$$

I-1. John, R. R., Recesso, J., "Ablation Characteristics of a Subliming Material Using Arc Heated Air," ARS Journal, Sept. 1959.

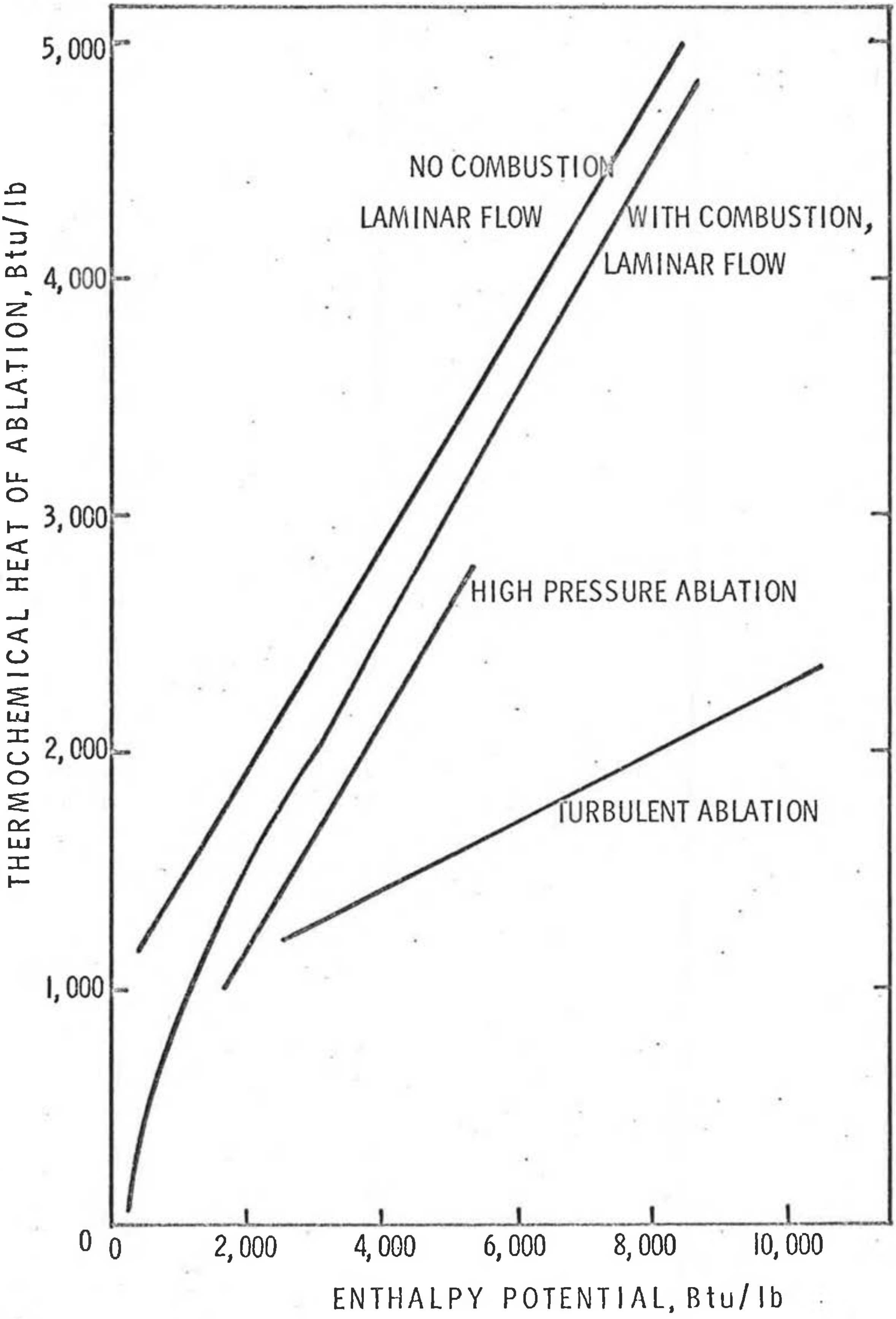

Figure I-1. Thermochemical Heat of Ablation of Teflon.

In a simplified, steady state analysis the heat input to an ablating sample is blocked or absorbed by three mechanisms, neglecting re-radiation:

1. Heat conducted to the sample's interior:

$$\dot{q}_{cond} = \rho V_w C_p \Delta T \qquad \text{(I-6)}$$

2. Energy absorbed by surface vaporization:

$$\dot{q}_{vap} = \Gamma \rho V_w H_p \qquad \text{(I-7)}$$

where Γ is the fraction of material which is vaporized - assumed unity for Teflon - and H_p is the effective heat of vaporization.

3. Energy absorbed by transpiration cooling:

$$\dot{q}_{trans} = \beta \Gamma \rho V_w (h_s - h_w) \qquad \text{(I-8)}$$

when β is the transpiration factor.

Combining Equations I-6 through I-8 an energy balance at the ablating surface yields:

$$\dot{q}_c = \rho V_w \left[C_p \Delta T + \Gamma \beta (h_s - h_w) + \Gamma H_p \right] \qquad \text{(I-9)}$$

Comparing Equations I-5 and I-9 yields:

$$Q^* = C_p \Delta T + \Gamma H_p + \beta \Gamma (h_s - h_w) \qquad \text{(I-10)}$$

which gives the desired result that the thermochemical heat of ablation is a linear function of enthalpy difference. For Teflon, with $\Gamma = 1$, the slope of the curve shown in I-1 is a direct measure of the transpiration factor β. Similarly, the value of the thermochemical heat of ablation at $h_s - h_w = 0$ is a measure of the material heat capacity and heat of vaporization (i.e., $C_p \Delta T + H_p$).

When using the thermochemical heat of ablation, it is implied that steady state conditions are present. For simple ablators, the work of Brogan, Figure 5, has shown that steady state is achieved quickly.

At steady state conditions Brogan assumed that the temperature distribution, T_x, in an ablator was that of an infinite plate whose surface is moving at constant velocity, V_w:

$$T_x = T_w \, e^{(-x/\delta_1)} \qquad \text{(I-11)}$$

where $\delta_1 = \alpha/V_w$

The steady state ablation velocity or ablation is from Equation I-5:

$$V_w = \frac{\dot{q}_c}{\rho \, Q^*} \qquad \text{(I-12)}$$

Brogan empirically determined that to establish steady state ablation, the heat diffusion depth must be of the order of δ_1 (i.e., when $x = \delta_1$):

$$T = T_s \, e^{-1} \qquad \text{(I-13)}$$

Since velocity, $V = x/t$ setting $x = \delta_1$ and substituting in Equation I-12 yields the time to reach steady state as:

$$t_{ss} = \frac{k}{\rho \, C_p} \left(\frac{\rho Q^*}{\dot{q}_c} \right)^2 \qquad \text{(I-14)}$$

To demonstrate how the thermochemical heat of ablation is used as a preliminary design tool a few additional relations will be presented.

The thickness of material required for ablation is:

$$L_o = \frac{\dot{q}_c t}{\rho Q^*} \tag{I-15}$$

The amount of material required in lbs/ft^2 is:

$$W = \frac{\dot{q}_c t}{Q^*} \tag{I-16}$$

The time to burnthrough a thickness L_o is:

$$t = \frac{L_o \rho Q^*}{\dot{q}_c} \tag{I-17}$$

The quantity $\dot{q}_c t$ can be replaced by the total convective heat minus total reradiation for a heat pulse which is not constant.

APPENDIX II

Method of Reducing Partial Differential Equations by Finite Differences

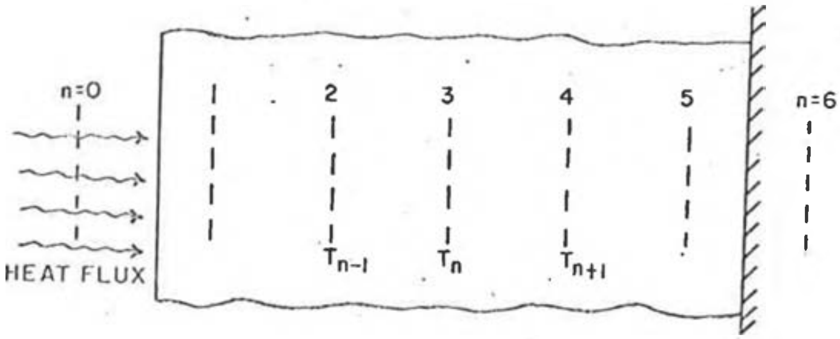

Figure II-1. Selection of Temperature Stations.

The heat conduction equation in one-dimension:

$$\frac{\partial T}{\partial t} = \alpha \frac{\partial^2 T}{\partial x^2} \tag{II-1}$$

is a partial differential equation having derivatives with respect to both time, t, and distance, x, and cannot be solved in this form on an analog computer or by the MIMIC computer program for the reason that only one independent variable is available in both methods.

Whenever we wish to solve partial differential equations by means of an electronic differential analyzer or by MIMIC, it is necessary first to convert the equations to ordinary differential equations since MIMIC can integrate with respect to only one variable. For the purpose of solving Equation II-1 we chose the variable of integration to be time. If the partial differential equation is linear, this conversion to ordinary differential equations can often be done by separation of variables, which result in ordinary differential equations of the eigenvalue type. The eigenfunction can then be found after which the complete series solution is obtained by combining the eigenfunctions. This technique is not possible if the partial differential equation and its boundary conditions are non-linear. However, it is possible to solve a partial differential equation on an analog computer or by numerical means on a digital computer. This can be done by replacing some of the partial derivatives by finite differences in order to convert the original partial differential equations into a system of ordinary differential equations.

The normal approach to solving a partial differential equation, such as Equation II-1, is to make the assumption that we are not interested in knowing the behavior of temperature versus time at every point in the slab shown in Figure II-1; instead, a finite number of points will be selected for further analysis.

Equation II-1 is a partial differential equation in which the dependent variable $T(x,t)$ is a function of both a distance variable, x, and a time variable, t. Instead of measuring the variable T at all distances, x, let us measure T only at certain stations along x. Thus, let T_1 be the value of T at the first station, T_2 be the value of T at the second x station, and T_n be the value of T at the nth station. Further, let the distance between stations be a constant, Δx, as shown in Figure II-1. This, however, is not a necessary assumption and an uneven spacing would be desirable for an irregular shaped specimen or for the first node which symbolizes the surface temperature.

A good approximation to $\left.\frac{\partial T}{\partial x}\right|_{\frac{1}{2}}$ (i.e., the partial derivative of T with respect to x at the $\frac{1}{2}$ station) is given by Equation II-2.

$$\left.\frac{\partial T}{\partial x}\right|_{\frac{1}{2}} \approx \frac{T_1 - T_0}{\Delta x} \qquad \text{(II-2)}$$

In fact, the limit of Equation II-2 as $\Delta x \longrightarrow 0$ is just the definition of the partial derivative at that point.

Thus, if the temperature at some station, n, is designated as T_n, the temperature gradients on either side of that station can be approximated by:

$$\left.\frac{\partial T}{\partial x}\right|_{n+\frac{1}{2}} \approx \frac{T_{n+1} - T_n}{\Delta x} \qquad \text{(II-3)}$$

and

$$\left.\frac{\partial T}{\partial x}\right|_{n-\frac{1}{2}} \approx \frac{T_n - T_{n-1}}{\Delta x} \qquad \text{(II-4)}$$

The second derivative, $\frac{\partial^2 T}{\partial x^2}$, can be approximated in a similar manner:

$$\left.\frac{\partial^2 T}{\partial x^2}\right|_n \approx \left[\left.\frac{\partial T}{\partial x}\right|_{n+\frac{1}{2}} - \left.\frac{\partial T}{\partial x}\right|_{n-\frac{1}{2}}\right]\frac{1}{\Delta x} \qquad \text{(II-5)}$$

or from Equations II-3 and II-4:

$$\left.\frac{\partial^2 T}{\partial x^2}\right|_n \approx \frac{T_{n+1} - 2\,T_n + T_{n-1}}{(\Delta x)^2} \qquad \text{(II-6)}$$

The incremental distance, Δx, should be kept small but finite. For the slab shown in Figure II-1, $\Delta x = L_o/5$ where L_o is the thickness of the slab. Thus, we have converted a partial derivative with respect to x into algebraic differences. The only differentiation needed now is with respect to the time variable, t, so that we are left with a system of ordinary differential equations involving dependent variables $T_o(t)$, $T_1(t)$, ... $T_n(t)$.

By substituting Equation II-6 into Equation II-1 the temperature behavior in a slab can be approximated by a set of differential equations that can be expressed as:

$$\frac{dT_n}{dt} = \frac{\alpha}{(\Delta x)^2} (T_{n+1} - T_n) - \frac{\alpha}{(\Delta x)^2} (T_n - T_{n-1}) \qquad \text{(II-7)}$$

where n = 1, 2, ... 5.

The complete set of five equations for the slab shown in Figure II-1 will be:

$$\frac{dT_1}{dt} = \frac{\alpha}{(\Delta x)^2} (T_2 - T_1) - \frac{\alpha}{(\Delta x)^2} (T_1 - T_o)$$

$$\frac{dT_2}{dt} = \frac{\alpha}{(\Delta x)^2} (T_3 - T_2) - \frac{\alpha}{(\Delta x)^2} (T_2 - T_1)$$

$$\frac{dT_3}{dt} = \frac{\alpha}{(\Delta x)^2} (T_4 - T_3) - \frac{\alpha}{(\Delta x)^2} (T_3 - T_2) \qquad \text{(II-8)}$$

$$\frac{dT_4}{dt} = \frac{\alpha}{(\Delta x)^2} (T_5 - T_4) - \frac{\alpha}{(\Delta x)^2} (T_4 - T_3)$$

$$\frac{dT_5}{dt} = \frac{\alpha}{(\Delta x)^2} (T_6 - T_5) - \frac{\alpha}{(\Delta x)^2} (T_5 - T_4)$$

From Equation II-8 the first equation in the set can be used to define T_1, the second T_2, etc., but that leaves two terms in the set of equations, namely T_o and T_6 that have not been specified as yet. To do this it is necessary to specify the appropriate boundary conditions for the problem.

In order to solve Equation II-1, two boundary conditions and one initial condition are required. Determination of the boundary conditions can be done by considering the rate of heat flow at both the front and rear surface of the slab. Typical boundary conditions may be:

$$\text{B.C. 1 at } x = 0; \qquad -k \frac{\partial T}{\partial x} = \dot{q}$$

$$\text{B.C. 2 at } x = L_o; \qquad -k \frac{\partial T}{\partial x} = 0$$

$$\text{I.C. at } t = 0; \qquad T = T_i$$

The first boundary condition signifies that a heat rate, $\dot{q}$, is applied to the front surface. The second boundary condition signifies that the rear surface is perfectly insulated (i.e., the heat flow at the rear will be zero). The rate of heat flow at the front and rear surfaces boundary conditions one and two can be approximated by:

$$\dot{q}\Big|_{x=0} \approx \frac{-KA\,(T_1 - T_o)}{\Delta x} = \dot{q}\,A$$

$$\dot{q}\Big|_{x=L_o} \approx \frac{-KA\,(T_6 - T_5)}{\Delta x} = 0 \qquad \text{(II-9)}$$

Substituting Equation II-9 into the first and last set of Equation II-8, we obtain the final set of the five equations:

$$\dot{T}_1 = \frac{dT_1}{dt} = \frac{\alpha}{(\Delta x)^2}(T_2 - T_1) + \frac{\alpha}{k\Delta x}\,\dot{q}$$

$$\dot{T}_2 = \frac{dT_2}{dt} = \frac{\alpha}{(\Delta x)^2}(T_3 - T_2) - \frac{\alpha}{(\Delta x)^2}(T_2 - T_1) \qquad \text{(II-10)}$$

$$\dot{T}_3 = \frac{dT_3}{dt} = \frac{\alpha}{(\Delta x)^2}(T_4 - T_3) - \frac{\alpha}{(\Delta x)^2}(T_3 - T_2)$$

$$\dot{T}_4 = \frac{dT_4}{dt} = \frac{\alpha}{(\Delta x)^2}(T_5 - T_4) - \frac{\alpha}{(\Delta x)^2}(T_4 - T_3)$$

$$\dot{T}_5 = \frac{dT_5}{dt} = - \frac{\alpha}{(\Delta x)^2}(T_5 - T_4)$$

Before the heat is applied, the slab will be considered to be at a uniform temperature distribution, T_i. The system of equations given by Equation II-10 can be solved by the MIMIC computer program which integrates the system of equations using a variable step Runge Kutta technique. The temperature distribution is obtained from:

$$T_n = T_i + \int \dot{T}_n \, dt \qquad \text{(II-11)}$$

where n = 1, 2, ... 5.

The method of reducing partial differential equations to set of ordinary differential equations can readily be extended to solve two and three dimensional heat transfer problems. The two dimensional counterpart of Equation II-1 can be expressed as:

$$\frac{\partial T}{\partial t} = \alpha \left(\frac{\partial^2 T}{\partial x^2} + \frac{\partial^2 T}{\partial y^2} \right) \qquad \text{(II-12)}$$

Applying Equation II-6 to Equation II-12, the two dimensional difference equation for the temperature $T_{n,m}$ becomes:

$$\frac{dT_{n,m}}{dt} = \frac{\alpha}{(\Delta x)^2}(T_{n+1,m} - 2T_{n,m} + T_{n-1,m}) + \frac{\alpha}{(\Delta y)^2}(T_{n,m+1} - 2T_{n,m} + T_{n,m-1})$$

(II-13)

or for $\Delta x = \Delta y$

$$\dot{T}_{n,m} = \frac{\alpha}{(\Delta x)^2} (T_{n+1,m} + T_{n-1,m} - 4T_{n,m} + T_{n,m+1} + T_{n,m-1}) \qquad \text{(II-14)}$$

To solve a set of equations described by Equation II-13 one needs four boundary conditions and one initial condition.

Extension of this method to three dimensions presents no difficulty. A partial differential equation in cylindrical or spherical coordinates can also be reduced to a system of ordinary differential equations (Ref. II-1).

There are many techniques of solving Equation II-1 by numerical methods. Generally the methods fall into two categories (Ref. II-2) explicit and implicit finite difference methods. Equation II-12 is approximated by the following explicit finite difference equation:

$$\frac{T_{i,j}^{n+1} - T_{i,j}^{n}}{\Delta t} = \frac{\alpha}{(\Delta x)^2} (T_{i+1,j}^{n} - 2T_{i,j}^{n} + T_{i-1,j}^{n}) +$$

$$\frac{\alpha}{(\Delta y)^2} (T_{i,j+1}^{n} - 2T_{i,j}^{n} + T_{i,j-1}^{n}) \qquad \text{(II-15)}$$

where i,j are the lattice parameters in the two-dimensional grid used ($i = 1$ corresponds to $x = 0$, and $j = 1$ corresponds to $y = 0$) and n denotes the time level t ($t = n \Delta t$).

II-1. Howe, R. M., Hoveman, V. S., "The Solution of Partial Differential Equations by Difference Methods Using the Electronic Differential Analyzer," Proc. Western Computer Conf., (Joint IRE-AIEE-ACM Conference), Los Angeles, Calif., Feb. 4-6, 1953.
II-2. Barakat, H. Z., Clark, J. A., "On the Solution of the Diffusion Equations by Numerical Methods," Journal of Heat Transfer, Transactions of the ASME, Nov., 1966.

The primary difficulty encountered in using the explicit formulation is the time required to obtain solutions on the digital computer. The equations are integrated stepwise over time, and the maximum time interval for which the solution is stable with the explicit formulation is obtained from the following stability criterion (Ref. II-1):

$$\alpha \Delta t \left[\frac{1}{(\Delta x)^2} + \frac{1}{(\Delta y)^2} \right] \leq \frac{1}{2} \qquad \text{(II-16)}$$

Furthermore, it can be proven (Ref. II-1) that the solution of Equation II-15 will converge to that of Equation II-12 as both time and space increments Δt, Δx, and Δy approach zero assuming that inequality (II-16) is satisfied. This method has the advantages of being simple to program, but the restriction of small Δt usually requires a very large number of time steps and thus much computer time.

To alleviate the difficulty various implicit methods have been devised (Ref. II-1). The first known implicit method has the form:

$$\frac{T_{i,j}^{n+1} - T_{i,j}^{n}}{\Delta t} = \frac{\alpha}{(\Delta x)^2} (T_{i+1,j}^{n+1} - 2T_{i,j}^{n+1} + T_{i-1,j}^{n+1}) +$$

$$\frac{\alpha}{(\Delta y)^2} (T_{i,j+1}^{n+1} - 2T_{i,j}^{n+1} + T_{i,j-1}^{n+1}) \qquad \text{(II-17)}$$

More accurate, but more sophisticated and more difficult to program, implicit methods have been devised such as the Crank-Nicolson Method and the Peaceman-Rachford Method (Ref. II-1). The main advantage of the implicit method is the fact that the method is

---

II-1. Ibid.

unconditionally stable. However, the use of these methods requires the solution of a large number of simultaneous linear, algebraic equations at each time step. Iterative methods are usually utilized to accomplish the solution. Regardless of the iterative method used, the number of iterations required to achieve a modest numerical accuracy may become large, particularly for large time increments and small grid sizes. The advantages of these methods from the standpoint of savings in the cost of machine time is then of doubtful value.

The method which we have proposed to solve Equation II-12 is basically an explicit method and the solution is stable if the time interval is dictated by Equation II-16. To briefly recapitulate the method proposed to solve partial differential equations: (a) reduce the partial differential equation to a set of ordinary differential equations, and (b) solve the set of ordinary differential equations by simultaneous integration by a Runge-Kutta technique. The resulting truncation errors will be discussed in Appendix III. The method is extremely simple to program and does not require excessive machine time. The truncation errors which result in implicit and explicit formulations can be found in (Ref. II-1).

II-1. Ibid.

APPENDIX III

MIMIC Computer Program

The MIMIC language is classed as a digital analog simulation (DAS) language, denoting continuous simulation rather than discrete simulation such as the SIMSCRIPT language. The language is based largely on the use of FORTRAN-like expression to represent simulation variables. Special functions are included which are oriented toward continuous simulation, especially the integration function, INT. The logical control variable, LCV, and other logical functions preserve the sense of parallelism, as contrasted to FORTRAN which is procedural in nature. This means that in programming the MIMIC language the order of the statements which simulate events need not be observed. This is in contrast to FORTRAN which executes the first statement before executing the second unless specifically programmed to do otherwise. Simplified input/output operations and fixed formats divorce the user from the complexities of these operations. Plots of a variable can be easily obtained as functions of any other five parameters. The plotting can be obtained either as an online plot or by a Stromberg-Carlson 4020 Plotter. All that is required to obtain a plot of a temperature distribution as a function of time is the statement PLO (T, T1, T2, ...). The MIMIC language will determine a scale for the axis, label the axis, and label the plots.

The MIMIC language is basically a digital computer program for solving systems of ordinary differential equations on an IBM 7090 (7094) computer with a FORTRAN IV IBYSYS Monitor. Since the MIMIC language was originally written to simulate an analog computer, many of the logical variable names resemble and function as their analog computer counterparts. In fact, MIMIC can be easily coded by listing the connections indicated on a detailed analog computer diagram. However, it can also be coded directly from the equations of the system and MIMIC will then sort the program. The MIMIC user has a wide set of functions at his disposal, may write MIMIC or FORTRAN subroutines, add new functions, and exercise control over the execution of his program (Ref. 8).

The heart of the MIMIC processor is a variable-interval fourth-order Runge-Kutta integration subroutine. The processor contains the subroutine linkages which control this subroutine and connect it with the program generated from the user's problem description. A sorting routine converts the user's problem description, which is essentially non-procedural, into a satisfactorily-ordered description, which is in turn used to produce a procedural program.

All integrations in MIMIC are performed by the centralized integration routine which employs a fourth-order variable step Runge-Kutta method. The mechanics of this method can be described in terms of an initial value problem:

$$\dot{T} = f(T,t) \qquad \text{(III-1)}$$

where T may be a vector or scalar

$T\ (t_n) = T_n$

$T\ (t_n + \Delta t) = T_{n+1}$

---

8. Ibid.

Given that $T = T_n$ at $t = t_n$, then T at $t_n + \Delta t$ can be computed from (Ref. III-1):

$$T_{n+1} = T_n + \frac{\Delta t}{6} (k_1 + 2k_2 + 2k_3 + k_4) + 0 \left[\Delta t\right]^5 \qquad \text{(III-2)}$$

where:

$$k_1 = f(t_n, T_n)$$

$$k_2 = f(t_n + \tfrac{1}{2} \Delta t, T_n + \tfrac{1}{2} \Delta t\, k_1)$$

$$k_3 = f(t_n + \tfrac{1}{2} \Delta t, T_n + \tfrac{1}{2} \Delta t\, k_2)$$

$$k_4 = f(t_n + \Delta t, T_n + \Delta t\, k_3)$$

This is a two parameter family of formulas of fourth-order accuracy which reduces to Simpson's rule of integration if the function, f, were independent of t. These formulas can be generalized and used to solve simultaneous differential equations (Ref. III-1).

The value of Δt that is used is determined by the values of the computer printout interval, DT, the maximum integration step size allowed, DTMAX, and the minimum integration step size allowed, DTMIN. If the values of DTMIN and DTMAX are not assigned by the programmer, they are set to zero and DT respectively by the computer. The step size, Δt, is automatically changed by the integration routine to keep the local relative error below 5×10^{-6}. The error is computed by comparing the values of T_{n+1} obtained by computing with two half steps and one full step. The step size may change over the range:

$$\text{DTMIN} \leq \Delta t \leq \text{DTMAX} \leq \text{DT} \qquad \text{(III-3)}$$

The error criterion can be changed from a relative error to an absolute basis at the discretion of the user.

III-1. Hildegrand, F. B., Introduction to Numerical Analysis, McGraw Hill Book Co., Inc., New York, 1956.

No simple expressions are known for the precise truncation errors when the Runge-Kutta method is used to solve simultaneous differential equations (Ref. III-1). An estimate of the error can be obtained, in practice, in the following way. Let the truncation error associated with a formula of r^{th}-order accuracy, in progressing from the ordinate at t_n to that at $t_{n+1} = t_n + \Delta t$, in a single step, be denoted by $C_n(\Delta t)^{r+1}$, and suppose that C_n varies slowly with n and is nearly independent of Δt when Δt is small. Then, if the true ordinate at t_{n+1} is denoted by Y_{n+1}, the value obtained by two steps starting at t_{n-1} by T_{n+1}, and the value obtained by a single step with doubled spacing $2\Delta t$ by $T_{n+1}^{(2\Delta t)}$, the following approximate equations are obtained (Ref. III-1):

$$Y_{n+1} - T_{n+1}^{(\Delta t)} \approx 2\, C_n\, (\Delta t)^{r+1} \qquad \text{(III-4)}$$

$$Y_{n+1} - T_{n+1}^{(2\Delta t)} \approx 2^{r+1}\, C_n\, (\Delta t)^{r+1} \qquad \text{(III-5)}$$

when Δt is small.

The result of eliminating C_n from these approximate relations is the Richardson extrapolation formula (Ref. III-1):

$$Y_{n+1} \approx T_{n+1}^{(\Delta t)} + \frac{T_{n+1}^{(\Delta t)} - T_{n+1}^{(2\Delta t)}}{2^r - 1} \qquad \text{(III-6)}$$

Thus, if at certain stages of the advancing calculation, the newly calculated ordinate, T_{n+1}, is recomputed from T_{n+1} with a double spacing, the truncation error in the originally calculated value is

III-1. Ibid.

approximated by the result of dividing the difference between the two values by the factor 2^{r-1} which is 15 in the formulas of fourth-order accuracy.

According to (Ref. III-1) an arbitrary change in spacing can be introduced at any stage of the forward progress, when a method of the Runge-Kutta type is used, without introducing any appreciable complications.

It should be pointed out that what was said in the preceding paragraphs pertained only to truncation errors. This does not say anything about what error is introduced when we simulate the heat conduction equation by a set of ordinary differential equations employing large nodes (i.e., large Δx). Estimates of this type can be obtained by comparing approximate solutions with known exact solutions, as was done in Section IV.

III-1. Ibid.

APPENDIX IV

Equations of Motion

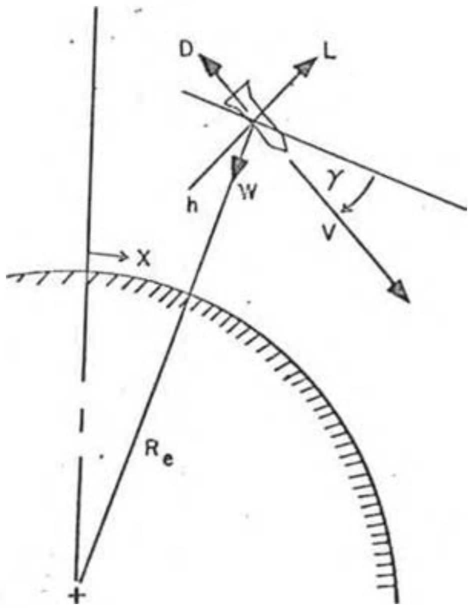

Figure IV-1. Forces Acting on a Re-entry Vehicle.

In order to obtain trajectory information for a vehicle re-entering the earth's atmosphere, the equations of motion of a body in flight will be derived. Simplified equations of motion for a point mass moving in a vertical plane of a round non-rotating earth will be subsequently derived. The mass is subjected to aerodynamic and gravitational force. The drag coefficient, lift coefficient, cross-sectional area, and the mass are assumed constant during re-entry. The re-entry body is assumed to be an uncontrolled ballistic type that may have drag and lift, but no thrust force.

The Euler equations of motion along and normal to the vehicle's velocity vector are:

$$D - W \sin \gamma = - \frac{w}{g} \frac{dV_\infty}{dt} \qquad \text{(IV-1)}$$

$$L + \left(\frac{w}{g} \frac{V_\infty^2}{R} - w \right) \cos \gamma = - \frac{w}{g} V_\infty \frac{d\gamma}{dt} \qquad \text{(IV-2)}$$

where: $R = R_e + H$ (R_e is the radius of the earth and assumed to be 3438 nautical miles) and the gravity, g, varies with altitude as:

$$g = 32.174 \left(\frac{R_e}{R_e + H} \right)^2 \qquad \text{(IV-3)}$$

If the thrust force, Th, is desired, Th cos $\bar{\alpha}$ is subtracted from the left hand side of Equation IV-1 and Th sin $\bar{\alpha}$ is subtracted from the left hand side of Equation IV-2. The propulsive thrust force is given by:

$$Th = I_{o_{SP}} \dot{w}_p + A_E (P_E - P_\infty) \qquad \text{(IV-4)}$$

where $I_{o_{SP}}$ is the fuel's specific impulse at sea level (sec.):

$\dot{w}_p$ is the fuel flow (lb/sec)

A_E is the exit area of the nozzle (ft^2)

P_E is the static pressure at nozzle exit ≈ 2116 lb/ft^2

P_∞ is the ambient static pressure

The thrust force can be included in the equation of motion if the boost trajectory, for the purpose of computing the ascend heating, is desired. However, the angle of attack, $\bar{\alpha}$, and the flight path angle, γ, as a function of time must be specified until boost burnout.

Defining the aerodynamic drag, D, and the aerodynamic lift, L, by:

$$D = \tfrac{1}{2} \rho_\infty V_\infty^2 C_D A \qquad \text{(IV-5)}$$

$$L = \tfrac{1}{2} \rho_\infty V_\infty^2 C_L A \qquad \text{(IV-6)}$$

and the ballistic parameter as $W/C_d A = BP$, Equations IV-1 and IV-2 reduce to:

$$\dot{V}_\infty = \frac{d V_\infty}{dt} = g \sin \gamma - \frac{g \rho_\infty V_\infty^2}{2\ BP} \qquad \text{(IV-7)}$$

and

$$\dot{\gamma} = \frac{d V_\infty}{dt} = \frac{1}{V_\infty} \left(g \cos \gamma - \frac{V_\infty^2}{R} \cos \gamma - \tfrac{1}{2} \frac{L}{D} \frac{\rho_\infty g V_\infty^2}{BP} \right) \qquad \text{(IV-8)}$$

The flight path angle, γ, is assumed to be positive downward.

A direction parallel, but opposite, to the flight path of the vehicle and a normal to this direction pointing away from the surface of the earth, are assumed to be the positive directions to our coordinate system. The kinematic equations can be written in this coordinate system. The kinematic equations are the rate of change of the vertical distance, H, which yields the altitude and the rate of change in the horizontal distance, X, which yields the ground range. These equations can be written as:

$$\dot{H} = \frac{dH}{dt} = - V_\infty \sin \gamma \qquad \text{(IV-9)}$$

$$\dot{X} = \frac{dX}{dt} = V_\infty \cos \gamma \qquad \text{(IV-10)}$$

Thus, the velocity, V_∞, flight path angle, γ, altitude, H, and ground range, X, can be expressed as shown on the following page.

$$
\begin{aligned}
V_\infty &= V_o + \int \dot{V}_\infty \, dt \\
\gamma &= \gamma_o + \int \dot{\gamma} \, dt \\
H &= H_o + \int \dot{H} \, dt \\
X &= X_o + \int \dot{X} \, dt
\end{aligned}
\qquad \text{(IV-11)}
$$

A complete trajectory can be obtained by specifying the initial conditions, V_o, γ_o, H_o, X_o, the ballistic parameter, W/C_dA, and the lift to drag ratio has a value only for the vehicles which are lifting bodies. For a ballistic re-entry vehicle the value of lift to drag ratio is zero. The system of equations given by Equation IV-11 is non-linear and must be solved by numerical means. This system of equations is easily solved by the MIMIC computer program.

For simplification the atmospheric density, ρ_∞, may be expressed as an exponential function of altitude for an isothermal atmosphere:

$$\rho_\infty = \rho_{SL} \, e^{-H/23700} \qquad \text{(IV-12)}$$

where ρ_{SL} is the sea level atmospheric density and has a value of 2.378×10^{-3} lb sec^2/ft^4.

The atmospheric pressure, P in lb/ft^2, at any altitude, assuming the perfect gas law is found from:

$$P_o = 1716 \, \rho \, T \qquad \text{(IV-13)}$$

where an average value of 400° R can be assumed for the temperature T.

An alternate method of programming atmospheric density, pressure and temperature variation with altitude is by means of table lookups. This is especially simple using the MIMIC computer program, since the program is equipped to do the required interpolation.

Since the equations of motion were modeled to primarily obtain aerodynamic heating, the initial values used to start the trajectory are representative of the beginning of re-entry. Re-entry will be assumed to start at an altitude of 300,000 to 400,000 feet, depending on the vehicle's initial speed. For manned re-entry the normal g-loadings, obtained from $\dot{V}_{\infty}$, should be kept under ten.

APPENDIX V

Materials Properties

The following tables will summarize the thermophysical and mechanical properties of Teflon and Carbon Phenolic. The data was obtained from many sources, including:

a. Hillberg, L. H., "Influence of Material Properties on Re-entry Vehicle Heat Shield Design," AIAA/ASME 8th Structures, Structural Dynamics and Materials Conference, Palm Springs, Calif., Mar. 29-31, 1967.

b. Slevin, G. S., "Heat Transfer and Ablative Heat Shields for Re-entry Vehicles," TR 3421, Picatinny Arsenal, Dover, N. J., Jan. 1967.

c. Air Force Materials Laboratory - unpublished data.

The term Teflon is used loosely as a generic term. It should be noted that Teflon is a registered trademark of the DuPont Company, covering fluorocarbon resins. When we talk of Teflon as an ablative material, we mean the compound polytetrafluorethylene. The properties listed in Tables V-1 and V-2 are representative of this material.

Carbon phenolic materials are carbon fiber or carbon cloth reinforced phenolic resin composites. The carbon can be in the form of individual fiber mats, woven yarn, chopped yarn, chopped cloth squares, filament wound, or various fabric weaves, including three dimensional weave or yarn layups. The phenolic resin can be any one of the various phenolformaldehyde condensation products commercially available.

The Carbon Phenolic whose properties are presented in Tables V-3 and V-4 is made with a carbon fiber content of about sixty-five per cent by weight and a nominal resin content of thirty-five per cent by weight. The carbon fibers are parallel to the specimen's length.

TABLE V-1 NOMINAL THERMOPHYSICAL PROPERTIES OF TEFLON

Virgin Material	
Density, lb/ft^3	136
Emissivity	0.5
Absorptivity	0.2
Conductivity, $^{BTU\ in}/_{ft^2\ sec\ ^oR}$	(1)
Specific Heat, $^{BTU}/_{lb\ ^oR}$	(2)
Heat of Pyrolysis, $^{BTU}/_{lb}$	750-800
Decomposition Temperature, ^oF	800-1000
Collision Frequency, $^1/_{sec}$	9.8×10^{18}
Activation Temperature, ^oR	73800
Reaction Order	1.0
Gas	
Transpiration Factor for Ablating Gasses:	
Laminar	0.41
Turbulent	0.18
Gasification Ratio	1.0
Ablation Gas Heat of Combustion, $^{BTU}/_{lb}$	10000
Specific Heat, $^{BTU}/_{lb\ ^oR}$	0.4
Average Molecular Weight ($C_2 F_4$), $^{lb}/_{lb\text{-}mole}$	100

(1) $k_v = 8.25 \times 10^{-7}\ T$ (T in ^oR)

(2) $C_{Pv} = 0.1544 + 1.389 \times 10^{-4}\ T$ (T in ^oR)

TABLE V-2 NOMINAL MECHANICAL PROPERTIES OF TEFLON

Tensile Strength, psi	3940
Tensile Elastic Modulus, 10^6 psi	0.58
Tensile Elongation at Failure, %	110
Compressive Strength, psi	16,900
Compressive Elastic Modulus, 10^6 psi	0.10
Flexural Strength, psi	8,500
Flexural Elastic Modulus, 10^6 psi	0.08
Impact Strength, ft-lb	4.0
Thermal Expansion Coefficient, 10^{-5} in/in/^{o}F	5.6

TABLE V-3 NOMINAL THERMOPHYSICAL PROPERTIES OF CARBON PHENOLIC

Virgin Material	
Density, lb/ft^3	91.1
Emissivity	0.85
Absorptivity	0.85
Conductivity, $^{BTU\ in}/ft^2\ sec\ ^oR$	1.5×10^{-3}
Specific Heat, $^{BTU}/lb\ ^oR$	0.40
Heat of Pyrolysis, $^{BTU}/lb$	2200
Decomposition Temperature, ^oF	900-1100
First Term Decomposition Constants	
Collision Frequency, $^1/sec$	4.5×10^{-3}
Activation Temperature, ^oR	5700
Reaction Order	1.0
Second Term Decomposition Constants	
Collision Frequency, $^1/sec$	6.0×10^{14}
Activation Temperature, ^oR	88700
Reaction Order	1.0
Gas	
Transpiration Factor for Ablating Gasses:	
Laminar	0.7
Turbulent	0.25
Gasification Ratio	0.62
Ablation Gas Heat of Combustion $^{BTU}/lb$	6000
Average Molecular Weight, $^{lb}/lb\text{-mole}$	20
Specific Heat, $^{BTU}/lb\ ^oR$	0.4

Char

Density, lb/ft^3	70.0
Emissivity	0.85
Absorptivity	0.85
Conductivity, $^{BTU\ in}/ft^2\ sec\ ^oR$	(1)
Specific Heat, $^{BTU}/lb\ ^oR$	(2)
Arrhenius Decomposition Constants	
Effective Collision Frequency, lb/ft^2 sec	286
Activation Temperature, ^oR	20100
Reaction Order	0.5
Heat of Combustion, $^{BTU}/lb$	14000
Sublimation Constants	
Effective Collision Frequency, $^{lb}/ft^2$ sec	1.6×10^7
Activation Temperature, ^oR	1.11×10^5
Reaction Order	0.67
Heat of Sublimation, $^{BTU}/lb$	25300

(1) $k_c = 3.2 \times 10^{-3} + 2.4 \times 10^{-14}\ T^3$ (T in ^oR)

(2) $Cp_c = 0.03 \times 3.14 \times 10^{-4}\ R - 5.33 \times 10^{-8}\ T^2 + 2.97 \times 10^{-12}\ T^3$ (T in ^oR)

TABLE V-4 NOMINAL MECHANICAL PROPERTIES OF CARBON PHENOLIC

Virgin Material	
Porosity	0.01
Thermal Expansion Coefficient, $^{in}/in\ ^{o}R$	6.5×10^{-6}
Compressive Elastic Modulus, 10^6 psi	1.57
Poisson's Ratio	0.2
Tensile Strength, psi	
75^oF	3.50
350^oF	2.80
Tensile Elongation at Failure %	
75^oF	1.08
350^oF	1.14
Shear Strength, psi	
75^oF	4000
350^oF	3230
Compressive Strength, psi	35000
Flexural Strength, psi	30000
Flexural Elastic Modulus, 10^6 psi	2.4
Hardness, Barcol	73
Char	
Porosity	0.3
Permeability (Darcy's) ft^2	1.0×10^{-10}
Thermal Expansion Coefficient, $^{in}/in\ ^{o}R$	6.0×10^{-8}
Elastic Modulus, $11_f/in^2$	5.0×10^5
Poisson's Ratio	0.2
Ultimate Tensile Strength, psi	
3000^oF	1800

Tension Elastic Modulus, 10^6 psi	
3000°F	0.28
Compression Elastic Modulus, 10^6 psi	
3000°F	0.3
Failure Strain in Tension %	
3000°F	0.5
Failure Strain in Compression %	
3000°F	1.0
Ultimate Compressive Strength, psi	
3000°F	4000